INFORMATION TO USERS

This dissertation was produced from a microfilm copy of the original document. While the most advanced technological means to photograph and reproduce this document have been used, the quality is heavily dependent upon the quality of the original submitted.

The following explanation of techniques is provided to help you understand markings or patterns which may appear on this reproduction.

1. The sign or "target" for pages apparently lacking from the document photographed is "Missing Page(s)". If it was possible to obtain the missing page(s) or section, they are spliced into the film along with adjacent pages. This may have necessitated cutting thru an image and duplicating adjacent pages to insure you complete continuity.

2. When an image on the film is obliterated with a large round black mark, it is an indication that the photographer suspected that the copy may have moved during exposure and thus cause a blurred image. You will find a good image of the page in the adjacent frame.

3. When a map, drawing or chart, etc., was part of the material being photographed the photographer followed a definite method in "sectioning" the material. It is customary to begin photoing at the upper left hand corner of a large sheet and to continue photoing from left to right in equal sections with a small overlap. If necessary, sectioning is continued again — beginning below the first row and continuing on until complete.

4. The majority of users indicate that the textual content is of greatest value, however, a somewhat higher quality reproduction could be made from "photographs" if essential to the understanding of the dissertation. Silver prints of "photographs" may be ordered at additional charge by writing the Order Department, giving the catalog number, title, author and specific pages you wish reproduced.

University Microfilms

300 North Zeeb Road
Ann Arbor, Michigan 48106

A Xerox Education Company

Reproduced with permission of the copyright owner. Further reproduction prohibited without permission.

72-17,156

PILBEAM, Carol Coke, 1941-
ACOUSTIC VELOCITIES AND ENERGY LOSSES
IN GRANULAR AGGREGATES.

Yale University, Ph.D., 1971
Geophysics

University Microfilms, A XEROX Company, Ann Arbor, Michigan

© 1972

CAROL COKE PILBEAM

ALL RIGHTS RESERVED

THIS DISSERTATION HAS BEEN MICROFILMED EXACTLY AS RECEIVED

Reproduced with permission of the copyright owner. Further reproduction prohibited without permission.

ACOUSTIC VELOCITIES AND ENERGY LOSSES IN GRANULAR AGGREGATES

Carol Coke Pilbeam

1971

A Dissertation Presented to the Faculty of the Graduate School of Yale University in Candidacy for the Degree of Doctor of Philosophy

Reproduced with permission of the copyright owner. Further reproduction prohibited without permission.

PLEASE NOTE:

Some pages may have

indistinct print.

Filmed as received.

University Microfilms, A Xerox Education Company

Reproduced with permission of the copyright owner. Further reproduction prohibited without permission.

SUMMARY

Unconsolidated aggregates occur in several geologic settings of interest. Examples are marine sediments and beach sands, lunar surface soils, and, if the fluid pressure should be about equal to the overload pressure, partial melts in the earth at depth. The properties of such aggregates are not well known. When studying the behavior of a complex system, it is important to know what factors can contribute to the behavior in order to extrapolate the observed properties to other conditions. At low net pressures (intergranular contact areas small compared to grain size), the bulk dynamic properties of aggregates are determined in large part by the interparticle contact properties. A set of relations, collectively called contact theory, have been used to describe the dynamic behavior of pairs and regular arrays of uniform spheres in elastic contact. It was the purpose of this study to compare some of the predictions of contact theory with experimental studies on irregularly packed aggregates of various types and sizes of clean and lubricated particles.

Extensional and torsional velocities in granular aggregates were found to increase with confining pressure (from 0 to 1 bar), while the associated fractional energy losses per cycle ($2\pi Q^{-1}$) decreased. Velocities varied as the 1/3 power of pressure for aggregates of clean, spherical particles, as the 1/3.5-1/5 power for lubricated spherical particles, and as the 1/4-1/6 power for clean and lubricated angular particles. Lubrication raised the velocities, at a given pressure, of the spherical particle aggregates but not of the angular particle aggregates. The above results can be interpreted in terms of contact theory modified to include the changing number of interparticle contacts with pressure and lubrication. Also interpretable within the framework of contact theory are the observed decrease of velocity with decreasing spherical grain size and increasing angularity and the approach of the velocity of aggregates of particles with some plastic deformation at contacts to a terminal velocity at about 1 bar pressure. Values of Q^{-1} were independent of vibration frequency (1 to 20 kHz) and amplitude. Lubrication generally increased relative energy losses, sometimes by a factor of 10. The energy dissipation at these pressures, which is thought to be related to lightly made contacts, is not adequately described by any present theory.

The measured extensional velocities of clean aggregates at pressures of about 1 bar ranged from about 0.3 to 0.6 km/sec and the associated values of Q^{-1}, from 4×10^{-3} to 2×10^{-2}. Extrapolations of these values to lunar conditions agree well with the low velocities and low Q^{-1}'s observed in studies of man-made impacts on the moon.

Reproduced with permission of the copyright owner. Further reproduction prohibited without permission.

TABLE OF CONTENTS

Page

LIST OF TABLES iii

LIST OF ILLUSTRATIONS iv

INTRODUCTION 1

ACKNOWLEDGMENTS 3

I. GRANULAR AGGREGATES: THEORETICAL AND EXPERIMENTAL BACKGROUND 4

A. Two Spheres in Elastic Content 4
A-1. Contact theory 4
A-2. Experimental investigations on single contacts 13
A-3. Alternative mechanism for energy dissipation at contacts 16
B. Regular Arrays of Spheres 20
B-1. Stress-strain relations 20
B-2. Wave propagation 21
B-3. Experimental investigations 27
C. Real Aggregates of Particles 29
C-1. Random packings of particles 29
C-2. Contact of rough surfaces 34
C-3. Field and laboratory acoustic studies of randomly packed aggregates 39

II. EXPERIMENTAL PROCEDURE FOR THE ACOUSTIC TESTS . . 43

A. Method 43
A-1. Measurement techniques 43
A-2. Equipment 46
A-3. Preparation of rigid bars and effects of jacket 49
A-4. Support of specimens 54
B. Description of Specimens 56

Reproduced with permission of the copyright owner. Further reproduction prohibited without permission.

Page

III. RESULTS OF THE ACOUSTIC EXPERIMENTS 61

IV. DISCUSSION OF THE ACOUSTIC RESULTS 68

A. Comparison of Data with Theoretical Expressions for Regular Arrays of Spheres 68
B. Possible Modifications of Theoretical Expectations for Real Aggregates Suggested by the Experimental Data 73
B-1. Close and near contacts in aggregates of spherical particles 73
B-2. Particle size 92
B-3. Particle shape 94
B-4. Plastic deformation at contacts 97
B-5. Friction, lubrication, and Q^{-1} 101

V. COMPRESSION TESTS 104

A. Specimen Preparation and Experimental Method .104
B. Specimen Deformation 105
C. Unloading-Reloading Cycles 109

VI. LUNAR SEISMIC OBSERVATIONS 115

REFERENCES 119

Reproduced with permission of the copyright owner. Further reproduction prohibited without permission.

LIST OF TABLES

Table		Page
1.	Some Physical Properties of the Liquid lubricants	59
2.	Physical Properties of Some of the Granular Materials Studied	60
3.	Results of the Acoustic Experiments on Granular Aggregates	66
4.	Calculated Regular Array Velocities	69
5.	Experimentally Observed Velocities and Dependences	70
6.	Comparison of Predicted and Observed Dependences for Q^{-1}	71
7.	Comparison of Calculated and Observed Values of Q^{-1}	71
8.	Estimates of $dn'/d\alpha$	88
9.	Some Results of the Compression Tests	108

Reproduced with permission of the copyright owner. Further reproduction prohibited without permission.

LIST OF ILLUSTRATIONS

Figure		Page
1.	Traction Distribution over the Contact Surface between Two Like Spheres	124
2.	Tangential Force-Displacement Relation for Two Like Spheres under a Monotonically Increasing Tangential Force	125
3.	Ratio of "No-Slip" Tangential Compliance to "Slip" Compliance	126
4.	Tangential Force-Displacement Curve for Two Like Spheres Subjected to an Oscillating Tangential Force	126
5.	Rate of Energy Dissipation Versus Maximum Tangential Force Amplitude	127
6.	Comparison of Theoretical and Experimental Tangential Force-Displacement Relations for Circular Steel Contacts	128
7.	Comparison of Theoretical and Experimental Energy Dissipation for Circular Steel Contacts	129
8.	Comparison of Theoretical and Experimental Energy Dissipation for Circular Glass Contacts	130
9.	Force-Displacement Curve for a Block and Spring System	131
10.	White's Modified Tangential Force-Displacement Curve for Two Like Spheres	131

Reproduced with permission of the copyright owner. Further reproduction prohibited without permission.

Figure		Page
11.	Diagrammatic Sketch of Acoustic Experimental Setup	132
12.	Curves of Resonance Frequency Versus Confining Pressure for Clean Aggregates	133
13.	Curves of Resonance Frequency Versus Confining Pressure for Lubricated Aggregates	134
14.	Q^{-1} Versus Frequency	135
15.	Curves of Q^{-1} Versus Confining Pressure for Clean Aggregates	136
16.	Example of Q^{-1} Hysteresis with Pressure Cycling	137
17.	Comparison of Velocity and Q^{-1} Measurements as a Function of Confining Pressure for Lubricated Glass Beads	138
18.	Comparison of Velocity and Q^{-1} Measurements as a Function of Confining Pressure for Lubricated Alundum	139
19.	Velocity Versus Grain Size for Clean Glass Beads	140
20.	Q^{-1} Versus Weight Percent Lubricant	141
21.	Missing Contact Model	142
22.	Mohr Circle Diagrams for Lubricated Glass Beads	143
23.	Examples of Load-Displacement Hysteresis Curves Obtained in Compression Testing	144
24.	Area of Hysteresis Loop Versus Displacement Amplitude of Loop for Clean Alundum	145

Reproduced with permission of the copyright owner. Further reproduction prohibited without permission.

INTRODUCTION

Unconsolidated aggregates occur in several geologic settings of interest. Examples are marine sediments and beach sands, lunar surface soils, and, if the fluid pressure should be about equal to the overload pressure, partial melts in the earth at depth. The properties of such aggregates are not well known. When studying the behavior of a complex system, it is important to know what factors can contribute to the behavior in order to permit the extrapolation of the observed properties to other conditions. At low net pressures, the bulk dynamic properties of aggregates are determined in large part by the interparticle contact properties. The contact properties, in turn, are governed by the bulk material properties, the nature of the interparticle surfaces, the geometry of both particles and aggregate, the properties of whatever fluids are present, and by external conditions, such as pressure. A set of relations, collectively called contact theory, have been used to describe the dynamic behavior of pairs and regular arrays of uniform spheres in elastic contact. It was the purpose of

Reproduced with permission of the copyright owner. Further reproduction prohibited without permission.

the work reported here to compare the predictions of contact theory with experimental studies on irregularly packed aggregates of various types of particles.

In the first chapter the basic equations of contact theory for pairs and regular arrays of spheres in elastic contact are presented and discussed with regard to relevant experimental work done by other investigators. The chapter closes with a discussion of those properties of naturally occurring aggregates most likely to give rise to deviations from the theoretically expected behavior that might be inferred from the analysis of idealized regular arrays of spherical particles. In chapters II and III the experimental procedure used in this study of the acoustic properties of irregularly packed aggregates is described and a brief resume of the results of the study is given. Chapter IV discusses the acoustic results in more detail, using comparison of the results with theoretical relations to generate suggestions for general modifications of the theoretical expectations. Chapter V describes a series of quasi-static tests, performed on the same specimens used in the acoustic experiments, for the purpose of comparing dynamic behavior under high stress or strain amplitudes with the low amplitude acoustic results. In the last chapter the acoustic experimental results are applied to the interpretation of lunar seismic observations.

Reproduced with permission of the copyright owner. Further reproduction prohibited without permission.

ACKNOWLEDGMENTS

I wish to thank R. B. Gordon for his support and for his helpful comments on this work. I am especially grateful to J. R. Vaišnys for supervising this work and making countless sound criticisms and good suggestions, for being both tolerant and encouraging over many years, and for setting an excellent example as a scientist. Funds for this work were supplied by the Earth Science Division of the Office of Naval Research.

Reproduced with permission of the copyright owner. Further reproduction prohibited without permission.

I. GRANULAR AGGREGATES: THEORETICAL AND EXPERIMENTAL BACKGROUND

The following discussion deals first with the theoretical framework, and associated experiments, relevant to the mechanical description of pairs and regular arrays of spheres in elastic contact. The last part of the chapter is a survey of some of the properties of more complex granular aggregates and the difficulties involved in applying the theory to such aggregates.

A. Two Spheres in Elastic Contact

A-1. Contact theory

The mechanical properties of an assemblage of discrete particles in elastic contact are primarily determined by the behavior of the intergranular contacts within the constraints of the geometry of the system. Contact theory comprises the set of relations describing the deformation of such contacts under various applied forces. A detailed review of the theory and related experiments is given by Deresiewicz (1958a) and a brief review by White (1965).

Reproduced with permission of the copyright owner. Further reproduction prohibited without permission.

(a) Normal forces

If two elastic spheres of radii R_1 and R_2 are pressed together by a normal force N, an analysis by Hertz (Timoshenko and Goodier, 1951) predicts a plane circular area of contact of radius b given by

$$b = \left[(k_1 + k_2)\, N R_{12}\right]^{1/3}, \tag{1}$$

where $\frac{1}{R_{12}} = \frac{1}{2}\left(\frac{1}{R_1} + \frac{1}{R_2}\right)$, $k_1 = \frac{3(1-\nu_1^2)}{8E_1}$, and $k_2 = \frac{3(1-\nu_2^2)}{8E_2}$. The constants ν and E are, respectively Poisson's ratio and Young's modulus of the spheres. Equation (1) is based on the assumption that $b \ll R_1, R_2$ and that k_1 and k_2 are not so different that warping of the contact surface occurs. For two identical spheres equation (1) becomes

$$b = \left[\frac{3}{4}\frac{(1-\nu^2)\, N R}{E}\right]^{1/3}. \tag{2}$$

The hemispherical normal traction distribution over the contact surface described by equation (2) is given by

$$\sigma = \frac{3}{2}\frac{N}{\pi b^3}\left(b^2 - \rho^2\right)^{1/2}, \tag{3}$$

where ρ is the radial distance from the center of the contact circle (figure 1). The approach of the sphere centers is

$$\alpha = \frac{2b^2}{R} = \left[\frac{3(1-\nu^2)\, N}{\sqrt{2R'}\, E}\right]^{2/3}, \tag{4}$$

Reproduced with permission of the copyright owner. Further reproduction prohibited without permission.

and, hence, the normal compliance is

$$C_N = \frac{d\alpha}{dN} = \frac{1-\nu^2}{Eb} \quad . \tag{5}$$

These expressions and the assumptions underlying them are the foundation for the more complicated relations involving tangential components of static and oscillating forces. The requirement $b \ll R$ places an upper limit on the range of loads over which the Hertzian theory is applicable. Under very light loads the Hertzian relations may not apply to real spheres in contact simply because effects due to the roughness of their surfaces are predominant (Greenwood and Tripp, 1967).

(b) Tangential forces

Mindlin (1949) extended the Hertzian analysis to include tangential components of force. Consider a tangential force T applied across the contact surface of two identical spheres under normal load N. Mindlin showed that, for the case where there is no slip on the contact surface, the contact circle of radius b (equation 2) will move in the direction of T without change of shape or size. The relative displacement of the sphere centers is given by

$$\delta = \frac{(2-\nu)(1+\nu)}{2Eb} T, \tag{6}$$

Reproduced with permission of the copyright owner. Further reproduction prohibited without permission.

and the tangential compliance by

$$C_T = \frac{d\delta}{dT} = \frac{(2-\nu)(1+\nu)}{2Eb} . \qquad (7)$$

The distribution of tangential traction τ over the contact surface is shown in figure 1. From figure 1 it is seen that the solution to the elastic, or no slip, problem yields infinite tractions at the edge of the contact circle. In order to relieve these tractions Mindlin proposed that slip occurs over an annulus, beginning at the edge of the contact circle and progressing concentrically, radially inward. As slip occurs, the adhered portion of the surface within the annulus of slip is subjected to a change of traction and undergoes rigid-body or uniform tangential displacement, resulting in the relative displacement of the sphere centers. The basic assumption is that τ cannot anywhere exceed $\mu\sigma$, where μ is a limiting coefficient of friction; thus, over the adhered central portion, $\tau \leq \mu\sigma$, and over the annulus of slip, $\tau = \mu\sigma$ and has the same sense as the slip. The resulting distribution of traction is shown in figure 1. The inner radius of the annulus of slip is given by

$$c = b\left(1 - T/\mu N\right)^{1/3}, \qquad (8)$$

the relative displacement of the sphere centers by

$$\delta = \frac{3(2-\nu)(1+\nu)}{2Eb}\mu N\left[1-\left(1-T/\mu N\right)^{\frac{2}{3}}\right], \qquad (9)$$

Reproduced with permission of the copyright owner. Further reproduction prohibited without permission.

and the tangential compliance by

$$C_T = \frac{d\delta}{dT} = \frac{(2-\nu)(1+\nu)}{2Eb}\left(1-T/\mu N\right)^{-\frac{1}{3}} = \frac{(2-\nu)(1-\nu)}{2Ec} . \qquad (10)$$

Curves of a dimensionless form of the relative displacement versus T/N are shown in figure 2 for several values of μ. When $T=\mu N$, free sliding or gross slip takes place; when $T=0$, equation (10) becomes equation (7), the initial compliance. The ratio of the "slip" to "no-slip" compliance is $(1-T/\mu N)^{-\frac{1}{3}}$, and figure 3 shows the range over which the initial compliance is a useful approximation. With the inclusion of slip, both normal and tangential compliances are non-linear. In addition, the tangential force-displacement relation is inelastic, energy being dissipated during slip.

The effects of a small oscillating tangential force were examined by Mindlin and coworkers (1951). Suppose that the tangential force T on two spheres under load N is monotonically increased to a maximum value T*, where $T^*<\mu N$. The depth of slip and the relative displacement are given by equations (8) and (9) with T replaced by T*. A reduction in T will give rise to infinite tractions at the boundary of the contact, and hence slip must begin again at the edge of the contact, progressing now in a direction opposite to that for increasing T. The change of traction over the slipped region, due to the reversal of T, is -2μ , and this change

Reproduced with permission of the copyright owner. Further reproduction prohibited without permission.

produces uniform tangential displacement in the adhered region. For T decreasing from T*, the force-displacement relation is

$$\delta = \frac{3(2-\nu)(1+\nu)\mu N}{4Eb}\left[2\left(1-\frac{T^*-T}{2\mu N}\right)^{2/3}-\left(1-\frac{T^*}{\mu N}\right)^{2/3}-1\right], \qquad (11a)$$

and the inner radius of the annulus of counterslip is

$$c = b\left(1-\frac{T^*-T}{2\mu N}\right)^{1/3}. \qquad (11b)$$

From equation (11b) it is seen that there is a permanent set at T = 0. At T = -T* the slip has been completely reversed, and the situation is identical to that at T = T* except for sign reversal. For T increasing from -T*, the relations are

$$\delta = -\frac{3(2-\nu)(1+\nu)\mu N}{4Eb}\left[2\left(1-\frac{T+T^*}{2\mu N}\right)^{2/3}-\left(1-\frac{T^*}{\mu N}\right)^{2/3}-1\right] \qquad (12a)$$

and

$$c = b\left(1+\frac{T^*+T}{2\mu N}\right)^{1/3}. \qquad (12b)$$

The force-displacement curve over a cycle is shown in figure 4. The area enclosed by the loop gives the energy lost per cycle:

$$\Delta W = \frac{18(2-\nu)(1+\nu)\mu^2 N^2}{5Eb}\left\{1-\left(1-\frac{T^*}{\mu N}\right)^{5/3}-\frac{5T^*}{6N}\left[1+\left(1-\frac{T^*}{\mu N}\right)^{2/3}\right]\right\}. \qquad (13)$$

Curves of a dimensionless form of the energy dissipated per cycle versus T*/μN are plotted in figure 5 for several values of μ. For small values of T*/μN, equation (13) becomes

Reproduced with permission of the copyright owner. Further reproduction prohibited without permission.

$$\Delta W = \frac{(2-\nu)(1+\nu)T^{*3}}{9Eb\mu N}. \tag{14}$$

Since for small $T^*/\mu N$ the elastic force-displacement relations can be approximated by equation (6), the maximum elastic energy stored during a cycle is approximately

$$W = \int_0^{T^*} C_T T\,dT = \frac{(2-\nu)(1+\nu)}{4Eb} T^{*2}. \tag{15}$$

The fractional energy loss per cycle is then, for small $T^*/\mu N$,

$$\frac{\Delta W}{W} = \frac{4}{9}\frac{T^*}{\mu N}, \tag{16}$$

or in terms of displacement,

$$\frac{\Delta W}{W} = \frac{8Eb\delta^*}{9(2-\nu)(1+\nu)\mu N}. \tag{17}$$

(c) Oblique forces

The next step in complexity is to consider the effects of an oscillating oblique force applied to the contact surface. This was done by Mindlin and Deresiewicz (1953). At this point, it should be noted that with the introduction of slip and its associated permanent set the tangential displacements and tractions became dependent upon the loading history. An additional complication with oblique forces is that the displacements and tractions are also dependent upon the instantaneous relative rates of change of the normal and tangential components of force. A special, but useful, case

Reproduced with permission of the copyright owner. Further reproduction prohibited without permission.

is the following. Consider two spheres compressed by an initial load N_o resulting in a contact area of radius b_o. Now apply an oblique force F_{oB} such that its normal and tangential components, N and T, maintain a constant ratio while oscillating between maximum and minimum values. If N is denoted by $F_{oB}\cos\phi$ and T by $F_{oB}\sin\phi$, where ϕ is the angle between the normal to the contact surface and the force F_{oB}, the ratio of T to N is given by $\tan\phi$. Mindlin and Deresiewicz showed that if $\tan\phi \leq \mu$, the tangential traction τ on the contact surface is always less than $\mu\sigma$, and hence no slip occurs and no energy is dissipated. If $\tan\phi > \mu$, a hysteresis loop results, which stabilizes after three-quarters of a cycle. The tangential displacement during loading in the stabilized cycle is

$$\delta = \frac{b_o^2 \mu (2-\nu)}{2(1-\nu)} \left\{ (1+\theta L)^{2/3} + \left[1-(1+\theta)L^*\right]^{2/3} - 2\left[1-\frac{\theta}{2}(L^*-L)-\frac{1}{2}(L^*+L)\right]^{2/3} \right\}, \quad (18)$$

where $L = T/\mu N_o$, $L^* = T^*/\mu N_o$, and $\theta = \mu/\tan\phi$, $\tan\phi \geq \mu$. The unloading curve is obtained by reversing the signs of and L. For both loading and unloading, the normal component N will increase and decrease the contact area and the distance between sphere centers according to the Hertzian equations (2) and (4). The energy dissipation per cycle, obtained from the area of the hysteresis loop, is given by

Reproduced with permission of the copyright owner. Further reproduction prohibited without permission.

$$\Delta W = \frac{18(2-\nu)(1+\nu)\mu^2 N_o^2}{5Eb_o}\left\{\frac{1}{4\theta}\left[\frac{1+\theta}{1-\theta}\left(1-\theta L^*\right)^{5/3}-\frac{1-\theta}{1+\theta}\left(1+\theta L^*\right)^{5/3}\right]-\frac{1}{1-\theta^2}\left(1-\frac{1+5\theta^2}{6}L^*\right)\left(1-L^*\right)^{2/3}\right\}. \quad (19)$$

For small values of L*, equation (19) becomes

$$\Delta W = \frac{(2-\nu)(1+\nu)T^{*3}}{9Eb_o\mu N_o}\left(1-\theta^2\right). \quad (20)$$

Using the initial tangential force-displacement relation, equation (6), the maximum elastic energy stored per cycle, for small L*, calculated from the expression $dW = Nd\alpha + Td\delta$ is $W = \frac{(1+\nu)}{4Eb_o}\left[6(1-\nu)N^{*2}+(2-\nu)T^{*2}\right]$. The fractional energy loss per cycle, then, for $L^* \ll 1$ is, in terms of the maximum oblique force, F_{OB}^*,

$$\frac{\Delta W}{W} = \frac{4F_{OB}^*}{9\mu N_o}\left[\frac{(2-\nu)(\sin^3\phi)(1-\tan^2\phi)}{6(1-\nu)\cos^2\phi+(2-\nu)\sin^2\phi}\right]. \quad (21)$$

The force-displacement relations for two spheres in contact may be extended to irregularly shaped particles if the surface adjacent to the contact can be described as a surface of the second-degree. General expressions for the normal compliance have been derived by Hertz (Timoshenko and Goodier, 1951) and for the tangential compliance by Mindlin (1949) and Cattaneo (1938). The treatment is similar to that for two spheres, and the results are basically the same, although much more geometrically complicated. For spheres of different radii and/or elastic constants, the

Reproduced with permission of the copyright owner. Further reproduction prohibited without permission.

simple replacements indicated in section A-1 may be made in the above equations.

A-2. Experimental investigations on single contacts

Experimental support for the theoretical work of Mindlin and coworkers has been provided by Johnson (1955). He investigated the microdisplacements resulting from steady and oscillating tangential forces acting on the contact of a steel ball and a flat steel surface. Normal loads on the ball ranged from 4 to 20 pounds, and the ball diameter was varied from 0.188 to 1.565 inches ($\frac{b}{R} \approx 7 \times 10^{-3}$ to 5×10^{-2}). For all cases studied interfacial slip occurred, and the displacements as a function of tangential force closely followed equation (9) (see figure 6). Also, the areas of the annuli of slip, as indicated by fretting of the contact surfaces, were in reasonable agreement with Mindlin's theory. Energy losses were obtained from static hysteresis curves and from the decay of free vibrations (about 46 Hz). At small amplitudes of tangential force, $T \leq 1/5$ N, the energy dissipation per cycle was approximately $\frac{0.04(1+\nu)T^{*2}}{Eb}$ and, hence, varied with the square rather than the cube of the amplitude as predicted by equation (14). The fractional energy loss per cycle was constant (approximately 0.09), i.e., independent of tangential force amplitude or displacement,

Reproduced with permission of the copyright owner. Further reproduction prohibited without permission.

normal load, and ball size. At higher amplitudes there was satisfactory agreement between the measured values of energy loss per cycle and the theoretical predictions.

Goodman and Brown (1962) made similar tests on steel balls, varying in diameter from 1/4 to 3/4 inches, for a range of normal loads from 0.154 to 1.25 pounds. The balls were held between two steel plates and subjected to oscillations (60 Hz) parallel to the plates. The experiments covered the range of displacement amplitudes $0.45 < \delta^*/\delta_{max} < 1$, where δ_{max} is the displacement corresponding to gross slip. Within this range, the shapes of the experimental hysteresis curves agreed well with theoretical loops. Curves of a dimensionless form of the energy dissipation, $\Delta W/T_{max}\,\delta_{max}$ ($T_{max} = \mu N$), versus δ^*/δ_{max} compared satisfactorily with theoretical predictions (figure 7).

In a later paper Johnson (1961) studied the effects of an oscillating oblique force on the contact of a steel ball and flat. His experiments showed that energy dissipation varied with the angle of obliquity ϕ of the oscillating force, agreeing well with tne theoretical curves at high amplitudes of force. For $\tan\phi < \mu$ ($\phi < 29^\circ$), the energy dissipation differed very little from the small constant loss at $\phi = 0^\circ$. Since there is no tangential force at $\phi = 0^\circ$, there should be no energy dissipation due to slip. Johnson

Reproduced with permission of the copyright owner. Further reproduction prohibited without permission.

therefore suggested that this loss was a result of internal hysteresis in the steel. Such internal material losses could explain the constant Q^{-1} at small amplitudes of oscillating force, regardless of the angle of obliquity. However, some fretting damage to the surface of contact was observable even at $\phi = 10^{o}$, indicating some slip.

Mindlin, Mason, and coworkers (1951) looked at the contact of crown glass lenses under oscillating tangential forces. Comparison of the dimensions of the annuli of slip as a function of load agreed well with theoretical predictions. Fretting of the surfaces was not as obvious as with the steel balls, about half of the runs showing no surface damage after many hours of oscillation. Over the range of displacements investigated, the measured energy dissipation per cycle varied approximately as the square of the displacements rather than the cube, i.e., $\frac{\Delta W}{W}$ was independent of amplitude. At large displacements, nearing gross slip, the measured values approached the theoretical values (figure 8). Dissipation was significantly higher than predicted by theory and not explainable in terms of internal material losses.

In summary, the predictions of theory regarding compliances and areas of contact are substantiated by experimental investigations. Energy dissipation measurements on steel agree well with theoretical expectations except at very low

Reproduced with permission of the copyright owner. Further reproduction prohibited without permission.

amplitudes of force or displacement. For glass, the discrepancy between experiment and theory for the energy dissipation extends to higher amplitudes. This difference in the behavior of steel and glass may give some clue as to the dissipative mechanism characterized by constant values of fractional energy loss.

A-3. Alternative mechanism for energy dissipation at contacts

To account for the discrepancies between calculated and measured energy losses at small displacements, White (1965, 1966) suggested that the preceding theory might be modified by including the difference between the static and kinetic coefficients of friction, μ_s and μ_k. Static friction is generally higher than kinetic friction, even for lubricated surfaces. The difference between the two coefficients often results in "stick-slip" during sliding when the sliding motion is reasonably slow and one of the surfaces has some degree of elastic freedom. In the theory discussed above, the limiting coefficient of friction, μ, is defined as that value of the ratio T/N at which gross sliding occurs. White interprets this μ as μ_k and then proceeds to show that the inclusion of μ_s in the theory results in additional energy losses.

Reproduced with permission of the copyright owner. Further reproduction prohibited without permission.

The model proposed by White is based on a block and spring system with the block sliding on a flat surface. Displacement of the end of the spring will result in a force-displacement diagram like the one shown in figure 9. Initially only the spring is displaced. At point A the force exerted by the spring on the block is equal to the normal force F_N on the block times the static coefficient of friction μ_s, and the block begins to slide, at which point the acting coefficient of friction becomes μ_k. The block then slides under a constant force equal to $F_N\mu_k$ until the displacement is reversed at B. The total energy input to the system during the displacement cycle is proportional to the area enclosed by the loop ABCD. The extra energy expended against static friction is given by the area under the shaded triangles. For one triangle the area is

$$\Delta W' = \frac{F_N}{2S}\left(\frac{\mu_s - \mu_k}{\mu_k}\right)^2, \tag{22}$$

where S is the spring modulus. Note that if the block just barely begins to slide before the displacement is reversed, the energy dissipation represented by the shaded triangles will be the majority of the energy lost during the cycle.

Now consider the contact surface of two spheres under a normal force N and acted upon by a tangential force. Each increment in the annulus of slip discussed previously may be

Reproduced with permission of the copyright owner. Further reproduction prohibited without permission.

thought of as analogous to a spring and block system. Suppose that slip has progressed inward to radius c, where c is given by equation (8). The normal force F_N over the increment of annulus just inside c that is about to slip is given by

$$F_N = \sigma(c)2\pi c\Delta c = \frac{3N}{2\pi b^2}\left(1-\frac{c^2}{b^2}\right)^{1/2} 2\pi c\,\Delta c .$$

The spring stiffness S (reciprocal of the compliance) of the annulus element Δc is equal to the decrease of stiffness that occurs when Δc breaks loose and slides and is (see equation 10):

$$S = \frac{2E\,\Delta c}{(2-\nu)(1+\nu)} .$$

Putting S and F_n into equation (22) yields the extra energy dissipated in "unsticking" the annulus increment Δc:

$$\Delta W' = \frac{18N^2(2-\nu)(1+\nu)(\mu_s-\mu_k)^2c^2(1-c^2/b^2)\,\Delta c}{8Eb^4} . \qquad (23)$$

Then, since the slipping of Δc results in an increment of displacement between the sphere centers, $\Delta\delta = 3(2-\nu)(1+\nu)\mu_k N c\Delta c/2Eb^3$, which follows from equation (8) and (9), equation (23) may be rewritten as

$$\Delta W' = \left(\frac{\mu_s-\mu_k}{\mu_k}\right)^2 \frac{2Ec}{(2-\nu)(1+\nu)}\delta\Delta\delta = T'\Delta\delta , \qquad (24)$$

where T' is the extra force due to static friction. It will

Reproduced with permission of the copyright owner. Further reproduction prohibited without permission.

now be assumed that $T/\mu_k N$ is so small that the energy loss due to slip, that is, the loss calculated from equation (14), is negligible compared to losses due to "sticking." In other words, the tangential force amplitude is small, slip does not penetrate very far, and the force-displacement curve over a cycle (figure 4) can be approximated by a straight line. With this assumption, c may be replaced by b, the initial contact radius, and T' may be added to T, as given by equation (6), to yield the total force-displacement relations. The curve obtained for oscillatory motion between δ^* and $-\delta^*$ is shown in figure 10. From the area enclosed, the energy loss per cycle is

$$\Delta W = \frac{8 E b \delta^{*2}}{(1+\nu)(2-\nu)} \left(\frac{\mu_s - \mu_k}{\mu_k} \right)^2. \tag{25}$$

The maximum elastic energy stored per cycle, W, is given by equation (15), and the fractional energy loss per cycle is

$$\frac{\Delta W}{W} = 8 \left(\frac{\mu_s - \mu_k}{\mu_k} \right)^2. \tag{26}$$

For an oblique force acting on the contact, the maximum displacement in equation (25) will be the tangential component of displacement only, while the energy stored will be a function of both normal and tangential components of displacement.

Reproduced with permission of the copyright owner. Further reproduction prohibited without permission.

Note that the fractional energy loss per cycle is independent of normal load, displacement or force amplitude, and sphere radius, in agreement with the experimental single contact data for small displacements discussed earlier. Numerically, equation (26) fits Johnson's values for steel balls (1955) if $\mu_s \approx 1.1\,\mu_k$ for steel.

B. Regular Arrays of Spheres

B-1. Stress-strain relations

Stress-strain relations including the effects of both normal and tangential components of contact forces have been derived for several cases of regularly packed spheres (Duffy and Mindlin, 1957; Deresiewicz, 1958b; Duffy, 1959; and Thurston and Deresiewicz, 1959). Since These relations are dependent on the loading history, they must be given in differential or incremental form, and a total stress-strain law for any particular case involves integration over the whole loading history.

The differential relations are obtained from the requirements of equilibrium of forces and compatibility of displacements. For each packing a volume element representative of the geometry of the packing is chosen. This unit volume is preloaded by an average isotropic stress or confining pressure, P_o, resulting in uniform contact forces

Reproduced with permission of the copyright owner. Further reproduction prohibited without permission.

$N_o \propto R^2 p_o$, and the loading history to this point is restricted to variations in P_o. An arbitrary increment of traction is then applied to the faces of the unit volume, and, from equilibrium and symmetry considerations, a set of equations is derived relating the increments in contact forces to the increment of applied force. Displacement compatibility requirements give a second set of relations relating relative incremental displacements of sphere centers, or equivalently, contact force increments and compliances, to the deformation of the unit volume. Solution of these two sets of equations yields differential stress-strain (σ-ε) relations of the usual form,

$$d\sigma_{ij} = C_{ijkl}\, d\varepsilon_{kl}\,, \tag{27}$$

where the indices can be x, y, or z and double indices indicate summation. The elastic coefficients C_{ijkl} are combinations of the reciprocal compliances and are dependent on the loading history.

B-2. Wave propagation

For small variations of stress compared to the initial state, the differential or incremental form of the relations may be used directly. Furthermore, the contact compliances may be taken as constants; that is, the initial values corresponding to the isotropic average stress p_o may be used.

Reproduced with permission of the copyright owner. Further reproduction prohibited without permission.

The elastic coefficients are then of the form $K\left[\frac{3E^2p_o}{8(1-\nu^2)^2}\right]^{1/3}$, where K is a constant for each coefficient depending on the array geometry and on Poisson's ratio ν of the spheres. For any particular packing, K will depend on the orientation of the array with respect to the direction of wave propagation. Assuming small amplitude disturbances, equations (27) may be inserted directly in the equations of motion,

$$\frac{\partial \sigma_{ij}}{\partial x_j} = \bar{\rho}\frac{\partial^2 u_i}{\partial t^2}, \tag{28}$$

where $\bar{\rho}$ is the bulk density and u_i are the components of displacement (recall that $\varepsilon_{ij} = \frac{1}{2}\left(\frac{du_i}{dx_j} + \frac{du_j}{dx_i}\right)$). Solution of these equations for the appropriate conditions yields the various wave velocities, V, as the square root of some combination of the elastic coefficients divided by the bulk density, i.e.,

$$\bar{\rho}V^2 = K\left[\frac{3E^2p_o}{8(1-\nu^2)^2}\right]^{1/3}. \tag{29}$$

Note that all velocities will depend on the one-sixth power of the initial stress or confining pressure, p_o. As a specific example for later reference, extensional or bar velocity along an axis in a face-centered cubic array is given by

$$\bar{\rho}_{fcc}V_{fcc}^2 = \bar{E}_{fcc} = \frac{2(8-7\nu)}{(8-5\nu)}\left[\frac{3E^2p_o}{8(1-\nu^2)^2}\right]^{1/3}, \tag{30}$$

where $\bar{\rho}_{fcc} = (\pi/3\sqrt{2})\rho$ and ρ is the solid material density (Duffy and Mindlin, 1957). $\bar{E}_{fcc}$ is the bulk elastic modulus

Reproduced with permission of the copyright owner. Further reproduction prohibited without permission.

equivalent to the Young's modulus of a continuous system. Along an axis in a simple cubic array the extensional velocity is given by

$$\bar{\rho}_{sc} V_{sc}^2 = \bar{E}_{sc} = \left[\frac{3 E^2 p_o}{8(1-\nu^2)^2}\right]^{1/3}, \tag{31}$$

where $\bar{\rho} = (\pi/6)\rho$ (White, 1965).

The energy dissipation accompanying the small variations of stress during wave propagation may be calculated from either Mindlin's or White's expressions. Once the displacement is specified with respect to the geometry of the array, the dissipation at all contacts may be summed to give the total dissipation for the array. To look at the general form of fractional energy loss expected with either Mindlin's or White's type of dissipation, an example of a granular bar in longitudinal resonance will be examined. The bar is taken to be rectangular, with length ℓ, and composed of uniform spheres of radius R packed in a regular array. The dimensions of the bar are assumed to be much greater than the radius of the spheres and the wavelength of vibration to be large compared with the lateral dimensions of the bar. The array is held together by an isotropic confining pressure p_o. To excite longitudinal vibrations a uniaxial increment of stress, $\sigma(x,t) \ll p_o$, is applied to one end of the bar, and the resulting stress-strain relation is of the form

Reproduced with permission of the copyright owner. Further reproduction prohibited without permission.

$$\sigma(x,t) = K\left[\frac{3E^2 p_o}{8(1-\nu^2)^2}\right]^{1/3} \varepsilon(x,t),$$

where the differential notation has been dropped for convenience. During resonance the displacement along the bar (ends free) is given by

$$u(x,t) = A \sin n\pi\omega t \cos \frac{n\pi x}{\ell},$$

where A is the maximum amplitude of displacement, n is the number of half-wavelengths in the bar, and ω is the frequency of vibration in radians/sec. Consider now an element of volume, Δv, located at some x, $0 \leq x \leq \ell$, representative of the array and containing contacts j = 1...m. At any contact within Δv the maximum tangential component of the increment of contact force corresponding to the increment of stress is of the form

$$T_j^*(x) = k_j R^2 \sigma^*(x),$$

where k_j is a constant for each contact whose value is a function of the geometry and orientation of the array and of Poisson's ratio ν of the spheres. Noting that $\varepsilon^*(x) = \frac{\partial u^*(x)}{\partial x}$, the maximum absolute stress, $\sigma^*(x)$, expressed in terms of the displacement is

$$\sigma^*(x) = K\left[\frac{3E^2 p_o}{8(1-\nu^2)^2}\right]^{1/3} A \frac{n\pi}{\ell} \sin \frac{n\pi x}{\ell}.$$

Looking first at the dissipation due to slip (Mindlin), $T_j^*(x)$ is cubed and summed over the m contacts in ΔV yielding

Reproduced with permission of the copyright owner. Further reproduction prohibited without permission.

$$\sum_{j=1}^{m} T_j^{*3}(x) = \left[\frac{3E^2 p_o}{8(1-\nu^2)^2}\right] R^6 \left(KA\frac{n\pi}{\ell}\sin\frac{n\pi x}{\ell}\right)^3 \sum_{j=1}^{m} k_j^3 .$$

As given by equation (20) the rate of energy dissipation in Δv per unit volume is of the form (recall that $N_o \propto R^2 p_o$ and $\Delta V \propto R^3$)

$$\Delta W' = \frac{\bar{K} E^{4/3}}{\mu p_o^{1/3}} \left(\frac{An\pi}{\ell}\sin\frac{n\pi x}{\ell}\right)^3 (a-\mu^2),$$

where $\bar{K}$ and a have replaced all constants depending on geometry, orientation, and ν. To obtain the rate of dissipation for the bar, $\Delta W'$ is multiplied by $dV = Sdx$, where S is the cross-sectional area of the bar, and integrated over the length of the bar to yield

$$\Delta W = \frac{4\bar{K} E^{4/3}}{3\mu p_o^{1/3}} \left(\frac{SA^3 n^3 \pi^2}{\ell^2}\right)(a-\mu^2).$$

The maximum elastic energy per cycle per unit volume stored in the bar may be calculated from the relation

$$dW = \sigma^*(x)\, d\varepsilon^*(x)$$

and is

$$W' = \frac{K}{2}\left[\frac{3E^2 p_o}{8(1-\nu^2)^2}\right]^{1/3} \varepsilon^{*2}(x),$$

or, in terms of displacement,

$$W' = \frac{K}{2}\left[\frac{3E^2 p_o}{8(1-\nu^2)^2}\right]^{1/3} \left(A\frac{n\pi}{\ell}\sin\frac{n\pi x}{\ell}\right)^2 .$$

The total energy stored per cycle is given by

Reproduced with permission of the copyright owner. Further reproduction prohibited without permission.

$$W = \int_0^{\ell} W' S \, dx$$

and is

$$W = \frac{K}{4}\left[\frac{3E^2 p_o}{8(1-\nu^2)^2}\right]^{1/3} S A^2 \frac{n^2\pi^2}{\ell} = \frac{1}{4}\bar{\rho} V^2 S A^2 \frac{n^2\pi^2}{\ell}. \qquad (32)$$

The fractional energy loss per cycle is

$$\frac{\Delta W}{W} = K'\left(\frac{E}{p_o}\right)^{2/3}\left(\frac{nA}{2\ell}\right)\left(\frac{a-\mu^2}{\mu}\right), \qquad (33)$$

where K' is another constant depending on array geometry and orientation and on ν. Thus $\frac{\Delta W}{W}$ is inversely proportional to $p_o^{2/3}$ and to wavelength, $\frac{2\ell}{n}$, and directly proportional to wave amplitude, A.

White's expression for the rate of energy loss per cycle for two spheres in contact may be written as

$$\Delta W = \frac{8 E b_o}{(2-\nu)(1+\nu)}\left(\frac{\mu_s - \mu_k}{\mu_k}\right)^2 T^{*2}(1-\theta^2)$$

or

$$\Delta W = \frac{2(2-\nu)(1+\nu)}{E b_o}\left(\frac{\mu_s - \mu_k}{\mu_k}\right)^2 T^{*2}(1-\theta^2).$$

The term $(1-\theta^2)$ has been added to White's formulation to account for oblique forces at contacts as discussed in section A-1 (see equation [18]), and the limiting coefficient μ in this term has been interpreted as μ_s. Proceeding in the same fashion as before, the energy dissipated in ΔV per cycle per unit volume is

Reproduced with permission of the copyright owner. Further reproduction prohibited without permission.

$$\Delta W' = K'' W' (a - \mu_s^2) \left(\frac{\mu_s - \mu_k}{\mu_k}\right)^2,$$

where K'' is a constant whose value depends on the array geometry and orientation and on ν. The fractional energy loss per cycle for the bar is

$$\frac{\Delta W}{W} = K'' \left(\frac{\mu_s - \mu_k}{\mu_k}\right)^2 (a - \mu_s^2). \qquad (34)$$

Note that $\frac{\Delta W}{W}$ is a constant once the difference between μ_s and μ_k is specified.

B-3. Experimental investigations

Experiments have been performed on granular bars to test the differential stress-strain relations. Duffy and Mindlin (1957) determined wave velocities and accompanying rates of energy dissipation in bars composed of a face-centered array of 1/8 inch diameter steel bearing balls. Duffy (1959) measured velocities of granular bars of similar steel balls arranged in hexagonal close packing. The balls were held rigid in a rubber container by drawing a vacuum inside the container. Confining pressure p_o was varied from 0 to about 1 bar. Resonance tests were used to determine extensional velocities for two modes of vibration, and energy dissipation was found from the decay of free vibrations. Velocity increased with the 1/6 power of pressure from about 0.7 bar to 1 bar; at lower pressures the variation was more rapid, going as the 1/3 to 1/4 power. Measured velocity was

Reproduced with permission of the copyright owner. Further reproduction prohibited without permission.

lower than theory predicted, presumably because some contacts were not made. Balls of two dimensional tolerances were used, $\pm$ 50 X 10^{-6} inches and $\pm$ 10 X 10^{-6} inches. Velocities for the higher tolerance balls approached theoretical prediction somewhat better and showed more change in slope with pressure, probably because more contacts were made than with the poorer tolerance balls. The number of contacts in the array of higher tolerance balls was probably closer to the theoretically expected number for an array of perfectly smooth balls than in the array of lower tolerance balls. Also, the normal contact forces were probably more uniform in the array of higher tolerance balls. The rate of energy dissipation, ΔW, was found to increase as the square of the maximum tangential contact force rather than the cube, in agreement with tests on single contacts. Also, ΔW varied with confining pressure raised to approximately the -1/6 power, with some variation with tolerance, while theory predicts the -1/3 power. The rate of energy dissipation was higher and $\frac{\Delta W}{W}$ was about 25% greater for the higher tolerance balls than for the poorer tolerance balls. In general, the rate of energy dissipation decreased by a factor of two as the cleanliness (or surface friction) of the balls increased.

Reproduced with permission of the copyright owner. Further reproduction prohibited without permission.

C. Real Aggregates of Particles

C-1. Random packings of particles

There are many difficulties in using contact theory to make predictions for general aggregates of particles. Consider initially a random packing of uniform spheres in elastic contact, preloaded by a confining pressure p_o. A wave propagating in such a system can be thought of as an oscillating stress or strain applied to some combination of springs in series and/or parallel. Each tangential or normal compliance is equivalent to a spring stiffness and proportional to p_o. If the distributions of interparticle contacts and associated contact forces are such that the packing configuration, including coordination, is invariant with pressure except for volume changes, the modulus for the system should be proportional to p_o. The losses at each contact may be summed as was done for regular arrays and the energy stored calculated similarly. Thus the same dependences found for the velocity and Q^{-1} in regular arrays might be expected in irregular packings.

A major difficulty that arises in attempting to apply the theory exactly, even to such an idealized system as described above, is the lack of symmetry of contact orientation. As a result of the random orientation of contacts around a sphere, preloading by an external stress p_o may

Reproduced with permission of the copyright owner. Further reproduction prohibited without permission.

give rise to a variety of normal contact forces as well as tangential forces, thus making the initial state very difficult to define. One approach might be to describe the bulk medium as a combination of volume elements of two regular packings in appropriate proportions to yield the observed porosity and number of contacts per sphere. For example, Smith, Foote, and Busang (1929) found that, for the purposes of statistical descriptions, randomly packed homogeneous steel spheres could be regarded as a mixture of hexagonal and simple cubic arrays.

A second, and more serious, problem in random packings of spheres is that the contacts around any sphere range from close (spheres in direct contact) to near (spheres almost in contact). Bernal and Mason (1960) experimentally investigated the coordination in randomly packed aggregates of uniform steel ball bearings. The number of close and near contacts was determined by soaking the sphere arrangement with paint and then draining it off. Close contacts were marked by rings of paint and near ones by spots due to surface tension effects. Near contacts were recorded by this method up to distances 5% greater than the ball diameter (1/4 inch). Two modes of random packing were found. Random close packing had a porosity of 36% and an average of 8.5 total contacts. Random loose packing had a porosity of 40% and an

Reproduced with permission of the copyright owner. Further reproduction prohibited without permission.

average of 7.1 total contacts with 5.5 close contacts per sphere. As a consequence of the near contacts, the modulus for the system will have an additional dependence on the confining pressure p_o reflecting the making or breaking of contacts with variations in p_o. For any sphere in the aggregate there will be a distribution of contact forces arising from the fact that some contacts will be heavily displaced while others are barely made.

Statistical equations, applicable to beds of randomly packed uniform spheres, have been developed by Beresford (1969) for predicting the expected number of spheres having a specific number of close and/or near neighbors and the expected number of near neighbors of an average sphere. The bed porosity, η, and the average number of close contacts, $\bar{M}$, are the only undetermined constants, and the theoretical predictions compare quite favorably with the experiments of Bernal and Mason (1960). His expression for the expected number of sphere centers within a radial distance r from the center of an average sphere is

$$M = \bar{M} + \left[\frac{4(1-\eta)}{2-\sqrt{3}} - \bar{M}\right] \exp\left[-\bar{M}\left(\frac{r}{R} - 2\right)\right], \quad r \geq 2R,$$

where R is the sphere radius. The expected change in number of centers between r and r + dr is

$$\frac{dM}{dr} = \frac{\bar{M}}{R}\left[\frac{4(1-\eta)}{2-\sqrt{3}} - \bar{M}\right] \exp\left[-\bar{M}\left(\frac{r}{R} - 2\right)\right]. \qquad (35)$$

Reproduced with permission of the copyright owner. Further reproduction prohibited without permission.

Equation (35) may also be interpreted as the expected change in the number of contacts as the radial distance between the central sphere and all of its neighbors is decreased by dr. If $r \ll R$, $\frac{dM}{dr}$ is approximately independent of r.

At this point it should be noted that the preceding discussion is strictly applicable only to smooth spheres. The roughness of some materials may have significant effects on the number of near contacts per sphere and on $\frac{dM}{dr}$.

A further problem restricting the general applicability of the theory is the dependence of packing geometry on grain size and shape. Theoretically the porosity of a packing of uniform spheres is independent of the size of the spheres. However, there is a size effect on the porosity in random packings of some spheres like glass beads or rounded sand grains, porosity increasing for the finer sizes. For example, Westman and Hugill (1930) obtained the following experimental data on random packings of round washed sand:

Diameter (in.)	Porosity (%)
0.176	37.7
0.028	38.2
0.0097	38.6
0.0035	42.5

Mixing different sizes of particles generally increases the bulk density and the number of contacts per sphere over those of packings of equal sizes. Westman and Hugill's

Reproduced with permission of the copyright owner. Further reproduction prohibited without permission.

experiments (1930) indicated that for mixtures of two size grades of spherical particles the density increased as the difference in average radii increased.

Packings of irregularly shaped particles have been studied very little compared to sphere packings. In general, angular particle aggregates are characterized by more non-uniformity (Brown and Hawksley, 1945) and have higher porosities than aggregates of spheres. Brain (1958) found an almost linear relationship between the increase in porosity and the weight percent of angular particles in random packings of sand grains of approximately uniform size. White and Walton (1937) obtained the following experimental data on random packings:

Material		Mesh Size	Porosity (%)
silicon carbide	rounded	-0.066 + 0.055	44.72
	angular		53.12
aluminum oxide	rounded	-0.066 + 0.055	40.75
	angular		45.25

There is also some evidence that porosity increases with decreasing size (Brown and Hawksley, 1945). The higher porosity of angular particle aggregates reflects the more interlocking geometry of such packings and does not necessarily imply fewer contacts per particle than found in spherical particle aggregates. Studies by El Boushi (1969) of random packings of angular particles of crushed rock of nearly

Reproduced with permission of the copyright owner. Further reproduction prohibited without permission.

equal median diameter indicated an average number of contacts per particle of between 9 and 12. This number includes both close and near contacts.

From this discussion it is clear that use of contact theory to predict acoustic properties in general aggregates of particles will probably require a rather extensive knowledge of the geometrical properties of the aggregate. It is expected that the acoustic properties of such aggregates will depend on grain size and shape and on confining pressure in ways not specified by Mindlin's or White's theories.

C-2. Contact of rough surfaces

The theory discussed earlier in this chapter presumed that all surfaces were smooth and all contacts continuous and also that the materials deformed elastically up to the point of slipping. On a microscopic scale, however, there are no absolutely smooth surfaces. All solid surfaces are characterized by protuberances or asperities. Since local pressures on the asperities may be very high, even under relatively light loads, asperity deformation may be in large part plastic, especially in the case of metals and some ductile non-metals such as NaCl. An extensive treatment of the frictional and deformational properties of surfaces may be found in Bowden and Tabor (1954, 1964).

Reproduced with permission of the copyright owner. Further reproduction prohibited without permission.

Based on the usual assumption that frictional force is proportional to the real area of contact between surfaces, two sorts of relations are expected, depending on the mode of deformation at asperity contacts. For a single metallic or ductile asperity contact, where deformation is plastic and the contact welds together, the real area of contact is given by $A = F/p_m$, where F is the load on the contact and p_m is the mean yield pressure. In this case the frictional force f is equal to As_m, where s_m is the mean shear strength of the welded asperity junction. Hence Amonton's Law can be derived,

$$f = \frac{s_m}{p_m} F \simeq \frac{s}{p} F = \mu F,$$

where s and p are the bulk material properties and $\mu (= s/p =$ constant) is the coefficient of friction. For a single asperity contact between brittle materials, the deformation should be largely elastic (Hertzian), and elasticity theory predicts a dependence of A on the 2/3 power of F. The frictional force f should then be proportional to $F^{2/3}$, and the coefficient of friction, $\mu = f/F$, should be proportional to $F^{-1/3}$.

Experimentally it is found that the above relations are true for <u>single</u> contacts if the effects of work-hardening are included for metals (e.g., see Bowden and Tabor, 1954 and 1964; Archard, 1957; and Courtney-Pratt and Eisner,

Reproduced with permission of the copyright owner. Further reproduction prohibited without permission.

1957). However, Amonton's Law appears to be approximately obeyed by both ductile and brittle materials in contact over a large number of asperities. Originally this observation was thought to indicate that all asperities deformed plastically and adhered. Now, however, analytical and experimental studies have shown that the frictional properties of nominally flat or curved surfaces in multipoint contact are determined primarily by the statistical distribution of asperities, or more simply, their roughness (e.g., Archard, 1953; Archard, 1957; Greenwood, 1967; Greenwood and Williamson, 1966; Greenwood and Tripp, 1967; O'Conner and Johnson, 1963). The general law for multipoint contact is that $f \propto A$, and whether or not Amonton's Law ($f \propto F$) is obeyed depends primarily on the surface topography rather than on the mode of asperity deformation. For example, for surfaces in elastic multipoint contact, assuming that each asperity contact is Hertzian, f is found analytically to be proportional to F^n, where $n \approx 1$, the exact value of n depending on the asperity distribution chosen. Related to this conclusion are experiments by Archard (1957) on Perspex and brass which showed that $f \propto A \propto F$ and that μ was constant as long as there were many contacts. At high loads, where the asperities were flattened and separate contacts ran together, μ decreased with increasing F for both brass and Perspex, as

Reproduced with permission of the copyright owner. Further reproduction prohibited without permission.

would be expected for contact over only a few asperities which were deforming elastically. As pointed out by Greenwood in several papers (e.g., Greenwood, 1967), probably the real basis for the relationship $F \propto A$ is that the size of an average microcontact area is relatively constant, i.e., independent of load, in the case of multipoint contact.

The question now arises as to what frictional relationship should be expected for elastic particle contacts in a general aggregate. Should each particle contact be considered a single or a multipoint contact, or, equivalently, should μ be taken as a constant? This question is particularly relevant to the description of the energy dissipated at the contacts.

For two rough spheres in contact over a wide range of loads and types of materials, the surface roughness has no effect on the distribution of elastic stresses in the bulk of the solid, and the bulk displacement under normal or tangential loading is given by elasticity theory. The experiments by Johnson (1955, 1961) discussed earlier showed that for hard steel balls the observed displacements under tangential and oblique loading were predicted accurately by elasticity theory. Later experiments by O'Connor and Johnson (1963) on curved metallic surfaces with a variety of hardness and roughness characteristics showed that the

Reproduced with permission of the copyright owner. Further reproduction prohibited without permission.

contribution of asperity deformation to tangential compliance was negligible compared to the bulk elastic component of compliance. Theoretically, however, under very light loads the surface roughness may extensively modify the force-displacement relations. Greenwood and Tripp (1967) looked at the effect of roughness on the contact between a rough sphere and a smooth surface. Both the deformation of asperities and the bulk deformation of the sphere were included in the analysis. The asperities were assumed to have spherical tops and uniform radii, and each asperity contact was assumed to be Hertzian. The distribution was taken to be Gaussian, an assumption with some physical support (Greenwood and Williamson, 1966). The statistical analysis concluded that the pressure distribution over the contact at very low loads, where the squashing of asperities is important, was lower and extended over a much larger effective area than the Hertzian distribution. At higher loads the bulk deformation of the sphere became more important and the pressure distribution over the contact was essentially Hertzian, although the distribution tailed off instead of dropping sharply to zero. The changeover load is approximately equal to $\frac{2\sigma_s(1-\nu^2)}{E}\sqrt{2R\sigma_s}$, where σ_s is the "roughness" or standard deviation of the height distribution, E and ν are Young's modulus and Poisson's ratio, and R is the sphere

Reproduced with permission of the copyright owner. Further reproduction prohibited without permission.

radius. Note that the more uniform the asperity heights, the lower the changeover load.

C-3. Field and laboratory acoustic studies of randomly packed aggregates

Acoustic properties of wet and dry sands and of other unconsolidated aggregates have been investigated by many workers in both laboratory and field environments for the purposes of studying marine sediments, simulating lunar soils, interpreting well-logging records, and modeling porous materials such as crustal rocks. In general, the velocity through dry aggregates with some degree of structural rigidity is a function of confining pressure, aggregate density and porosity, and bulk material properties. For aggregates saturated with a liquid but still having structural rigidity, the aggregate velocity depends on the differential pressure and, if the liquid velocity is of the same order of magnitude as or higher than that of the solid, on the velocity of the liquid. The fractional energy loss per cycle is generally found to depend on confining or differential pressure, at least at low pressures, and to be independent of vibration frequency and wave amplitude. Consolidated aggregates or rocks at low confining pressures exhibit similar velocity and loss characteristics.

Reproduced with permission of the copyright owner. Further reproduction prohibited without permission.

Velocities and fractional energy losses were measured in resonance bar experiments by Gardner et. al. (1964) on several unconsolidated sands and glass sphere aggregates. Torsional and extensional velocities were found to increase with confining pressure, raised to about the 1/4 power over a pressure range of 3 to 300 bars . (Previous experiments by Wyllie et. al. [1958] showed that a terminal velocity, such as found for rocks at high confining pressures, was not reached for glass sphere aggregates at differential pressures as high as 600 bars.) Measurements of the fractional energy loss per cycle decreased with about the 1/6 power of confining pressure from about 10 to 100 bars, becoming almost independent of pressure by 300 bars ($Q^{-1} \approx 10^{-3}$). In addition, the fractional energy losses were independent of porosity, grain size, vibration frequency ($< 10^5$ Hz), and vibration amplitude and were lower than losses obtained for consolidated sandstones at similar confining pressures.

A variety of other data suggest a similar pressure dependence for the velocity. For example, field measurements reported by White and Sengbush (1953) of velocities in sand indicate an approximate increase of velocity with the 1/6 power of the depth of burial. Similar results were found by Faust (1951) for shale and sand-shale sections. Velocity measurements on sandstones as a function of confining

Reproduced with permission of the copyright owner. Further reproduction prohibited without permission.

pressure are also frequently characterized by an approximate 1/6 power dependence on pressure (e.g., see Hicks and Berry [1956] and Hughes and Kelly [1952]).

A relation of velocity to grain size has been noted in some cases. For example, in in-situ acoustic measurements by McCann and McCann (1969) on water-saturated sand and silt-size sediments at a mean depth of burial of 2 m, a small increase of velocity with grain diameter was found. A statistical analysis by Morgan (1969) of longitudinal velocities through water-saturated cores of fresh-water sediments indicated an approximate linear dependence of velocity on median grain diameter. This same study showed an inverse dependence of velocity on the square of the porosity. Both bulk density and porosity were found to be related to the median grain diameter in a complicated manner.

In summary, the available observational and experimental acoustic data obtained for granular aggregates are ambiguous and sometimes contradictory. The best defined relation, the 1/4 to 1/6 power dependence of velocity on pressure or depth of burial, is similar to the dependence predicted by contact theory. However, the occasionally observed dependence of velocity on grain size has no analogy at all in contact theory. Furthermore, although the contancy of the observed values of Q^{-1} with wave amplitude and frequency fits White's

Reproduced with permission of the copyright owner. Further reproduction prohibited without permission.

theory for energy dissipation, variations of Q^{-1} with pressure do not appear to support either Mindlin's or White's theories. Finally, nothing but fragmentary data is available to evaluate the contributions of grain shape, type of deformation at contacts, or interfacial lubrication to the measurements of velocity and Q^{-1}. The experiments to be discussed in the next three chapters were undertaken with the aim of separating the effects of some of the important aggregate variables on acoustic measurements and of comparing the measured relations with the predictions of contact theory in order to provide a more complete description of the acoustic properties of aggregates at low confining pressures.

Reproduced with permission of the copyright owner. Further reproduction prohibited without permission.

II. EXPERIMENTAL PROCEDURE FOR THE ACOUSTIC EXPERIMENTS

A. Method

A-1. Measurement techniques

A resonance method was used to obtain longitudinal and torsional velocities and energy losses in bars of granular media over a range of frequencies. For a bar with free ends the resonance condition is

$$\ell = \frac{n\lambda}{2} ,$$

where λ is the wavelength of the vibration; ℓ, the length of the bar; and n, the number of wave nodes along the bar. Because of geometrical considerations, vibrations in bars are generally dispersive; that is, the velocities depend on λ. The equation for computing the longitudinal velocity of a bar, as given by Spinner and Tefft (1961), is

$$V_L(\lambda) = \frac{\ell \omega_n}{n\pi} \frac{1}{\sqrt{\beta_n(\lambda)}} ,$$

where $\omega_n = 2\pi$ times the frequency corresponding to n nodes. If the diameter to wavelength ratio for the bar is $\ll 1$, Rayleigh's correction factor, β_n, may be expressed as

$$\beta_n \approx 1 - \frac{\pi^2 n^2 \nu^2 d^2}{8\ell^2} ,$$

Reproduced with permission of the copyright owner. Further reproduction prohibited without permission.

where ν is Poisson's ratio. For a rectangular bar with lateral dimensions a_1 and a_2, and $a_1 \approx a_2$, $d^2 = 2/3(a_1^2 + a_2^2)$; for a cylindrical bar, d is equal to the diameter. For all samples studied, $\beta_n \approx 1$ for the fundamental and first overtone, and the working equation was simply

$$V_E = \frac{\ell \omega_n}{n\pi}, \tag{36}$$

where V_E is the extensional or "bar" velocity. The basic equation for torsional velocity in a bar (Spinner and Tefft, 1961),

$$V_T(\lambda) = \frac{\ell \omega_n}{n\pi} \sqrt{\gamma(\lambda)}, \tag{37}$$

is similar to that for longitudinal velocity, although for cylindrical bars, the shape factor γ is equal to 1 and the equation is exact. For rectangular bars of cross-section $a_1 a_2$, where $a_1 \approx a_2$, $\gamma \approx 1.19$ for the fundamental mode of vibration. The errors involved in the use of equations (36) and (37) for calculating velocities from the experimentally determined frequencies are negligible compared to experimental errors.

In dissipative systems the modulus relating stress and strain may be considered to have both real and imaginary components. Specifically, Young's modulus may be taken as $E = E_1 + iE_2$, where E_1 is the elastic modulus and E_2 is a

Reproduced with permission of the copyright owner. Further reproduction prohibited without permission.

measure of the energy dissipated. The ratio E_{2/E_1} is equal to $1/2\pi$ times the fractional energy loss per cycle, $\frac{\Delta W}{W}$. By definition the internal friction, Q^{-1}, is equal to $\frac{1}{2\pi}\frac{\Delta W}{W}$; hence $E_2/E_1 = Q^{-1}$. The measured velocity is related to E_1 and E_2 in the following manner (McSkimin, 1964):

$$V_E^2 = \frac{2E_1\left[1+(E_2/E_1)^2\right]}{\rho\left\{\left[1+(E_2/E_1)^2\right]^{1/2}+1\right\}}$$

where ρ = density. If Q^{-1} is about 10^{-1} or less, $V_E^2 = \frac{E_1}{\rho}$ to a very good approximation. The rigidity modulus may be treated similarly. In all the experiments reported here, the modulus calculated from the measured velocity was taken to be the elastic modulus. The error in calculating elastic modulus based on this assumption was less than +3% for the highest damping specimens.

Most of the energy losses per cycle for longitudinal and torsional vibrations were calculated in terms of the internal friction or the inverse quality factor, $Q^{-1} = \frac{1}{2\pi}\frac{\Delta W}{W}$, from the width of the resonance peak. For a linear system with low damping (Q^{-1} equal to or less than about 10^{-1}), $Q^{-1} = \Delta\omega/\omega_n$, where $\Delta\omega$ is 2π times the difference between the frequencies at which the amplitude is $\frac{1}{2}$ the peak amplitude at resonance. The linearity of the systems investigated, and hence the applicability of this method of measurement,

Reproduced with permission of the copyright owner. Further reproduction prohibited without permission.

was indicated by the lack of any significant dependence of energy loss on vibration amplitude and by the symmetry of the resonance peaks.

A second method of determining energy dissipation, the decay of free oscillations, was used for most of the preliminary tests and as check for some of the later experiments. Again assuming a linear system, the amplitude of a harmonic wave at a fixed point in space decays by a factor $e^{-\gamma t}$ in time t, where $\gamma = \frac{\omega}{2\pi} Q^{-1}$. In these experiments a resonance frequency was excited, the excitation suddenly removed, and the subsequent decay of vibrations was displayed on an oscilloscope and photographed. The log of the amplitude of vibration was then plotted against time and the slope, γ, of the resulting straight line was calculated. (If the system had been nonlinear, the plot would not have been a straight line.) Values of Q^{-1} obtained in this manner agreed well with those calculated from the resonance curves.

A-2. Equipment

The basic equipment was the same for all experiments (figure 11). The frequency generator was an audio oscillator with a range of about 60 Hz to 20 kHz. The generator output was connected to the horizontal plates of an oscilloscope and to a frequency counter. Frequency was measured

Reproduced with permission of the copyright owner. Further reproduction prohibited without permission.

to 1 Hz. Output from the pickup was sent to a differential amplifier with matching impedance. The amplified signal was connected to a 20 Hz - 200 kHz band-pass filter and to an AC voltmeter. The filtered output was fed to the vertical plates of the oscilloscope.

Two methods of exciting the specimen were used. In the preliminary experiments the driver was a Pye-Ling Type 47 vibration generator with approximately the same frequency range as the oscillator. For longitudinal vibrations the vibrator was placed facing the end of the sample opposite the pickup. Coupling was either through air, for the low damping samples, or through light contact with the end of the sample. Torsional vibrations were excited by placing the vibrator perpendicular to the long axis of the specimen and coupling it to the edge of the specimen end by a thin thread. The vibrator was wired to a switch that could disconnect it from the oscillator and trigger the oscilloscope while simultaneously retracting or advancing the vibrator spindle. When the switch was thrown, free decay of the received wave form was displayed on the oscilloscope and could be photographed with a Polaroid scope camera.

The second method, electrodynamic drive (Biesterfeldt, et. al., [1960]), was much more satisfactory and was used to obtain most of the data. This method supplied more power to

Reproduced with permission of the copyright owner. Further reproduction prohibited without permission.

drive the specimen, the magnitude being essentially limited by heating of the coils, while minimizing the loading of the specimen by the driver. The output was smooth over the frequency range studied and independent of frequency. With the vibration generator, on the other hand, various spurious resonances were always present, either generated within the vibrator itself or in the auxiliary equipment by air-coupling of the sound accompanying the high frequencies. Also, the power output of the vibrator dropped at the higher frequencies, making it difficult to drive the specimen without undesirable loading.

The driving coil for the electrodynamic method consisted of several turns of thin copper wire cemented to the end of the sample opposite the pickup. The coil was connected directly to the oscillator and placed in the field of a strong permanent magnet. For longitudinal vibrations a magnet was modified with a removable pole piece and a one-inch air gap to concentrate the flux lines. For torsional vibrations the coil was cemented to the edge of the specimen end, parallel to the long axis of the specimen. The end of the sample was then placed between the poles of a U-shaped magnet.

Reproduced with permission of the copyright owner. Further reproduction prohibited without permission.

A stereo phonograph crystal cartridge with a one-volt output and a high frequency limit of about 20 kHz was used as a signal detector for all experiments. The cartridge was placed in light contact with the end of the bar opposite the driver. Coupling was improved by removing the stylus. Various other sorts of pickups were tried during the course of the experiments, including microphones, magnetic cartridges, and a coil and magnet arrangement similar to the driver. However, the large output of the crystal cartridge and the relative lack of electrical cross-coupling with the driver made the crystal pickup the most convenient. A disadvantage was that it picked up the sound generated by the vibrator.

A-3. Preparation of rigid bars and effects of jacket

Rigid bars of granular media were prepared in the following fashion. Cylindrical rubber containers with one open end were placed in partial forms and filled with the granular material. The open end was then sealed and a vacuum pulled inside the container through a connection made at the center of the specimen. Measurements of velocity and internal friction as a function of pressure were made by varying the vacuum inside the container.

Reproduced with permission of the copyright owner. Further reproduction prohibited without permission.

The preliminary experiments were done with latex containers approximately 0.007 inches thick. With these containers, the sample nearly filled the whole container and only a small amount of excess rubber was left at the sealed end of the bar. All these specimens were cylindrical and from 4 to 5 inches long and about 1/2 inch in diameter. A small copper tube connected to the vacuum pump, via a pressure gage, was inserted in the center of the container before filling.

In the second set of experiments, thinner (approximately 0.002 inches thick) and more homogeneous latex containers were used. These containers were larger in diameter than the final sample and hence there was some excess rubber along the length of the bar. All of the bars made in this manner were approximately square in cross-section, about 1/2 by 1/2 inch, and about 4 inches long. The connection to the pressure gage and vacuum pump was made through a hypodermic needle inserted in the center of the specimen.

The measured resonance frequencies and internal friction of the jacketed samples include some contribution from the rubber jacket. Formulas for correcting the observed values for the jacket effect are given by Gardner et. al. (1964). The expression applicable to extensional vibrations is

Reproduced with permission of the copyright owner. Further reproduction prohibited without permission.

$$V_m = \frac{E_b v_b + B_1 E_j v_{sj}}{\rho_b v_b + \rho_j v_j} \quad , \quad B_1 = \frac{\nu_b^2 - 2\nu_b\nu_j + 1}{1 - \nu_j^2} \, ,$$

where V_m is the measured velocity; E_b and E_j are Young's moduli for the specimen and the jacket; v_b and v_j are the volumes of the specimen and the jacket; ρ_b and ρ_j are the densities of the specimen and the jacket; v_{sj} is the jacket volume, excluding the ends; and ν_b and ν_j are Poisson's ratios for the specimen and the jacket.

For the purposes of estimation, approximate values for the microbead specimens will be taken to be $\nu_b = .22$, $V_m = 4 \times 10^4$ cm/sec, and $\rho_b = 1.55$ gm/cc. Specific values for the 0.002-inch thick rubber jacket modulus must be estimated. An attempt was made to calculate the jacket modulus using the above expression and a specimen that could be tested independently of the jacket. The rubber modulus was so small, however, compared to the modulus of the test bar (lucite) that the other variables in the expression could not be determined accurately enough to obtain the modulus. (There was excess rubber along the bar as with the aggregate specimens.) A static tension test on the rubber yielded a value for E_j of about 2.0×10^7 dynes/cm^2 for a strain of about 1%. Similar values are reported by Nolle (1949) at low frequencies for the rubber used in these experiments (natural latex or gum rubber). Both the modulus and Q^{-1} of this type

Reproduced with permission of the copyright owner. Further reproduction prohibited without permission.

of rubber increase slowly with frequency, and values for E_j and Q^{-1} of approximately 4×10^7 dynes/cm^2 and 0.45 at 30° C, 5 kHz, are given in Nolle (1949). To estimate the maximum jacket effect for these experiments, which cover a frequency range of 1 to 20 kHz, E_j will be taken to be 1×10^8 dynes/cm^2 and Q^{-1} to be 1. The density of the rubber is 0.98 gm/cc, and Poisson's ratio is 0.45 - 0.50. An average value of $\frac{V_{sj}}{V_b}$ for all samples was about 0.016 and $V_{sj} \approx V_j$. With these values, $B_1 \approx 1$, and since $\rho_b V_b \gg \rho_j V_j$,

$$V_m^2 \approx \frac{E_b}{\rho_b} + \frac{E_j V_{sj}}{\rho_b V_b} \tag{38}$$

or

$$1.6 \times 10^9 \approx V_b^2 + 10^6,$$

where V_b is the velocity of the specimen. The correction is thus negligible for the microbeads and would be even more so for the higher velocity and/or higher density specimens studied.

For correcting the extensional internal friction, Gardner et. al. (1964) give the following expression:

$$Q_m^{-1} = \frac{E_b V_b Q_b^{-1} + B_2 E_j V_{sj} Q_j^{-1}}{E_b V_b + B_1 E_j V_{sj}}, \tag{39}$$

where Q_m^{-1}, Q_b^{-1}, and Q_j^{-1} are the measured internal friction, the specimen internal friction, and the jacket internal friction. The factor B_2 is a complicated function of ν_b, ν_j,

Reproduced with permission of the copyright owner. Further reproduction prohibited without permission.

and the jacket and specimen Q^{-1}'s and can be set equal to 1 for this estimation. Using the values given above for the microbeads and the maximum expected values for the 0.002-inch thick rubber jacket equation (39) becomes

$$Q_m^{-1} \approx Q_b^{-1} + 6 \times 10^{-4}.$$

The lowest Q_m^{-1} for the microbeads was about 2×10^{-2} and, hence, the correction for the microbeads is small. For the lower loss ($Q^{-1} \approx 4 \times 10^{-3}$) but higher velocity alumdum specimens, the correction is more important ($Q_m^{-1} \approx Q_b^{-1} + 2 \times 10^{-4}$) but still small.

Expressions for estimating the jacket effect for torsional vibration are similar to equations (38) and (39) and give similar results. The thicker rubber jacket (0.008 inches) should have approximately the same properties as the thinner rubber, but the corrections would be somewhat greater simply due to the larger volume of rubber per sample.

To test these estimations, velocity and Q^{-1} were measured on a lucite bar ($V_b = 1.88 \times 10^5$ cm/sec, $\rho_b = 1.18$ gm/cc, $Q_b^{-1} = 6 \times 10^{-3}$) with and without both kinds of jackets. The ratio $\frac{V_{sj}}{V_j}$ was approximately the same as for the aggregate samples. Addition of the 0.002-inch jacket lowered the fundamental frequency (about 5300 Hz) by 0.6% and the second overtone (about 15,860 Hz) by 0.8%. Hence, the effect on the velocities is considered to be negligible. The effect

Reproduced with permission of the copyright owner. Further reproduction prohibited without permission.

on Q^{-1} was more important. Q_m^{-1} was about 1.2 to 1.3 times Q_b^{-1} over the frequency range from 5 to 20 kHz. This increase is larger than can be reasonably accounted for by equation (39). The additional loss probably represents not only the jacket loss but also losses due to the coupling of the coil to the jacket and, possibly, viscous losses due to the added surface area of the rubber jacket including the excess rubber flap. If such is the case, then the extra loss would be approximately constant for all samples and would be significant only for the lower loss alumdum specimens.

Jacketing the lucite bar with the 0.008-inch thick rubber lowered both the fundamental and the second overtone by about 1.5%. Thus, the differences in measured velocities between the two sets of experiments, due to the differences in jackets, are expected to be small. Q_m^{-1} was about 6×10^{-4} higher than with the thinner jacket for the lower frequencies. Beginning about 15 kHz the jacketed sample showed a sharp increase of Q_m^{-1} with frequency. All measurements made with this jacket above about 10 kHz were therefore disregarded.

A-4. Support of specimens

All specimens used in the vibrator experiments were suspended horizontally by two long silk threads hung from a

Reproduced with permission of the copyright owner. Further reproduction prohibited without permission.

heavy cross bar. The threads formed a sling which was placed under the vacuum connection at the center of the specimen. If the suspension is exactly at a node, then, since there is no motion at a node, the vibration of the specimen is unaffected. The effects on measured internal friction of moving the suspension away from the node have been investigated by Wachtman and Tefft (1958). They derived the following expression:

$$Q_m^{-1} = \frac{Q_s^{-1} + k\,Q_a^{-1}\cdot(Y/Y_o)^2}{1 + k\cdot(Y/Y_o)^2},$$

where Q_m^{-1} is the measured internal friction, Q_s^{-1} is the internal friction of the specimen, and Q_a^{-1} is the internal friction of the suspension apparatus. For a given specimen and suspension, k is a constant expressing the ratio of energy stored in the suspension apparatus to that stored in the specimen when the suspension is at an antinode. For a bar with ends free in extensional resonance, the ratio of the displacement at the suspension point to the maximum displacement is $Y/Y_o = \sin \frac{n\pi x}{\ell}$, where x is the distance of the suspension away from a node (the two points of suspension are symmetrically placed). To estimate the suspension effects for the experiments described here, consider first the odd harmonics, which have a node at the center of the bar. Setting $k = .1$ and $Q_a^{-1} = 10^{-1}$ (Wachtman and Tefft, 1958) and

Reproduced with permission of the copyright owner. Further reproduction prohibited without permission.

using the average values $x = 0.2$ cm and $\ell = 10$ cm, $y/y_0 \approx 0.31$ for the fifth harmonic, usually the highest one measured. Then

$$Q_m^{-1} \approx Q_s^{-1} + 1 \times 10^{-4}.$$

The lowest Q_m^{-1} measured was about 4×10^{-3}. Hence, the error introduced by the suspension for the odd harmonics is negligible. For the even harmonics, $y/y_0 = 1$, the correction is still small, especially since the average Q_m^{-1} was greater than 10^{-2}.

In the preliminary experiments, all the samples were supported by a small foam rubber block placed at the center of the specimen. The effects of this support were not computed. For values of $Q^{-1} \geq 1 \times 10^{-2}$, data obtained using this type of support agreed with those obtained from suspended specimens.

B. Description of Specimens

The primary materials used in the experiments were glass microbeads, or glas-shot, manufactured by Microbeads, Inc., Jackson, Mississippi, for use as abrasives. The glass is described as optical crown glass, soda lime type, high in silica and free of lead. Approximate specifications for the glass are given in table 2. The microbeads are described as having a minimum of 85% true spheres, with less than 1%

Reproduced with permission of the copyright owner. Further reproduction prohibited without permission.

sharp angular particles and less than 1/2% foreign matter. A typical size distribution for the beads indicated that, for each sieve range given for the beads, 90 - 100% passed the larger sieve and 0 - 10% passed the smaller. The four sieve ranges of beads used in the experiments, and the nominal diameter for each, are listed in table 3. The manufacturer's specifications state that the maximum bulk density for the larger beads under zero confining pressure is approximately 1.55 gm/cc, and the minimum for the smaller sizes, 1.50 gm/cc.

Clean samples of the glass beads were prepared as follows. After several washings with acetone, the beads were rinsed with tap water then soaked several times with a cleanser (Alconox) used primarily for cleaning glass. After many rinsings with tap water, they were rinsed thoroughly with distilled water. Following a final rinsing with alcohol, they were dried in a furnace. Until they were used, they were kept either under vacuum in a desiccator jar or in tightly sealed containers. The beads were supplied from the dealer with a guarantee of cleanliness, and no significant difference in acoustic properties was observed between the cleaned and uncleaned samples. The cleansing procedure, however, insured uniformity of samples.

Reproduced with permission of the copyright owner. Further reproduction prohibited without permission.

To study the effects of varying contact friction, various types of lubricants were applied to the beads. Sodium stearate, oil (Gulf Security 205), and glycerol were applied by evaporation from solution in amounts estimated to form a film of several to many molecular layers of lubricant around each sphere. The general procedure was as follows. The oil and glycerol solutions were prepared by adding one ml of the lubricant to 1000 ml of heptane and ethanol, respectively. The sodium stearate solution was prepared by adding 2 gm of sodium stearate to 1000 ml of distilled water and heating until the solution became clear. A 200 gm sample of the microbeads was covered with the appropriate solvent, and the desired amount of solution added and mixed. The sample was then heated or air dried and subsequently stored in tightly sealed containers. The amounts of lubricants added to 200 gm samples of beads (and the corresponding weight percent of lubricant in the 200 gm sample) were: 0.001 ml (0.00063%), 0.010 ml (0.0063%), and 0.080 ml (0.0504%) of glycerol; 0.010 ml (0.0045%) and 0.020 ml (0.0090%) of Gulf oil; and 0.020 gm (0.005%) and 0.090 gm (0.045%) of sodium stearate.

Other lubricants used on the glass beads were silicone and molybdenum disulfide sprays, Ivory soap, water soluble silicone (Siliclad), Dow silicone fluid, and G. E. silicone fluid. The Dow and G. E. silicone fluids were degassed and

Reproduced with permission of the copyright owner. Further reproduction prohibited without permission.

applied in unmeasured amounts by covering the sample with the fluid and allowing the excess to drain away. The silicone and molybdenum sulfide sprays were simply sprayed on the beads as evenly as possible. The soap and water-soluble silicone were applied from solutions made with distilled water. Relevant physical properties of the liquid lubricants are given in the following table.

TABLE 1.--Some physical properties of the liquid lubricants

Lubricant	Specific Gravity	Viscosity (cs)
Gulf Security 205 oil	0.896	4.2×10^3 (20° C)
Glycerol	1.26	1.2×10^3 (20° C)
G. E. SF-96 silicone fluid . . .	0.958	50 (25° C)
Dow Corning 200 silicone fluid .	0.973	6.0×10^4 (25° C)

Other granular materials studied included alundum (electrically fused crystalline alumina), spherical alumina mounting filler, scientific-grade sodium chloride crystals, and crushed glass plate. The alundum was angular and approximately equiangular (-60 mesh). Two samples of alundum were lubricated, in the same manner as the microbeads, with

Reproduced with permission of the copyright owner. Further reproduction prohibited without permission.

0.01% sodium stearate and with 0.045% Gulf oil. The alumina mounting filler covered a range of sizes (-80 mesh) and was available in two types, "hard" and "soft", depending on the temperature at which it was fired. The relevant physical properties of the two types of filler were unavailable. All samples of the sodium chloride (approximately -25 + 60 mesh) were stored under vacuum for several days before use. The crushed glass plate was similar in composition to the glass beads and was cleaned in the same manner. The following table gives approximate physical properties of the glass, alundum, and sodium chloride for comparison.

TABLE 2.--Physical properties of some of the granular materials studied

Material	Density (gm/cc)	Young's Modulus (dynes/cm^2)	Poisson's Ratio	Hardness	
				Mohs	Indentation (kg/mm^2)
Glass	2.5	7.0×10^{11}	0.25(3)	6.0	600(2)
Alundum	3.99(1)	4.0×10^{12}(1)	0.24(1)	9.0	2000(2)
Sodium Chloride	2.16(1)	3.7×10^{11}(1)	0.25(1)	2.5	60(2)

(1) Anderson and Liebermann (1966)

(2) Bowden and Tabor (1964)

(3) Kolsky (1963)

Reproduced with permission of the copyright owner. Further reproduction prohibited without permission.

III. RESULTS OF THE ACOUSTIC EXPERIMENTS

The acoustic data are summarized in table 3 and in figures 12 through 20. Data from the coil and magnet experiments are more accurate than data obtained from the vibrator experiments; the latter experiments were made in the sense of a reconnaissance and no attempt is made to estimate the errors involved. It is noted, however, that in areas of overlap data from both types of experiments were in satisfactory agreement (i.e., within the range of experimental error estimated for the coil and magnet experiments).

The densities given in table 3, except for those in parentheses, were obtained from weight and dimension measurements of the larger specimens prepared for the compression tests. The errors involved in these measurements are estimated to be less than $\pm 2.5\%$. Densities calculated from similar measurements on the acoustic specimens were less reliable due to the small volumes of the specimens and, with two exceptions, are not included.

Measured velocities were independent of vibration frequency, except for some geometrical dispersion, and of

Reproduced with permission of the copyright owner. Further reproduction prohibited without permission.

amplitude over the range studied. The extensional velocities in table 3 were calculated according to equation (36) at maximum confining pressure ($p = 0.95$ bar). Errors in extensional velocity values obtained with the coil and magnet apparatus due to errors in length and frequency measurements are estimated to be less than 1%. The biggest problem inherent in the velocity determination was the dependence of velocity on time and pressure cycling. The velocities at maximum confining pressure of almost all bead specimens increased with time, and, initially, with the pressure cycling involved in determining the dependence of velocity on confining pressure. The velocities in table 3 are the maximum values recorded after a number of pressure cycles had been completed and the experiment was approximately one day old. Approximate rates of change of velocity observed in the first two days of the experiments are given in table 3. Despite these difficulties, the maximum difference in velocities so obtained for different specimens of the same material was about 0.4×10^4 cm/sec, which is equivalent to a maximum error of $\pm$ 5% for the lowest velocities measured.

Poisson's ratios were calculated in the coil and magnet experiments from the ratios of extensional to torsional velocities, yielding an average value of 0.22 for all the bead specimens. The measurement of torsional velocities followed

Reproduced with permission of the copyright owner. Further reproduction prohibited without permission.

the extensional measurements and always required some handling of the samples in preparation for the measurement. Such handling may have decreased the torsional velocity observed relative to the immediately preceding extensional velocity; hence, the calculated Poisson's ratios may be several percent too high.

The variation of velocity with confining pressure, determined by cycling the pressure over a range from about 0.2 to 1 bar, was best expressed as the pressure raised to some exponent. The variation with pressure was found to be independent of frequency or mode of propagation and insensitive to time of measurement, at least over short periods. Many of the exponents given in table 3 are averages of exponents determined for several harmonics and/or for both torsional and extensional vibrations. (The arrows in table 3 indicate a change in the $\partial \ln V / \partial \ln p$ slope with increasing pressure.) Before each recorded pressure cycle, the pressure was cycled a number of times. An average of ten minutes was spent at each pressure in the cycle to allow the specimen to stabilize somewhat. Nevertheless, there was generally some hysteresis between the increasing and decreasing pressure measurements. Even including this hysteresis, however, the error in reproducibility of the exponents was generally less than 20%. Curves of resonance frequency versus confining pressure for

Reproduced with permission of the copyright owner. Further reproduction prohibited without permission.

a number of the specimens are shown in figures 12, 13, 17, and 18. Since length changes during the pressure cycling were too small for measurement, these curves are equivalent to velocity versus pressure curves.

Values of Q^{-1} for all specimens were independent of vibration frequency and amplitude. The values recorded in table 3 are averages of measurements made over a range of frequencies at maximum confining pressure. (For any one specimen, values of Q^{-1} which were greater by as much as 50% or more than the average of the lowest values were disregarded.) Figure 14 shows the relation of average extensional Q^{-1} values for many of the specimens over the frequency range covered by the measurements.

Q^{-1} was also dependent on time and pressure cycling, generally decreasing whenever the velocity increased. The Q_E^{-1} values recorded are those corresponding to an approximate experimental duration of one day. Very approximate initial rates of decrease of Q^{-1} with time (including pressure cycling) are given for some specimens. In comparing the extensional and torsional values of Q^{-1} it should be remembered that the torsional measurements followed the extensional ones and that preparation for the torsional measurements may have disturbed the specimen packing, resulting in an apparent Q_T^{-1}/Q_E^{-1} that is slightly too high.

Reproduced with permission of the copyright owner. Further reproduction prohibited without permission.

A power dependence on pressure was the most satisfactory means for describing the variation of Q^{-1} with confining pressure. Average values of the exponents are given in table 3, and curves of Q^{-1} versus pressure are shown in figures 15 through 18. The variation of Q^{-1} with confining pressure, determined simultaneously with the velocity variation, was generally not as well defined as the velocity variation (figure 17). Also, hysteresis during pressure cycling was often more pronounced (figures 16 and 17). No relation of the pressure variation of Q^{-1} to vibration frequency or mode was observed.

Reproduced with permission of the copyright owner. Further reproduction prohibited without permission.

Reproduced with permission of the copyright owner. Further reproduction prohibited without permission.

TABLE 3.--Results of acoustic experiments on granular aggregates (velocity and Q^{-1} values given for $p_o = 0.95$ bar)

Specimen	Grain Size: Diameter (microns)	Grain Size: Mesh	Lubricant (wt %)	Specimen Density (gm/cc)	Extensional Velocity, V_E (10^4 cm/sec)	Initial Time Dependence of V_E (per day)	Power Dependence of Velocity on Confining Pressure	$Q^{-1} \times 10^2$: Extensional, Q_E^{-1}	$Q^{-1} \times 10^2$: Torsional, Q_T^{-1}	Initial Time Dependence of Q^{-1} (per day)	Power Dependence of Q^{-1} on Confining Pressure	Apparatus
Glass beads	105-53	-140+270	clean	--	3.2	0.2%	1/3.2	1.2	1.4	--	-0.8	vibrator
Glass beads	210-105	-70+140	clean	1.55	3.8	2%	1/3.1	1.6-2.8	--	10-20%	-0.8	coil
Glass beads	590-297	-30+50	clean	--	4.5	1-2%	1/3.0	1.2	2.7	--	-0.3 to -0.8	vibrator
Glass beads	710-350	-25+45	clean	1.58	4.6	1-2%	1/3.3	1.8	2.6	10-20%	-0.5	coil
Crushed glass plate	--	-25+45	clean	(1.43)	4.1	1%	1/3.6→1/5.0	1.7	1.7	--	-0.4	vibrator
Spherical alumina (hard)	--	-80	none	(2.10)	4.6	--	1/4.1	1.3	1.3	--	-0.9	vibrator
Spherical alumina (soft)	--	-80	none	--	3.1	1%	1/3.0	0.8	--	5%	-0.8	coil
Alundum	--	-60	none	2.25	5.6	0%	1/4.6	0.4	--	0%	-0.4	vibrator and coil
Sodium chloride	--	-25+45	none	--	6.0	1-3%	1/5→1/15	1.1	--	--	-0.9 to -0.3	vibrator and coil
Glass beads	590-297	-30+50	~0.01% soap	--	5.6-6.1	2%	1/4.5	1.3	1.3	--	-0.9	vibrator
Glass beads	590-297	-30+50	excess soap	--	7.0	--	1/5.0	2.0	2.0	--	--	vibrator
Glass beads	710-350	-25+45	0.005% sodium stearate	1.68	5.6	2%	1/3.8	2.5	3.1	--	-0.5	coil
Glass beads	710-350	-25+45	0.045% sodium stearate	1.64	6.0	5%	1/3.9	2.3	--	23%	-0.6	coil
Glass beads	105-53	-140+270	excess GE silicone fluid	--	4.5	1%	1/3.3	(3 - 5)		--	-0.7	vibrator
Glass beads	105-53	-140+270	excess Dow silicone fluid	--	5.5	1%	1/4.6	10	10	--	-0.9	vibrator

Reproduced with permission of the copyright owner. Further reproduction prohibited without permission.

TABLE 3.--Continued

Specimen	Grain Size		Lubricant (wt %)	Specimen Density (gm/cc)	Extensional Velocity, V_E (10^4 cm/sec)	Initial Time Dependence of V_E (per day)	Power Dependence of Velocity on Confining Pressure	$Q^{-1} \times 10^2$		Initial Time Dependence of Q^{-1} (per day)	Power Dependence of Q^{-1} on Confining Pressure	Apparatus
	Diameter (microns)	Mesh						Extensional, Q_E^{-1}	Torsional, Q_T^{-1}			
Glass beads	590-297	-30+50	silicone spray	--	5.8	--	1/4.0	7.4	7.4	--	--	vibrator
Glass beads	710-350	-25+45	Siliclad	--	5.1	-0.6%	1/3.8	3.7	5.8	12%	-0.5	coil
Glass beads	710-350	-25+45	0.00063% glycerol	--	5.1	4%	1/3→1/4	1.6	2.6	0%	-1	coil
Glass beads	710-350	-25+45	0.0063% glycerol	--	5.2	5%	1/3→1/4	4.4	--	12%	-0.8	coil
Glass beads	710-350	-25+45	0.0504% glycerol	1.62	5.6	4%	1/4→1/3	9.1	1.0	18%	-0.6	coil
Glass beads	710-350	-25+45	0.0045% oil	1.62	5.5	--	1/3.5→1/4.5	12	9.2	--	-0.6	coil
Glass beads	710-350	-25+45	0.0090% oil	1.62	5.4	--	1/4→1/5	17	--	--	-0.8	coil
Glass beads	710-350	-25+45	MoS_2 spray	--	5.7	0.2%	1/5	2.1	3.1	14%	-0.3→?	coil
Alundum	--	-60	0.0045% oil	2.22	5.6	0%	1/4→1/6	1.2	--	0%	-0.3	coil
Alundum	--	-60	0.010% sodium stearate	2.24	5.8	0%	1/3→1/6	0.9	--	0%	-0.4	coil
Sodium chloride	--	-25+45	excess Dow silicone fluid	--	6.5	5%	1/12.5	6.5	6.5	0%	-0.3	vibrator

IV. DISCUSSION OF ACOUSTIC RESULTS

A. Comparison of Data with Theoretical Expressions for Regular Arrays of Spheres

Extensional velocities and elastic moduli calculated from equations (30) and (31) for propagation along an axis in simple cubic and face-centered cubic arrays of spheres, under a confining pressure of 0.95 bars, are given in table 4 for several materials. The variation in velocity with direction of propagation in the array is small (about 1 - 2% for $\nu = 1/4$) relative to the velocity difference between the arrays. Table 4 is to be compared with table 5 in which the relevant aspects of the data in table 3 have been summarized. (Recall that the predicted power dependence of velocity on confining pressure is 1/6.)

Theoretically expected dependences for Q^{-1}, discussed previously, are reviewed in table 6 for small amplitude wave propagation in a bar of uniform spheres in elastic contact under an isotropic confining pressure and compared with the experimentally observed dependences. Not shown in the table is the dependence of Q^{-1} on contact friction for a given

Reproduced with permission of the copyright owner. Further reproduction prohibited without permission.

contact orientation predicted by both theories. Recall that in Mindlin and Deresiewicz's theory Q^{-1} depends inversely on a limiting coefficient of friction, μ, which, for the purposes of calculation, may be interpreted as either μ_s of μ_k, the usually small difference between the two being unimportant. In White's theory, this difference is very important since $Q^{-1} \propto (\frac{\mu_s - \mu_k}{\mu_k})^2$.

Approximate values of the expected damping associated with the face-centered cubic bars of the different materials are shown in table 7 and compared with experimental values for clean aggregates. In applying the theory of Mindlin and Deresiewicz (equation [33]), the following assumptions were made for all materials: $A = 10^{-6}$ cm, $\lambda = 17.8$ cm, and $p_o = 0.95$ bars. It was assumed that $\mu_s = 1.1\mu_k$ for all calculations according to White's theory (equation [34]).

TABLE 4.--Calculated regular array velocities ($p_o = 0.95$ bars)

Material	Simple Cubic Array			Face-centered Cubic Array		
	$\bar{\rho}$ (gm/cc)	E (dynes/cm^2)	V_E (cm/sec)	$\bar{\rho}$ (gm/cc)	E (dynes/cm^2)	V_E (cm/sec)
Glass	1.31	5.9×10^9	6.7×10^4	1.85	11×10^9	7.7×10^4
Alundum	2.09	25×10^9	9.7×10^4	2.95	36×10^9	11×10^4
Sodium Chloride	1.13	3.8×10^9	5.8×10^4	1.60	7.2×10^9	6.7×10^4

Reproduced with permission of the copyright owner. Further reproduction prohibited without permission.

TABLE 5.--Experimentally observed velocities and dependences

Specimen	Mesh	V_E (10^4 cm/sec) $p \approx 0.95$ bar	Power Dependence of Velocity on Confining Pressure
Glass beads:			
clean	-140+270	3.2	
lubricated		4.5-5.5	
clean	-70+140	3.8	clean 1/3
			lubricated 1/3 to 1/5
clean	-30+50	4.5	
lubricated		5.6-7.0	
clean	-25+45	4.6	
lubricated		5.1-6.0	
Crushed glass:			
clean	-25+45	4.1	1/4→1/5
Angular alundum:			
clean	-60	5.7	1/4 to 1/5
lubricated		5.6-5.8	1/4 → 1/6
Sodium chloride:			
clean	-25+45	6.0	
lubricated		6.5	1/5 to 1/15

Reproduced with permission of the copyright owner. Further reproduction prohibited without permission.

TABLE 6.--Comparison of predicted and observed dependences for Q^{-1}

Theory or Experiment	Form of Dependence for Q^{-1}		
	Wave Amplitude, A	Wavelength, $\lambda = 2\ell/n$	Confining Pressure, P
Mindlin and Deresiewicz	$\propto A$	$\propto 1/\lambda$	$\propto P^{-2/3}$
White	none	none	none
Experimentally observed	none	none	$\propto P^{-1}$ to $P^{-1/3}$

TABLE 7.--Comparison of calculated and observed values of Q^{-1} for clean aggregates

Material	Q^{-1}				
	Mindlin & Deresiewicz		White		Experimental Observations
	$\mu = .25$	$\mu = .1$	$\mu_s = .25$	$\mu_s = .1$	
Glass	2.5×10^{-4}	6.7×10^{-4}	1.5×10^{-2}	1.6×10^{-2}	1.5×10^{-2}
Alundum	8.1×10^{-4}	22×10^{-4}	1.5×10^{-2}	1.6×10^{-2}	0.4×10^{-2}
Sodium chloride	1.6×10^{-4}	4.4×10^{-4}	1.5×10^{-2}	1.6×10^{-2}	1.1×10^{-2}

Reproduced with permission of the copyright owner. Further reproduction prohibited without permission.

In comparing the theoretical expectations with the observed data, the following points should be noted. All measured exponents defining the velocity-pressure relations were greater than or equal to 1/6, except for the sodium chloride specimens, for which the exponents were always less than or equal to 1/5. The closest approach to the theoretically expected exponent was obtained with the lubricated angular alundum aggregates.

Measured velocities of the glass and alundum specimens were generally low compared to the calculated velocities. Lubrication brought the experimental velocities of the glass bead aggregates, but not of the alundum aggregates, into better agreement with the calculated velocities.

Q^{-1} was found to depend on friction, Q^{-1} increasing with lubrication, but the form of the dependence is unclear. The inverse dependence of Q^{-1} on the confining pressure found in all the experiments is inconsistent with both White's theory and the single contact experiments. The observed pressure dependence of Q^{-1} could be consistent with Mindlin and Deresiewicz's theory, but the dependence of Q^{-1} on amplitude and wavelength predicted by their theory was not observed for any of the specimens. It is concluded, therefore, that their theory for the losses associated with small amplitude vibrations is not applicable.

Reproduced with permission of the copyright owner. Further reproduction prohibited without permission.

B. Possible Modifications of Theoretical Expectations for Real Aggregates Suggested by the Experimental Data

Some of the difficulties involved in trying to apply contact theory to irregularly packed aggregates of various sizes and shapes of particles have been discussed earlier. The following discussion attempts to use the above experimental results to define the modifications of regular array contact theory necessary to explain the acoustic behavior of irregular granular assemblages.

B-1. Close and near contacts in aggregates of spherical particles

The velocity-pressure behavior of the specimens studied suggests that the principles of Hertzian contact apply but that there is interference from geometrical factors not considered in the theory. Further support for this argument comes from the agreement of single contact experiments with the theoretically predicted force-displacement relations. The observation that the dependence of velocity on pressure is larger than predicted suggests that the number of close contacts varies with pressure. In addition, the lower than expected values of velocity observed at a given pressure may indicate that there are fewer close contacts per particle than in regular arrays. These suggestions are reasonable in

Reproduced with permission of the copyright owner. Further reproduction prohibited without permission.

view of the earlier discussion of the experiments of Bernal and Mason on random packings of spheres (1960). Exact calculation of the elastic moduli for random aggregates of spheres, including the variation of contacts from near to close, is not possible. Therefore, some limiting approximations will be tried.

Consider the models in figure 21. Both are sections of a simple cubic array of spheres of radius R under an applied confining pressure p. In figure 21b some of the spheres are slightly asymmetrical and, hence, some contacts are not made. The normal force-displacement relation for any contact is given by equation (4):

$$\alpha = \left[\frac{3(1-\nu^2)N}{\sqrt{2R}\,E}\right]^{2/3} \tag{40}$$

The normal force per contact, N, is related to p in the following manner,

$$N = \frac{4R^2 n_s p}{n_c} \quad , \tag{41}$$

where n_s is the number of spheres in either layer, n_c is the number of contacts made in the plane of contacts, and $4R^2 n_s$ is the gross area over which p is applied. If an increment of displacement, $\Delta\alpha$, is now imposed, the corresponding increment of force is

$$\Delta F_N = n_c \Delta N . \tag{42}$$

Reproduced with permission of the copyright owner. Further reproduction prohibited without permission.

The increment of average stress is defined as

$$\Delta\sigma_{yy} = \Delta F_N / 4R^2 n_s \ , \tag{43}$$

and the increment of average strain as

$$\Delta\varepsilon_{yy} = \Delta\alpha / 2R \ . \tag{44}$$

The modulus for extensional wave propagation is, from equations (40) through (44),

$$\frac{\Delta\sigma_{yy}}{\Delta\varepsilon_{yy}} = \left(\frac{n_c}{n_s}\right)^{2/3}\left[\frac{3E^2p}{8(1-\nu^2)^2}\right]^{1/3} \ . \tag{45}$$

Note that for $n_c = n_s$ equation (45) is equivalent to equation (31). Letting primed quantities refer to figure 21b and unprimed quantities to figure 21a, the modulus for figure 21b may be written in terms of that for figure 21a ($n_c = n_s$),

$$\bar{E}' = \left(\frac{n_c'}{n_c}\right)^{2/3}\bar{E} \ , \tag{46}$$

and, if the bulk densities ($\bar{\rho}$) of the two models differ only slightly,

$$V_E' = \left(\frac{n_c'}{n_c}\right)^{1/3}V_E = \left(\frac{n_c'}{n_c}\right)^{1/3}\left[\frac{3E^2p}{8(1-\nu^2)^2}\right]^{1/6}\frac{1}{\sqrt{\bar{\rho}}} \ . \tag{47}$$

The expected value of n_c'/n_c is n'/n, where n is the average number of close contacts per sphere based on geometrical considerations and n' is the actual average number. If n'/n increases with pressure, the exponent giving the dependence of velocity on pressure will be greater than 1/6 until n' reaches some constant value, $n' \leq n$. Thus, not only is the velocity decreased by missing contacts, but the velocity-pressure dependence may be increased.

Reproduced with permission of the copyright owner. Further reproduction prohibited without permission.

No energy is dissipated during the displacements as described above since no slip occurs (or is permitted) at any of the contacts. If a tangential displacement is imposed instead of a normal displacement, maximum energy will be dissipated. Following the same procedure as above, the tangential modulus for figure 21b is

$$\frac{\Delta\sigma_{xy}}{\Delta\varepsilon_{xy}} = \left(\frac{n'}{n}\right)^{2/3} \frac{2(1-\nu)}{2-\nu} \left[\frac{3E^2p}{8(1-\nu^2)^2}\right]^{1/3} . \tag{48}$$

The expression for the energy dissipated per cycle per contact as determined by single contact experiments and derived by White is of the form (see equations [6] and [25])

$$\Delta W_c = \frac{2B(2-\nu)(1+\nu)}{Eb} \Delta T^{*2}, \tag{49}$$

where B is a constant $\left[B = \left(\frac{\mu_s-\mu_k}{\mu_k}\right)^2 \text{ in White's theory}\right]$. Noting that

$$\Delta T^* = 4R^2\left(\frac{n}{n'}\right)\Delta\sigma^*_{xy}$$

and, from equations (2) and (41), that

$$b = R\left[\frac{3(1-\nu^2)np}{En'}\right]^{1/3},$$

equation (49) may be rewritten as

$$\Delta W_c = 64B\frac{(1-\nu)}{(2-\nu)}R^3\left(\frac{n}{n'}\right)^{1/3}\left[\frac{3E^2p}{8(1-\nu^2)^2}\right]^{1/3}\varepsilon^{*2}_{xy} .$$

The number of contacts losing energy per unit volume is $n'/8nR^3$, and, hence, the energy dissipated per unit volume

Reproduced with permission of the copyright owner. Further reproduction prohibited without permission.

per cycle is

$$\Delta W = 8B \frac{(1-\nu)}{(2-\nu)} \left(\frac{n}{n'}\right)^{1/3} \left[\frac{3E^2 p}{8(1-\nu^2)^2}\right]^{1/3} \varepsilon_{xy}^{*2} \cdot \qquad (50)$$

The maximum energy stored per unit volume per cycle may be calculated from the expression $W = 1/2\, \Delta\sigma_{xy}^{*}\, \Delta\varepsilon_{xy}^{*}$ and is

$$W = \frac{(1-\nu)}{(2-\nu)} \left(\frac{n}{n'}\right)^{1/3} \left[\frac{3E^2 p}{8(1-\nu^2)^2}\right]^{1/3} \varepsilon_{xy}^{*2} \cdot \qquad (51)$$

From equations (50) and (51),

$$Q^{-1} = \frac{\Delta W}{2\pi W} = \frac{4}{\pi} B \cdot$$

Thus, although both ΔW and W depend on n'/n and p, Q^{-1} is independent of both.

A more realistic model is obtained if the previous models are expanded vertically to include more layers of spheres. If an increment of normal displacement is applied along any axis in such an expanded array with all contacts made, the modulus is again given by equation (45) with $n_c = n_s$ and no energy is dissipated. Now, however, removal of one contact, perpendicular to the direction of displacement as before, in the interior of the array gives rise to tangential forces at contacts merely as a result of the preloading pressure. Application of an increment of normal displacement during wave propagation will result in additional tangential forces or displacements with their accompanying energy

Reproduced with permission of the copyright owner. Further reproduction prohibited without permission.

dissipation. The modulus for the array is again lowered by the missing contact, but the relation is now modified by the inclusion of tangential contact moduli. The maximum energy stored per cycle, which is proportional to the array modulus, decreases with the removal of the contact, while the energy dissipated per cycle increases as a result of the added tangential contact displacements. Q^{-1} is, therefore, no longer zero, as it was for normal displacements in the simpler array discussed above, and is expected to decrease as the confining pressure increases (and more close contacts are made).

A somewhat different approach to the problem of close and near contacts is to assume a distribution of forces among the contacts supporting the load. The following discussion, which treats this latter approach, is a modification of Archard's model of microscopic contact between macroscopically flat surfaces (1953).

Consider a model similar to that in figure 21, but now let the vertical and horizontal arrangement of spheres in the bottom layer be defined by a distribution function h. Relative to any sphere in the uniform top layer, the function h describes the change in the number of neighbors (and, therefore, possible contacts) with distance as measured perpendicularly from the top plane. For small normal displacements of the layers, $y << R$, where R is the sphere radius, h

Reproduced with permission of the copyright owner. Further reproduction prohibited without permission.

may be taken to be approximately independent of displacement. (See earlier discussion of Beresford's radial distribution function in chapter I, section C-1.) The expected total number of contacts that will be made by a sphere in the top layer on application of a displacement (or decrease in separation) y is hy. Now let the bottom plane be fixed and the separation between the two layers be such that, initially, contact is just about to be made between spheres in the two layers. The initial position, so defined, of the top plane will be taken as $y = 0$. All contacts will be considered to be normal ones, i.e., tangential forces are ignored in this approximation. Recall that the normal force on two spheres compressed by an amount y is (equation[4])

$$N = \frac{\sqrt{2R}\, E\, y^{3/2}}{3\,(1-\nu^2)} \quad .$$

If the top layer of spheres is now rigidly displaced toward the bottom layer by an amount $y = \Delta y + 2\Delta y \ldots + m\Delta y$, or equivalently, $y = y_1 + y_2 + \ldots + y_m$, the total force on the layer is

$$F_N = \frac{\sqrt{2R}\, E}{3(1-\nu^2)} \sum_{k=1}^{m} n_s\, h\, \Delta y\, y_k^{3/2} \quad , \qquad (52)$$

where n_s = the total number of spheres in the top layer. Approximating the sum as an integral and integrating yields

$$F_N = \frac{2\sqrt{2R}\, E\, n_s\, h\, y^{5/2}}{15\,(1-\nu^2)} \quad . \qquad (53)$$

Reproduced with permission of the copyright owner. Further reproduction prohibited without permission.

If an additional increment of displacement is now applied, the corresponding increments of average stress and strain are

$$\Delta\sigma_{yy} \approx \frac{\Delta F_N}{4 n_s R^2}$$

and

$$\Delta\varepsilon_{yy} \approx \frac{\Delta Y}{2R} .$$

The elastic modulus for the system is, then,

$$\bar{E} = \frac{\Delta\sigma_{yy}}{\Delta\varepsilon_{yy}} \approx \frac{5}{4R}\left[\frac{2\sqrt{2R}\,E\,h}{15(1-\nu^2)}\right]^{2/5}\left(\frac{F_N}{n_s}\right)^{3/5},$$

or in terms of the average pressure p on the layers,

$$\bar{E} \approx 5\left[\frac{\sqrt{2}\,RE\,h}{30(1-\nu^2)}\right]^{2/5} p^{3/5} . \qquad (54)$$

The important result of this model is that the velocity varies as the 1/3.3 power of pressure rather than the 1/6 power. The dependence on R is cancelled by h, which is inversely proportional to R (see discussion of Beresford's distribution function). To obtain values of velocity comparable to the experimentally determined values for the clean -25+45 mesh glass beads, hR should be of the order 10^5.

Neither of these two illustrations has taken into account the case where no new contacts are added but instead the already existing contacts become more uniformly loaded as pressure increases. For example, assume that in the illustration 21a the height of the spheres above the planes

Reproduced with permission of the copyright owner. Further reproduction prohibited without permission.

varies slightly, such that some contacts are more heavily loaded than others under the same total force F_N as before. If the planes are now compressed by an amount $\Delta\alpha$ as before, the modulus calculated will be lower than that for the uniformly loaded case. Moreover, should increasing the total load on the array increase the uniformity of contact loads, the array modulus would increase with pressure faster than the 1/3 power of pressure. Consequently, the velocity-pressure exponent would be greater than 1/6 until all the contacts were uniformly loaded.

In both the second missing contact model (the modification of Archard's treatment) and the nonuniform contact case, no energy dissipation occurs when the applied displacement is normal. If an increment of tangential displacement is applied, the calculation of Q^{-1} based on White's theory or on single contact experiments again yields a constant value, as long as all contacts both store and dissipate energy. However, the possibility now arises of having lightly made contacts that slide (gross slip occurring when $T \geq \mu N$) under the increments of displacement or force associated with wave propagation. Such contacts would store no energy. As confining pressure is increased, these lightly made contacts would become "locked-in" contacts that dissipate energy through <u>slipping</u> ($T < \mu N$) rather than <u>sliding</u>

Reproduced with permission of the copyright owner. Further reproduction prohibited without permission.

and also store energy. The second missing contact model, with its linear distribution of contacts (hy), suggests a situation in which the number of light or sliding contacts ("new" contacts) remains constant with increasing pressure, while the number of "locked-in" contacts ("old" contacts) increases. For this case,

$$\Delta W = n_{slide}\ \Delta W_{slide} + n_{lock}\ \Delta W_{lock}$$

and

$$W = n_{lock}\ W_{lock},$$

where n = number of contacts. Assuming White's type of damping for the "locked-in" contacts, Q^{-1} is constant with increasing pressure if $n_{slide} = 0$; if n_{slide} is constant or if n_{slide} decreases with increasing pressure (i.e., if h decreases with y), Q^{-1} decreases with increasing pressure.

Simple cubic packings have been used in the above illustrations for computational convenience and because the number of contacts per sphere in simple cubic packings is comparable with the number of close contacts per sphere in random packings. Turning now to a closer examination of some of the experimental data, the model discussions suggest interpretations of several features of the data.

Time dependence of velocity and Q^{-1} in aggregates. With few exceptions, the velocities of all glass bead, spherical alumina, and sodium chloride specimens measured at maximum

Reproduced with permission of the copyright owner. Further reproduction prohibited without permission.

confining pressure increased from 1/2 to 10% during the first two days of the experiment. Part of the time effects were due to disturbances of the packing resulting from the pressure cycling used to determine the velocity dependence on pressure. The first few pressure cycles usually increased the velocity measured at their termination (at maximum confining pressure) and contributed to a steeper rise of velocity with time at the beginning of the experiment than was observed later. (Even without the pressure cycling, however, the rate of change was steepest during the initial part of the experiment.) By the second day of the experiment, the velocity measured after a pressure cycle was usually decreased, sometimes by several percent, the decrease being recoverable after several hours. One specimen of clean glass beads was studied for 30 days, at the end of which the velocity was still increasing with time at a rate of about 0.1% a day.

Although the Q^{-1} measurements were less consistent than the velocity measurements, Q^{-1} usually decreased whenever the velocity increased. The average change recorded over the two day period was 20-40%. In general, the increase in velocity, and hence in the energy stored, was not sufficient to account for the decrease in Q^{-1}; and therefore the energy dissipation, ΔW, must also have decreased.

Reproduced with permission of the copyright owner. Further reproduction prohibited without permission.

The increase of velocity with time, including the initial pressure cycling effects, may be explained by the making of more close or "locked-in" contacts or more uniformly loaded contacts. Excluding the packing disturbances due to cycling, the small relative displacements of grains with time, permitting the rearrangement, probably occurred by creep at tangentially stressed contacts. The relaxation of tangential stresses at contacts would also increase the velocity. The decrease of velocity resulting from the later pressure cycles indicates that a minimum volume for the packing, at that time, had been reached and any disturbance could only increase the volume, i.e., decrease the number of contacts. The decrease of ΔW with time or pressure cycling indicates that ΔW decreased with the making of more close or uniformly loaded contacts. In view of the previous discussion, this observation suggests that a major portion of the initial energy loss might have been due to slip at those contacts where the tangential stresses were being relaxed with time or relieved by rearrangements during pressure cycling, or to sliding at lightly loaded contacts, the number of which was being reduced with time or pressure cycling.

Increase of velocity of bead aggregates with lubrication. Lubrication of the glass bead aggregates increased the velocity from 10 to 50% and, in some cases, the rate of

Reproduced with permission of the copyright owner. Further reproduction prohibited without permission.

change of velocity with time. The highest velocity obtained for very small additions of lubricants to the glass bead specimens was 6.0×10^4 cm/sec. Addition of excess soap resulted in the maximum velocity measured, about 7.0×10^4 cm/sec. Note that these maximum values are approaching the velocities calculated above for regular arrays of glass spheres in complete elastic contact (table 4).

The bulk densities of the bead specimens also increased by about 3-4% with lubrication. This increase was not due to the added weight of the lubricant. For the maximum weight percent of lubricant added, the change in bulk density, assuming constant bulk volume, was about 0.05%.

The simplest and most consistent explanation for the velocity and density increases with lubrication is that the lubricants facilitated the same processes that occurred with time in unlubricated specimens by decreasing the contact friction. In addition to increasing the number of close contacts, it is possible that the lubricants also effected some sort of better acoustic coupling at contacts, analogous to the increased coupling observed when a thin film of liquid wets the interface between two glass plates. The small radius of curvature at contacts would work against this effect. If the lubricant coupling effect were strong, then some similar coupling should have occurred in the alundum

Reproduced with permission of the copyright owner. Further reproduction prohibited without permission.

specimens. However, the velocity (and density) of the alundum specimens were unchanged by lubrication, although changes in Q^{-1} and the velocity-pressure dependence did occur that were similar to those occurring with lubrication of the bead specimens.

The effects of lubrication on Q^{-1} are complicated by the variation of contact friction as well as the changing number of contacts and this subject will be taken up later.

Pressure dependence of velocity and Q^{-1} of spherical particle aggregates. The missing contact and the nonuniform contact illustrations predict a variation of velocity with pressure raised to a power greater than 1/6 as long as the number of close or uniform contacts continues to increase with increasing pressure. The velocity-pressure exponent of about 1/3 derived explicitly in the second missing contact model is the exponent obtained for specimens of clean glass beads and spherical alumina. Lubrication of the beads generally lowered the exponent to about 1/4 to 1/5. This lowering of the slope can be related to contacts becoming more uniformly loaded or to the changing numbers of near contact available to become close contacts with increasing pressure.

Consider the first missing contact model (figure 21). Taking $V_E = V_E(n', p)$, one obtains

$$dV_E = \left(\frac{\partial V_E}{\partial n'}\right)_p dn' + \left(\frac{\partial V_E}{\partial p}\right)_{n'} dp \,.$$

Reproduced with permission of the copyright owner. Further reproduction prohibited without permission.

If the form of V_E is similar to equation (47) and if n' = n'(p), the above equation may be rewritten as

$$\frac{d\ln V_E}{d\ln p} = \frac{1}{3}\frac{d\ln n'}{d\ln p} + \frac{1}{6} . \qquad (55)$$

The experimentally obtained values of $d\ln V_E/d\ln p$ for the glass beads were inserted in equation (55) to yield the values of $d\ln n'/d\ln p$ given in table 8. If it is assumed that the differences in velocity in table 8 are due to differences in n' as predicted by equation (47), then the ratios of velocities at a particular pressure give the ratios of n''s. For the purposes of comparison, n' for the clean -140+270 mesh beads was taken to be 1 and the remaining n''s calculated accordingly. The estimates in table 8 of $dn'/d\alpha$, the change in the number of close contacts with displacement, were then calculated from the relation

$$\frac{dn'}{d\alpha} = \frac{dn'}{dp}\frac{dp}{d\alpha} = \frac{n'}{p}\frac{d\ln n'}{d\ln p}\frac{dp}{d\alpha} , \qquad (56)$$

where

$$\frac{dp}{d\alpha} \approx \frac{1}{2R}\frac{\Delta\sigma_{yy}}{\Delta\varepsilon_{yy}} = \frac{1}{2R}\bar{\rho}V_E^2$$

and V_E is the experimentally determined velocity.

Comparing the estimates in table 8, $dn'/d\alpha$ is approximately constant (i.e., independent of n') for the clean bead specimens according to this missing contact model. Relative

Reproduced with permission of the copyright owner. Further reproduction prohibited without permission.

Reproduced with permission of the copyright owner. Further reproduction prohibited without permission.

TABLE 8.--Estimates of $dn'/d\alpha$, according to the first missing contact model, for bead aggregates ($p = 0.95$ bar)

Glass Bead Specimens	Measured Velocity V_E at $p = 0.95$ bars (cm/sec)	Measured Averages of $\frac{d \ln V_E}{d \ln p}$	Calculated Values of $\frac{d \ln n'}{d \ln p}$	Calculated Values of	
				$\frac{Rdn'}{d\alpha}$	$\frac{dn'}{d\alpha}$ (cm^{-1})
-25+45 mesh: clean	4.6×10^4	1/3.3	.41	2×10^3	7×10^4
lubricated	$5.1\text{-}6.0 \times 10^4$	1/3.95	.26	$2\text{-}5 \times 10^3$	$9\text{-}20 \times 10^4$
-30+50 mesh: clean	4.5×10^4	1/3.0	.50	2×10^3	10×10^4
lubricated	$5.6\text{-}6.0 \times 10^4$	1/4.2	.24	$3\text{-}5 \times 10^3$	$15\text{-}22 \times 10^4$
lubricated	7.0×10^4	1/5.0	.10	4×10^3	19×10^4
-70+140 mesh: clean	3.8×10^4	1/3.1	.47	0.9×10^3	11×10^4
-140+270 mesh: clean	3.2×10^4	1/3.2	.42	0.3×10^3	8×10^4
lubricated	4.5×10^4	1/3.3	.41	2×10^3	45×10^4
lubricated	5.5×10^4	1/4.6	.15	2×10^3	44×10^4

to the corresponding clean specimens the lubricated specimens have significantly higher values of $dn'/d\alpha$. Also, based on the relations in (56), $dn'/d\alpha$ for the clean specimens is essentially independent of pressure (from 0 to 1 bar) but varies inversely with pressure for the lubricated specimens. Hence, the deductions from this model suggest that lubrication compresses the near neighbor distribution around any sphere, as well as increasing the number of close contacts. That is, the near neighbors (or near contacts) of a sphere have moved closer to the sphere, and the distribution of near contacts tails off more rapidly with distance from the sphere than is the case in the clean specimens. This conclusion is supported by the increase in bulk density with lubrication.

As indicated in table 8, for $n' = 1\text{-}10$, $R\,dn'/d\alpha$ must be of the order 10^3 to derive the experimentally obtained glass bead velocities at maximum confining pressure. The similar quantity, Rh, in the second missing contact model (the modification of Archard's treatment) must be of the order 10^5. This last observation points out once again that the velocity increases more rapidly with the addition of uniformly loaded close contacts (n') than with the same number of non-uniformly loaded contacts. Estimates of $Rdn'/d\alpha$ or Rh for the -25+45 beads calculated from Beresford's radial

Reproduced with permission of the copyright owner. Further reproduction prohibited without permission.

distribution function or directly from Bernal and Mason's experimental data (see chapter I, section C-1) are of the order $10\text{-}10^2$. The discrepancy between these estimates and the experimentally obtained estimates might be the result of neglecting the increasing uniformity of contacts with pressure or of assuming the contact areas between spheres to be continuous (i.e., neglecting asperities).

The second missing contact model can be modified to account for the lowering of $d\ln V_E/d\ln p$ with lubrication (more close contacts) if h is not constant but instead is allowed to decrease with the total number of close contacts made or with increasing pressure. The velocity-pressure exponent would then decrease with increasing pressure for any one specimen.

Since increasing pressure has the same effect as lubrication in that the number of close contacts are increased and the bulk volume decreased, $dn'/d\alpha$ (or h) and $d \ln V_E/d \ln p$ are expected to decrease at higher pressures with increasing pressure for any specimen. Finally, of course, all contacts will be made and $dn'/d\alpha$ (or h) will go to zero and $d \ln V_E/d \ln p$ should go to 1/6. Some turning over of the $d \ln V_E/d \ln p$ slope with pressure was observed for a number of the lubricated specimens described here. In the vibration experiments of Duffy (1959) and of Duffy and Mindlin

Reproduced with permission of the copyright owner. Further reproduction prohibited without permission.

(1957) on regular arrays of steel balls, $d\ln V_E/d\ln p$ turned over from about 1/3 to 1/6 as confining pressure increased from about 0 to 1 bar. However, in the experiments of Gardner et. al. (1964) on irregularly packed sands and glass sphere aggregates V_E was still increasing with about the 1/4 power of pressure at confining pressures greater than 10^2 bars. The greater stability of the slope for the sand and glass bead aggregates reflects the greater number of near contacts and perhaps nonuniformly loaded contacts in irregularly packed aggregates than in regularly packed arrays. An additional source of near contacts in glass bead or sand aggregates might result from the fracturing of grains with increasing load.

As discussed previously, the variation of Q^{-1} with confining pressure was less consistent than the velocity variation. There was frequently more change of slope ($d\ln Q^{-1}/d\ln p$) with increasing pressure and more pronounced hysteresis with pressure cycling than was observed in the velocity measurements for the same specimen (figure 17). On the average, Q^{-1} for both clean and lubricated beads decreased with the -1/1.2 to -1/2.5 power of pressure (figures 15 and 17). Noting that the pressure dependence of W is given by pV_E^2, the pressure dependence of ΔW may be derived from the variation of Q^{-1} with pressure. The ΔW-pressure exponents so

Reproduced with permission of the copyright owner. Further reproduction prohibited without permission.

obtained were generally negative and ranged from -1/3 to essentially zero. This decreasing of ΔW with increasing pressure is probably related to an increasing number of close or "locked-in" contacts, as discussed earlier with regard to the time dependence.

B-2. Particle size

A decrease in velocity with decreasing grain size was observed in the smaller sizes of clean glass beads (figure 19). The velocity-mean diameter relationship can be described by $V_E \propto d^m$, where m is about 1/5. It has been noted earlier that porosity increases with decreasing grain size for the finer sizes of beads, and this effect is probably related to the variation of velocity with grain size. Before further discussion, however, external factors or boundary conditions possibly contributing to this effect should be considered.

In samples of irregularly packed uniform spheres held in large non-rigid containers, the container boundaries have been found to produce a more regular packing in the outer layers of the sample (Bernal and Finney, 1967). These ordered layers have a higher density and a greater number of contacts per sphere than the interior packing. For constant container volume, the ordering penetrates deeper as the sphere size increases; hence, the sample velocity should increase as the sphere size increases.

Reproduced with permission of the copyright owner. Further reproduction prohibited without permission.

There are strong arguments against the observed velocity dependence on grain size being the result of such ordering. First, as Bernal and Finney (1967) point out, the ordered skin layers break down for containers with small radii of curvature such as those used in these experiments. Second, each bead specimen in these experiments consisted of a range of spherical particle sizes with some 10-15% irregular particles. Regular ordering in such aggregates is more difficult to achieve than in aggregates of uniform spheres.

The size effect is therefore considered to be real. It is possible to explain both the decrease in velocity and the increase in porosity in terms of the missing contact models. For example, n' at a particular pressure may decrease with decreasing grain size. Note that interpretation of the data in terms of the first missing contact model (table 8) indicates that $dn'/d\alpha$ is constant for all clean bead specimens regardless of bead size. This is equivalent to saying that the distance between neighboring sphere centers remains constant while the average sphere radius R decreases. The quantity that is expected to be independent of grain size or R is $R\, dn'/d\alpha$. In the second missing contact model if it is h rather than Rh that is independent of R, then the velocity given by equation (54) increases as the 1/5 power of R. Such changes in the near neighbor distribution with

Reproduced with permission of the copyright owner. Further reproduction prohibited without permission.

decreasing grain size might be related to the greater effect of surface forces or the increasing importance of surface roughness relative to the particle volume.

B-3. Particle shape

Neither the bulk density nor the velocity of the alundum aggregates increased with time or lubrication. Moreover, the log velocity-log pressure slope was generally lower and changed more with pressure for the clean angular particles than for the clean beads (figure 12). Lubrication of the alundum specimens resulted in slopes that approached 1/6 with increasing confining pressure, the expected Hertzian behavior (figure 18). In view of the previous discussion, these observations indicate that there were fewer close contacts being made with time or pressure in these aggregates than in the bead aggregates. That is, at a confining pressure of about 1 bar, the ratio n'/n was approaching a constant value or h was approaching zero. This conclusion is intuitively reasonable considering the interlocking structure of angular particle packings.

The difference between the experimentally determined velocities and the calculated regular array velocities is greater for the angular alundum and crushed glass aggregates than for the glass bead aggregates. Calculation of the alundum velocity according to the first missing contact

Reproduced with permission of the copyright owner. Further reproduction prohibited without permission.

model, using reasonably small values of n'/n, still results in a large discrepancy between the expected and the observed velocity. However, additional lowering of the expected velocity may be obtained through a correction to the spherical particle model to account for the difference between the average particle radius and the average radius of curvature near the contact. Consider the compression by load N of two approximately spherical particles of average radius R which have surface irregularities of small relief compared to R. Assuming that, for each particle, the region near the contact is spherical with radius of curvature R', the force-displacement relation is simply

$$\alpha = \left[\frac{3(1-\nu^2)N}{\sqrt{2R'}\,E}\right]^{2/3} .$$

The average pressure is defined in terms of the average particle radius R,

$$p \approx N/4R^2,$$

and similarly the ratio of average stress to average strain is given by

$$\frac{\Delta\sigma}{\Delta\varepsilon} \approx \left(\frac{\Delta N}{4R^2}\right) \Big/ \left(\frac{\Delta\alpha}{2R}\right) .$$

It follows then that the extensional velocity along an axis of a simple cubic packing of such particles, with all contacts made, is

Reproduced with permission of the copyright owner. Further reproduction prohibited without permission.

$$V_E' \approx \left(\frac{R'}{R}\right)^{1/6} \left[\frac{3E^2 P}{8(1-\nu^2)^2}\right]^{1/3} \frac{1}{\sqrt{\bar{\rho}}} = \left(\frac{R'}{R}\right)^{1/6} V_E \,, \qquad (57)$$

where V_E and $\bar{\rho}$ are the corresponding velocity and bulk density in a simple cubic array of uniform spheres. A second type of contact between irregular particles can be modeled by contact of one of the above described irregular particles with a plane (infinite radius of curvature). In this case, equation (57) becomes

$$V_E' \approx \left(\frac{2R'}{R}\right)^{1/6} V_E \,. \qquad (58)$$

Based on microscopic examination of the alundum and crushed glass aggregates, it is estimated that many contacts occurred at points where R' was 0.1R or less. For these aggregates, then, the velocity expected from equations (57) and (58) is approximately 2/3 to 3/4 V_E. This modification for shape may, of course, be included in either of the missing contact models.

Q^{-1} of the clean alundum specimens was the lowest measured. The small Q^{-1} might be related to the smaller number of contacts being made with increasing pressure than in the bead aggregates or to the surface properties of the alundum grains. Since the Q^{-1} of the clean crushed glass was essentially the same as that of the clean beads, the latter alternative is favored.

Reproduced with permission of the copyright owner. Further reproduction prohibited without permission.

Q^{-1}- pressure exponents of -1/2.5 to -1/3.7 were obtained for the clean and lubricated angular particle specimens, compared to exponents of -1 to -1/2.5 for the bead specimens (figures 15 and 18). Energy dissipation per cycle was approximately independent of pressure or tended to increase with increasing pressure. These observations suggest that the processes predominantly responsible for the energy dissipation in these experiments differed from those in the bead specimens.

B-4. Plastic deformation at contacts

The measured velocities of the sodium chloride aggregates are bracketed by the velocities calculated for the simple cubic and face-centered cubic arrays of sodium chloride spheres. In contrast, the measured velocities of all but a few of the aggregates of other materials fall significantly below their corresponding regular array values. Moreover, the velocity-pressure exponents for the sodium chloride aggregates ranged from 1/5 to 1/15 (and in one case 1/40), compared to 1/3 to 1/6 for all other aggregates. A possible explanation is that plastic deformation occurred at the sodium chloride contacts.

During the initial compression of two smooth spherical surfaces in contact, plastic deformation begins whenever the maximum shear stress at about 1/2 b (where b is the radius

Reproduced with permission of the copyright owner. Further reproduction prohibited without permission.

of the elastic contact circle) beneath the center of the contact surface exceeds the shear strength of the material. As the load N is further increased, the plastic deformation spreads rapidly to include the whole contact region (full plasticity). While the condition of full plasticity exists, the area of contact $a \approx N/Y$, where Y is the yield strength of the bulk material (see chapter I, section C-2). If the load N is now reversed at N* and cycled between 0 and N*, the contact area behaves elastically, i.e., $a \propto N^{2/3}$, if the surfaces do not adhere. Thus, although such contacts deform plastically during the initial application of a confining pressure, the velocity-pressure exponent obtained upon cycling the pressure should still have a value of 1/6 as predicted by the elastic relations. The magnitude of the velocity, however, will be greater than that calculated from the elastic relations in which the radius of curvature at the contact is equal to the particle radius. The discrepancy occurs because the radius of curvature near the contact, R', is greater than R, the initial radius of curvature, as a result of the plastic deformation. Following the same arguments that led to equation (57), the velocity after plastic deformation, V_{EP}, is given by the relation

$$V_{EP} = \left(\frac{R'}{R}\right)^{1/6} V_E \quad , \qquad (59)$$

Reproduced with permission of the copyright owner. Further reproduction prohibited without permission.

where V_E is the velocity without plastic deformation. Taking the yield stress Y of sodium chloride to be about 10^4 bars (Bowden and Tabor, 1964), the area of contact of two sodium chloride spheres of radius R deforming plastically under a pressure of 1 bar is about $2 \times 10^{-4} R^2$. To make the ratio of observed velocity to calculated velocity (calculated for a simple cubic array) for the sodium chloride aggregates equal to the same ratio for the clean glass beads, equation (59) predicts a contact area of about $5 \times 10^{-4} R^2$. However, as noted above, the difference in the radii of curvature does not explain the low velocity-pressure exponents obtained for the sodium chloride.

If the surfaces of contact weld together strongly during plastic deformation, the elastic recovery which occurs when the load is decreased from N* may be insufficient to break the adhered junctions. In this case, the area of contact will change only little during the pressure cycling. Consequently, the velocity-pressure exponent will have a value between 1/6 and 0. For the extreme case of zero exponent, the grains may be thought of as welded together at a number of asperities. If the asperities are then idealized and treated as parallelepipeds, the ratio of the longitudinal modulus for two cubic grains in welded contact, $\bar{E}$, to the material modulus, E, is

Reproduced with permission of the copyright owner. Further reproduction prohibited without permission.

$$\frac{\bar{E}}{E} \approx \frac{1}{1 + \frac{1}{2}\sqrt{\frac{a_a}{a_r}}} , \qquad (60)$$

where a_a is the apparent area of contact and a_r is the real area (i.e., the area of welded regions). Using the sodium chloride aggregate modulus obtained at maximum confining pressure for $\bar{E}$, $\bar{E}/E$ is approximately 1/50, and hence equation (60) predicts a value of a_r/a_a of 4×10^{-4}. This value is to be compared with that expected for plastic deformation at p = 1 bar, $a_r/a_a = p/Y \approx 10^{-4}$.

Explanation of the experimental data probably involves both types of behavior described above, as well as some making and breaking of contacts as discussed previously. The velocity of the sodium chloride aggregates increased to some extent with both time and lubrication, as did the glass bead velocities. Also, the damping or Q^{-1} dependence on pressure of the sodium chloride aggregates was similar to that observed for the glass bead and alundum aggregates. The Q^{-1}-pressure exponent varied from about -1 to -1/3 (figure 15), and the energy dissipated generally decreased with increasing pressure. Moreover, lubrication raised Q^{-1} as it did in the other aggregates. It is likely that the energy dissipation in the sodium chloride aggregates is the result of the same processes that occur in the elastically deforming aggregates.

Reproduced with permission of the copyright owner. Further reproduction prohibited without permission.

B-5. Friction, lubrication, and Q^{-1}

The decrease of Q^{-1} with increasing pressure indicates that losses other than internal material hysteretic losses are predominant in the pressure range investigated here. If the damping were a material property rather than a contact property, Q^{-1} would be independent of pressure in the experimental pressure range. In particular, the correlation between decreasing Q^{-1} and increasing velocity with time, pressure cycling, and increasing pressure suggests that the values of Q^{-1} observed in these experiments reflect in large part processes associated with light or missing contacts.

The increasing of Q^{-1} with lubrication of both bead and alundum specimens is attributed to the lowering of contact friction according to the following arguments. First, lubrication increased the number of close contacts in the bead specimens as well as increasing the values of Q^{-1}. However, the number of contacts also increased with time, while Q^{-1} decreased. Moreover, different lubricants had different effects on Q^{-1} but similar effects on velocity and density and hence on the number of contacts per particle. Therefore, the major effect of lubrication on the Q^{-1} at a particular pressure is concluded to be unrelated to the changing numbers of contacts with lubrication. Second, lubrication did not alter the Q^{-1} dependence on pressure, indicating the same processes at work in both clean and lubricated

Reproduced with permission of the copyright owner. Further reproduction prohibited without permission.

specimens. Fractional energy losses in the fluid lubricant films are expected to depend on frequency. As discussed previously, no frequency dependence was observed. Finally, the amounts of lubricants added were equivalent to the surface area of the samples, and there was no evidence from the velocity measurements that these small amounts affected the force-displacement relations at close contacts. It is concluded, therefore, that Q^{-1} for these aggregates is inversely related to contact friction.

Increasing the amount of a particular fluid lubricant increased Q^{-1} (figure 20). In addition, an increase of Q^{-1} with increasing fluid viscosity was indicated. The solid lubricants, soap or sodium stearate, were less effective than the fluid lubricants in raising Q^{-1}, and increasing the amount of soapy lubricant made little change in Q^{-1}. This difference in lubricant behavior is probably related to the adhesive properties of the soapy lubricants. Under low loads, as in these experiments, lubrication with such lubricants frequently leaves the coefficient of friction unchanged, although at higher loads they are very effective lubricants (Bowden and Tabor, 1954, 1964). An alternative explanation is that the fluid lubricants increased the difference between μ_s and μ_k more than the soapy lubricants, analogous to the increased stick-slip motion observed with

Reproduced with permission of the copyright owner. Further reproduction prohibited without permission.

many fluid lubricants (Bowden and Tabor, 1954, 1964). This latter explanation would support White's theory.

At higher pressures, Q^{-1} of glass bead aggregates becomes independent of pressure. In the experiments of Gardner et. al. (1964) on quartz sand and glass beads, Q^{-1} became approximately constant (0.8×10^{-3} and 2.7×10^{-3}, respectively) at pressures of 10 to 100 bars. In applying White's theory, μ_s would have to be about 1.03 μ_k in order to get these low values of Q^{-1}.

The observations may be summarized as follows. Energy dissipation in granular aggregates at low pressures predominantly results from slipping or sliding at contacts. Q^{-1} decreases with increasing friction, and the pressure dependence of Q^{-1} reflects the making of contacts or more uniformly loaded contacts with increasing pressure. At present, there is no theory which adequately explains these observations.

Reproduced with permission of the copyright owner. Further reproduction prohibited without permission.

V. COMPRESSION TESTS

Compression tests were performed on the same types of granular aggregates that were studied acoustically. The objectives of the tests were to study the effects of grain shape and of lubrication on specimen deformation, to investigate energy dissipation at large strains, and to look for possible comparisons with the acoustic tests.

A. Specimen Preparation and Experimental Method

The aggregates studied consisted of clean and lubricated glass beads and alundum prepared in the same manner as the acoustic samples. All specimens were jacketed with two of the 0.002 in. thick rubber containers used for jacketing the acoustic specimens. Circular end plates of 1/8 in. thick stainless steel were included in the containers to reduce end friction and ensure flat ends. Confining pressure was exerted on the specimens by drawing a vacuum inside the containers through a hypodermic needle connected to a vacuum system and gage. At maximum confining pressure of about 1 bar, all undeformed specimens were cylindrical and about 3.5 in. long and 1.5 in. in diameter.

Reproduced with permission of the copyright owner. Further reproduction prohibited without permission.

The testing apparatus was an Instron Universal Testing Machine, model TT-C. The specimens were uniaxially compressed between a fixed base plate, connected to a load cell, and an upper movable cross-head and anvil. The cross-head was advanced or retracted at a constant rate of 0.01 in./min. in almost all tests. Relative length changes of the specimens were measured by a linear differential transformer. Both the load cell and the transformer were connected to a Hewlett Packard X-Y Recorder, model 7, which sketched curves of load versus displacement. Absolute values of specimen displacement were recorded from the Instron length gage.

B. Specimen Deformation

Compressive deformation of a granular aggregate generally involves work to dilate the packing, either overall or locally or both, as well as work done against interparticle friction and in elastic deformation at contacts. A discussion of some of these different aspects of deformation is given in Rowe (1962) and Horne (1965). The magnitude and partitioning of the work required to deform a specimen depend on the initial geometry and state of compaction of the granular assemblage and on the particle shape and the particle surface and bulk properties. In these experiments the

Reproduced with permission of the copyright owner. Further reproduction prohibited without permission.

initial configurations of specimens differing only in degree of lubrication were similar enough so that the differences in compressive properties were largely due to variations in interparticle friction.

All specimens were compressed to yielding at several confining pressures, beginning at about 1 bar and then decreasing. The term yielding is used here to define the first observed constancy of load with increasing displacement of the specimen. Deformation was always accompanied by bulging at the center of the specimen. Relative length changes on yielding at maximum confining pressure averaged 5% for the bead samples and 8% for the alundum samples. All alundum specimens and the sodium stearate lubricated beads deformed and yielded smoothly, with uniform bulging and no evidence of faulting. The asymmetrical shapes of some of the deformed clean and oil- and glycerol-lubricated bead specimens indicated faulting. The load-displacement curves for these specimens were very jagged, on a small scale, and there were frequently large, rapid decreases in load, presumably corresponding to faulting in the specimens. Particularly noticeable for these same samples during yielding was a sharp peak in load that occurred after the displacement had been stopped and started again.

Reproduced with permission of the copyright owner. Further reproduction prohibited without permission.

A family of Mohr circles were constructed for each specimen from the pairs of principal compressive stresses σ_y and p, the yield stress and the confining pressure, respectively. Because of the central bulging of all specimens, the specimen area supporting the load was taken to be an average of measurements made in the deforming region of the specimen. Hence, the yield stresses were only approximate. The envelope curve tangent to each circle in a family of Mohr circles was generally a straight line. An example is shown in figure 22. The slope of the envelope, $\tan \theta_m$ is a measure of the work done on the specimen to bring it to the yield condition, as well as a convenient means for extrapolating the data. Lubrication generally decreased the slope for both bead and alundum specimens (table 9), reflecting the lowering of interparticle friction. Sodium stearate was the most effective lubricant in this regard. Finally, all alundum specimens supported greater stresses (higher $\tan \theta_m$) than the bead specimens at similar confining pressures, probably due largely to the more interlocking geometries of the alundum aggregates.

Reproduced with permission of the copyright owner. Further reproduction prohibited without permission.

TABLE 9.--Some results of the compression tests

Specimen	θ_m	Loop Displacement Amplitude (10^{-4} in.)	V_s (10^4 cm/sec)	Q_s^{-1}
		p = 0.95 bar		
clean beads, -70+140 mesh	29°	--	--	--
		--	--	--
clean beads, -25+45 mesh	29°	10	3.2	.22
		15	3.1	.24
		20	2.9	.27
0.0045% oil on -25+45 mesh beads	24°	10	--	--
		15	--	--
		20	2.7	.22
0.0090% oil on -25+45 mesh beads	24°	10	3.3	.32
		15	3.0	.38
		20	2.8	.39
0.0504% glycerol on -25+45 mesh beads	29°	10	--	--
		15	3.5	.27
		20	3.2	.21
0.005% sodium stearate on -25+45 mesh beads	20°	10	2.5	.26
		15	2.2	.36
		20	2.1	.38
clean alundum, -60 mesh	39°	10	4.2	.21
		15	3.8	.25
		20	3.5	.29
0.0045% oil on -60 mesh alundum	36°	10	--	.16
		15	--	.22
		20	3.2	.23
0.010% sodium stearate on -60 mesh alundum	34°	10	--	--
		15	--	.51
		20	3.2	.53

Reproduced with permission of the copyright owner. Further reproduction prohibited without permission.

C. Unloading-Reloading Cycles

After a specimen had yielded, the load was cycled between the yield load and a succession of lower loads. This was done by cycling the imposed displacement over measured intervals from 5×10^{-4} to 7×10^{-3} inches in amplitude. In this manner a series of load-displacement hysteresis loops were generated as a function of displacement amplitude at each confining pressure. The yield state was chosen as the starting point because it was the nearest approach to a consistent initial configuration possible. Representative hysteresis loops are shown in figure 23. The loops were generally somewhat asymmetrical, the initial unloading tangent modulus being greater than the initial reloading modulus. This asymmetry reflects the finite stress difference that must build up as the specimen recovers on unloading before grain sliding or slip is reversed.

Changing the displacement amplitude of the loop also changes the major frequency components of the unloading-reloading cycle. While most tests were run at a displacement rate of 0.01 in./min., some preliminary tests were at a rate of 0.1 in./min. The increase in rate by a factor of 10 increased hysteresis loop areas with equal displacement amplitudes by less than a factor of 1.5 and had little effect on the load-displacement relations. Hence, all the

Reproduced with permission of the copyright owner. Further reproduction prohibited without permission.

quantities discussed below were essentially independent of frequency, at least over the limited range investigated.

The load-displacement relations obtained from the maximum displacement and load amplitudes of the hysteresis loops were highly nonlinear. The displacement amplitude varied as the second or third power of the load amplitude at small loop amplitudes and as the third to fifth power at larger amplitudes. Since the ratio of the specimen length to cross-sectional area changed only slightly during any one series of cycles, the preceding dependence also describes the stress-strain relationship.

According to Rowe (1962), deformation up to the point of yielding occurs as a number of arrested slides at grain contacts initially at some preferred orientation to the major applied stress. Horne (1965) points out that the motion probably takes place between groups of instantaneously rigid particles, groups which are continuously dividing and coalescing. At any one time some contacts are sliding, some are about to fail, and many are subject to large tangential stresses with accompanying slip. Thus, from the introductory discussion of contact theory, nonlinearity of the stress-strain relations is to be expected.

Reproduced with permission of the copyright owner. Further reproduction prohibited without permission.

For comparison with the acoustic data, "velocities," V_s, were calculated from the hysteresis loops according to the formula

$$V_s = \frac{1}{\sqrt{m}} \sqrt{\frac{\Delta F}{\Delta x}}\, \ell,$$

where m is the specimen mass, ℓ is the specimen height at the beginning of the loop, and ΔF and Δx are, respectively, the load and displacement amplitudes of the loop. At the smallest displacements (10^{-4} inches) these static velocities were 70% or less of the acoustic velocities for similar specimens (table 9). Again, from previous theoretical considerations the tangential contact moduli (and hence the velocity) is expected to decrease with increasing tangential displacements at contacts. Also, the dilatancy accompanying the compressional deformation may result in fewer close contacts per grain than in the acoustic specimens and thus a lower specimen modulus. It is interesting to note that for both the clean bead and clean alundum specimens the static velocities were lower than the acoustic velocities by approximately the same fraction. This observation implies that the conclusions regarding the influence of shape on the acoustic results may be applicable to these tests as well.

Lubrication of the beads had little effect on V_s, except for sodium stearate which lowered V_s somewhat, in contrast to the acoustic tests where lubrication raised the

Reproduced with permission of the copyright owner. Further reproduction prohibited without permission.

bead aggregate velocities. When tangential contact displacements become large, theory predicts that friction will be an important factor in determining the tangential contact modulus, the modulus decreasing with decreasing friction (figure 2). Opposing this effect, however, was the greater densities (and hence more close contacts per particle) of the lubricated beads compared to the clean beads, both initially and at yielding. There was some indication that the bead densities at yielding depended not only on the initial density but also on the coefficient of friction. For example, a sodium stearate lubricated bead specimen had the same initial density as an oil lubricated specimen, but the yield densities of the former measured at various confining pressures were several per cent higher than those of the latter at equivalent confining pressures. Hence, the lower tangential moduli at contacts with lower friction may be partly compensated by more close contacts per grain, at least in the spherical particle aggregates.

For all specimens, regardless of particle shape, V_s increased with the 1/2 to 1/3 power of the confining pressure. Once again, the higher power dependence (higher than the 1/6 power dependence predicted for the acoustic tests) is predicted for a single contact at large tangential displacements by contact theory. Also, the data indicated that

Reproduced with permission of the copyright owner. Further reproduction prohibited without permission.

yield volumes generally increased, implying decreasing close contacts, as the confining pressure decreased, and hence the arguments pertaining to the effects on the acoustic properties of the changing numbers of close contacts with pressure may be applicable to these tests as well.

The area enclosed by the unloading-loading loop gives the energy dissipated per cycle of displacement, ΔW_s. For all specimens studied, ΔW_s increased as the square of the displacement amplitude of the loop (figure 24) and decreased, in no consistent manner, with decreasing confining pressure. Both contact theory and single contact experiments on steel balls predict a higher power dependence than obtained in these tests when the contact displacements are large and nonlinear (figures 5 and 7). It is interesting to note that this square power dependence on amplitude is the same as that found in the acoustic tests where the contact displacements were much smaller.

For comparison with the acoustic results a fractional energy loss per cycle $2\pi\, Q_s^{-1}$ was defined as $\Delta W_s/W_s$, where W_s was calculated from the relation (1/8) $\Delta x \times \Delta F$. From table 9 it can be seen that there is very little difference in Q_s^{-1} for any of the specimens except the sodium stearate lubricated alundum and that Q_s^{-1} is generally much higher than the acoustic Q^{-1}. Plots of Q_s^{-1} versus confining pressure

Reproduced with permission of the copyright owner. Further reproduction prohibited without permission.

were characterized by much scatter and no dependence on confining pressure within the limits of experimental accuracy. In all cases Q_s^{-1} increased with displacement amplitude raised to the 1 to 3/2 power.

In summary, the results of the compression tests are not adequately explained in terms of contact theory, although there are several features of the tests which are compatible with the theory.

Reproduced with permission of the copyright owner. Further reproduction prohibited without permission.

VI. LUNAR SEISMIC OBSERVATIONS

Seismic signals, generated by lunar impacts of the Apollo 12 Lunar Module ascent stage and the third stage of the Apollo 13 Saturn booster, were recorded by seismometers installed on the moon by Apollo 12 astronauts. Analysis of these signals suggests that the mare in the region of the Apollo 12 station has very low near-surface velocities, with velocity increasing rapidly with depth in the upper 20 km, and also very low seismic wave energy absorption (Latham, et. al., 1970). The value of Q^{-1} for this region for all modes of propagation, calculated from the rate of decay of the signal amplitude, is about 3×10^{-4} (Latham, et. al., 1970). The acoustic data presented in the preceding sections indicate that both low velocity and low energy absorption are compatible properties of granular aggregates in elastic contact.

Because of the high lunar vacuum, the coefficients of friction of lunar particle surfaces are almost certainly greater than those of similar terrestrial grains. The high vacuum prevents the usual surface films and oxidation layers, which generally reduce friction, from forming on lunar

Reproduced with permission of the copyright owner. Further reproduction prohibited without permission.

particle surfaces, and the surfaces are therefore cleaner than is possible to duplicate in the lower artificial vacuums. Furthermore, adhesion of lunar soil samples has been observed, probably due to dispersion forces and/or surface electrostatic charges preserved by the lack of gas contamination (Grossman, et. al., 1970). Such adhesion should be equivalent to increased surface friction. The acoustic experiments reported here show that Q^{-1} of granular aggregates decreases with increasing contact friction. Recall that lubrication increased the glass bead Q^{-1} by as much as a factor of ten and tripled the alundum Q^{-1}. Thus, values of Q^{-1} representing energy dissipation at contacts in lunar aggregates should be considerably less than the values directly extrapolated from these experiments. Neglecting the increase in friction and using the experimentally observed dependences on pressure, extrapolation of the experimental Q^{-1} values for clean glass beads and clean alundum to pressure conditions corresponding to a depth of 5 km on the moon gives approximate Q^{-1} values of 10^{-3} and 10^{-4}, respectively.

A compressional velocity of 0.108 km/sec for the top several meters was derived from the Lunar Module signals (Latham, et. al., 1970). The velocities of bulk alundum and bulk glass should be reasonable upper and lower bounds for the expected velocities of lunar soil constituents. Using

Reproduced with permission of the copyright owner. Further reproduction prohibited without permission.

the measured specimen densities to calculate the overload pressure, extrapolation of the experimental data for clean beads and clean alundum aggregates to pressures corresponding to a depth of about 1 m on the moon gives compressional velocities of about 0.2 km/sec and 0.4 km/sec, respectively. However, any extrapolation of aggregate velocities to lunar conditions must include a consideration of the high coefficients of friction and the interparticle adhesive forces present in lunar aggregates. Both high friction and adhesion enable fewer contacts per particle to constitute a stable packing than in cohesionless, low friction aggregates. The higher number of contacts in the lubricated acoustic specimens compared to the clean specimens is one example. In addition, a numerical analysis was made by Vold (1959) of the packing of glass spheres with short-range interparticle forces such that each sphere cohered firmly to the first sphere it contacted. She found that such a model resulted in a mean number of contacts per sphere of 2.0. Hence, if it is assumed that the experimental specimens reported here had 6 close contacts per particle, the above extrapolated velocities might be decreased by a factor of about $(2/6)^{1/3}$, or about 0.7 (see equation [47]).

Reproduced with permission of the copyright owner. Further reproduction prohibited without permission.

Finally, the compressional velocity is reported to rise with depth to about 5-6 km/sec at 20 km (Latham, et. al., 1970). Extrapolation of the clean alundum and glass bead results, according to their experimentally determined dependences, to the pressure corresponding to a lunar depth of 20 km yields compressional velocities of about 3 km/sec and 4 km/sec, respectively. The steep rise of velocity with depth can, therefore, be largely explained by elastic contact theory modified to include the making of new contacts with increasing pressure.

In summary, then, the velocities and damping capacities of granular aggregates compare quite favorably with the observed lunar seismic properties.

Reproduced with permission of the copyright owner. Further reproduction prohibited without permission.

REFERENCES

Anderson, O. L., and Liebermann, R. C., 1966, Sound velocities in rocks and minerals (VESIAC State-of-the-Art Report under Contracts SD-78 and DA-49-083 OSA-3137): Lamont Geological Observatory, Columbia University, Palisades, New York.

Archard, J. F., 1953, Contact and rubbing of flat surfaces: Jour. Appl. Phy., v. 24, p. 981-988.

_____, 1957, Elastic deformation and the laws of friction: Proc. Royal Soc., London, series A, v. 243, p. 190-205.

Bernal, J. D., and Finney, J. L., 1967, Random packing of spheres in non-rigid containers: Nature, v. 214, p. 265-266.

Bernal, J. D., and Mason, J., 1960, Co-ordination of randomly packed spheres: Nature, v. 188, p. 910-911.

Beresford, R. H., 1969, Statistical geometry of random heaps of equal hard spheres: Nature, v. 224, p. 550-553.

Biesterfeldt, H. J., Lange, J. N., and Skudrzyk, E. J., 1960, Vibrations of rods at frequencies below their radial resonance: Jour. Acoust. Soc. Am., v. 32, p. 749-764.

Bowden, F. P., and Tabor, D., 1954 (Part I), 1964 (Part II), The friction and lubrication of solids: London, Oxford University Press.

Brain, C. K., 1958, The Transvaal ape-man-bearing cave deposits: Transvaal Museum Memoir, no. 11.

Brown, R. L., and Hawksley, P. G. W., 1945, Packing of regular (spherical) and irregular particles: Nature, v. 156, p. 421-422.

Reproduced with permission of the copyright owner. Further reproduction prohibited without permission.

Cattaneo, C., 1938, Sul contatto di due corpi elastici: Accademia dei Lincei, Rendiconti, series 6, v. 27, p. 342-348, 434-436, and 474-478.

Courtney-Pratt, J. S., and Eisner, E., 1957, The effect of a tangential force on the contact of metallic bodies: Proc. Royal Soc., London, series A, v. 238, p. 529-550.

Deresiewicz, H., 1958a, Mechanics of granular matter: Advances in Applied Mechanics, v. 5, Academic Press, New York, p. 233-306.

_____, 1958b, Stress-strain relations for a simple model of a granular medium: Jour. Appl. Mech., v. 25, Trans. ASME, v. 80, p. 402-406.

Duffy, J., 1959, A differential stress-strain relation for the hexagonal close-packed array of elastic spheres: Jour. Appl. Mech., v. 26, Trans. ASME, v. 81, p. 88-94.

Duffy, J., and Mindlin, R. D., 1957, Stress-strain relations and vibrations of a granular medium: Jour. Appl. Mech., v. 24, Trans. ASME, v. 79, p. 585-593.

El Boushi, I. M., 1969, Water-retention characteristics of coarse rock particles: Jour. Hydrology, v. 8, p. 431-441.

Faust, L. Y., 1951, Seismic velocity as a function of depth and geologic time: Geophysics, v. 16, p. 192-206.

Gardner, G. H. F., Wyllie, M. R. J., and Droschak, D. M., 1964, Effects of pressure and fluid saturation on the attenuation of elastic waves in sand: Jour. Petroleum Tech., v. 16, p. 189-198.

Goodman, L. E., and Brown, C. B., 1962, Energy dissipation in contact friction: constant normal and cyclic tangential loading: Jour. Appl. Mech., v. 29, Trans. ASME, v. 84, p. 17-22.

Greenwood, J. A., 1967, The area of contact between rough surfaces and flats: Jour. Lubrication Tech., Trans. ASME, v. 89, p. 81-91.

Reproduced with permission of the copyright owner. Further reproduction prohibited without permission.

Greenwood, J. A., and Tripp, J. H., 1967, The elastic contact of rough spheres: Jour. Appl. Mech., vol. 34, Trans. ASME, v. 89, p. 153-159.

Greenwood, J. A., and Williamson, J. B., 1966, Contact of nominally flat surfaces: Proc. Royal Soc., London, series A, v. 295, p. 300-319.

Grossman, J. J., Ryan, J. A., Mukherjee, N. R., and Wegner, M. W., 1970, Microchemical, microphysical and adhesive properties of lunar material: Proc. Apollo 11 Lunar Sci. Conf., v. 3, p. 2171-2181.

Hicks, W. G., and Berry, J. E., 1956, Application of continuous velocity logs to determination of fluid saturation of reservoir rocks: Geophysics, v. 21, p. 739-754.

Horne, M. R., 1965, The behavior of an assembly of rotund, rigid, cohesionless particles, I and II: Proc. Royal Soc., London, series A, v. 286, p. 62-97.

Hughes, D. S., and Kelly, J. L., 1952, Variation of elastic wave velocity with saturation in sandstone: Geophysics, v. 17, p. 739-752.

Johnson, K. L., 1955, Surface interaction between elastically loaded bodies under tangential forces: Proc. Royal Soc., London, series A, v. 230, p. 531-549.

_____, 1961, Energy dissipation at spherical surfaces in contact transmitting oscillating forces: Jour. Mech. Eng. Sci., v. 3, p. 362-368.

Kolsky, H., 1963, Stress waves in solids: New York, Dover Publications.

Latham, G., Ewing, M., Dorman, J., Press, F., Toksoz, N., Sutton, G., Meissner, R., Duennebier, F., Nakamura, Y., Kovach, R., and Yates, M., 1970, Seismic data from man-made impacts on the moon: Science, v. 170, p. 620-626.

McCann, C., and McCann, D. M., 1969, The attenuation of compressional waves in marine sediments: Geophysics, v. 34, p. 882-892.

Reproduced with permission of the copyright owner. Further reproduction prohibited without permission.

McSkimin, H. J., 1964, Ultrasonic methods for measuring the mechanical properties of liquids and solids: Physical Acoustics, ed. W. P. Mason, v. 1, part A, Academic Press, New York, p. 271-334.

Mindlin, R. D., 1949, Compliance of elastic bodies in contact: Jour. Appl. Mech., v. 16, Trans. ASME, v. 71, p. 259-268.

Mindlin, R. D., and Deresiewicz, H., 1953, Elastic spheres in contact under varying oblique forces: Jour. Appl. Mech., v. 20, Trans. ASME, v. 75, p. 327-344.

Mindlin, R. D., Mason, W. P., Osmer, T. F., and Deresiewicz, H., 1951, Effects of an oscillating tangential force on the contact surfaces of elastic spheres: Proc. First Natl. Cong. Appl. Mech., Chicago, p. 203-208.

Morgan, N. A., 1969, Physical properties of marine sediments as related to seismic velocities: Geophysics, v. 34, p. 529-545.

Nolle, A. W., 1949, Dynamic mechanical properties of rubber-like materials: Jour. Polymer Sci., v. 5, p. 1-54.

O'Conner, J. J., and Johnson, K. L., 1963, The role of surface asperities in transmitting tangential forces between metals: Wear, v. 6, p. 118-139.

Rowe, P. W., 1962, The stress-dilatancy relation for static equilibrium of an assembly of particles in contact: Proc. Royal Soc., London, series A, v. 296, p. 500-527.

Smith, W. O., Foote, P. D., and Busang, P. F., 1929, Packing of homogeneous spheres: Physical Rev., v. 34, p. 1271-1274.

Spinner, S., and Tefft, W. E., 1961, A method for determining mechanical resonance frequencies and for calculating elastic moduli from these frequencies: Proc. Am. Soc. Testing Mats., v. 61, p. 1221-1238.

Thurston, C. W., and Deresiewicz, H., 1959, Analysis of a compression test of a model of a granular medium: Jour. Appl. Mech., v. 26, Trans. ASME, v. 81, p. 251-258.

Reproduced with permission of the copyright owner. Further reproduction prohibited without permission.

Timoshenko, S., and Goodier, J. N., 1951, Theory of elasticity, 2nd ed., New York, McGraw-Hill Book Company, Inc.

Vold, M. J., 1959, A numerical approach to the problem of sediment volume: Jour. Colloid Sci., v. 14, p. 168-174.

Wachtman, J. B., and Tefft, W. E., 1958, Effect of suspension position on apparent values of internal friction determined by Forster's method: Rev. Sci. Inst., v. 29, p. 517-520.

Westman, A. E. R., and Hugill, H. R., 1930, The packing of particles: Jour. Am. Ceramic Soc., v. 13, p. 767-779.

White, J. E., 1965, Seismic waves: New York, McGraw-Hill Book Company, Inc.

White, T. E., 1966, Static friction as a source of seismic attenuation: Geophysics, v. 31, p. 333-339.

White, J. E., and Sengbush, R. L., 1953, Velocity measurements in near-surface formations: Geophysics, v. 18, p. 54-69.

White, H. E., and Walton, S. F., 1937, Particle packing and particle shape: Jour. Am. Ceramic Soc., v. 20, p. 155-166.

Wyllie, M. R. J., Gregory, A. R., and Gardner, G. H. F., 1958, An experimental investigation of factors affecting elastic wave velocities in porous media: Geophysics, v. 33, p. 459-493.

Reproduced with permission of the copyright owner. Further reproduction prohibited without permission.

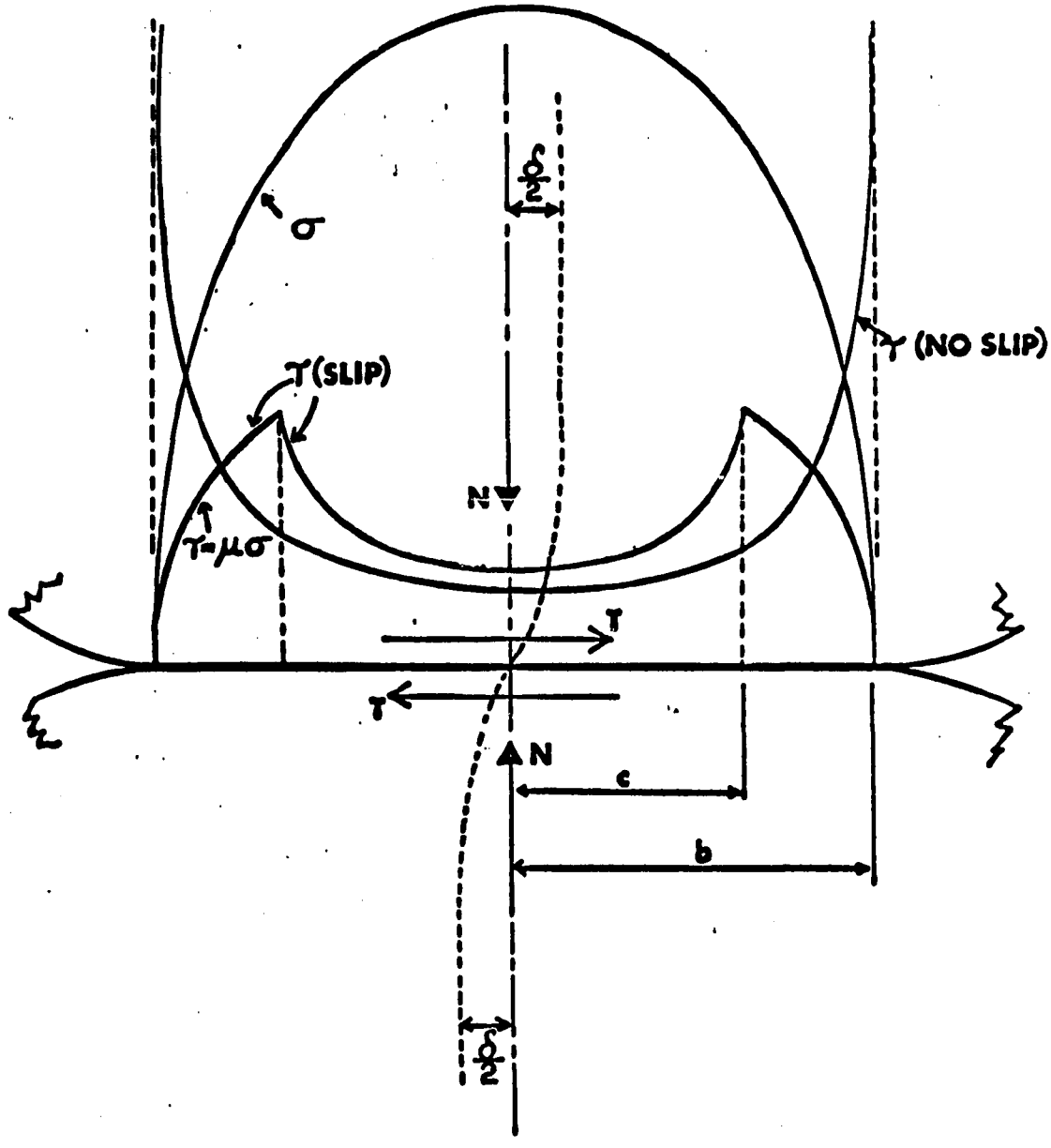

Fig. 1. Distribution of normal (σ) and tangential (τ) components of traction on the surface of contact between two identical spheres acted on by normal force N and tangential force T (Mindlin, 1949). See text for further explanation.

Reproduced with permission of the copyright owner. Further reproduction prohibited without permission.

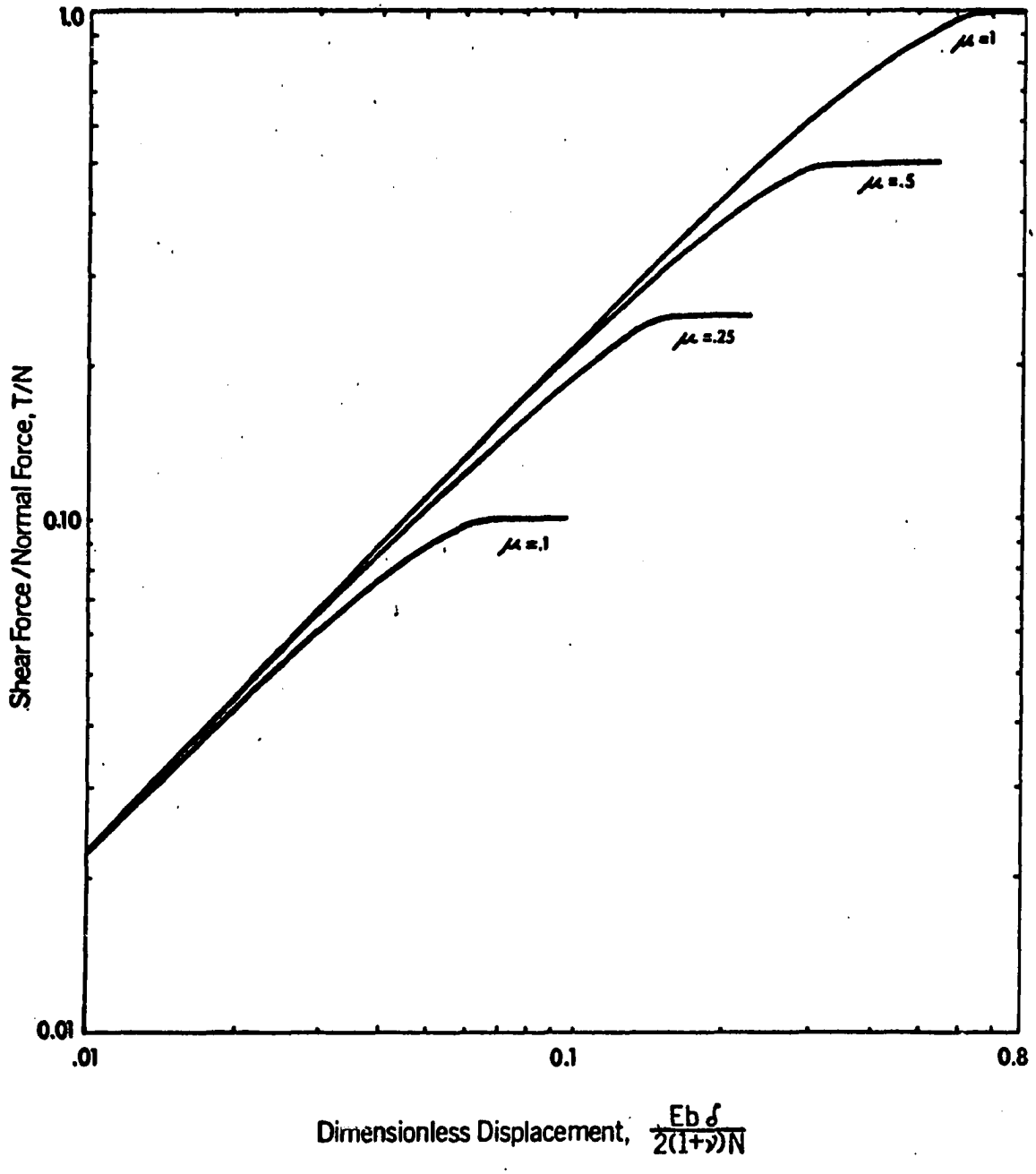

Fig. 2. Tangential force-displacement relation in dimensionless form for two like spheres under normal force N and acted on by a monotonically increasing tangential force T. Gross sliding occurs when T/N reaches the value μ, the limiting coefficient of friction.

Reproduced with permission of the copyright owner. Further reproduction prohibited without permission.

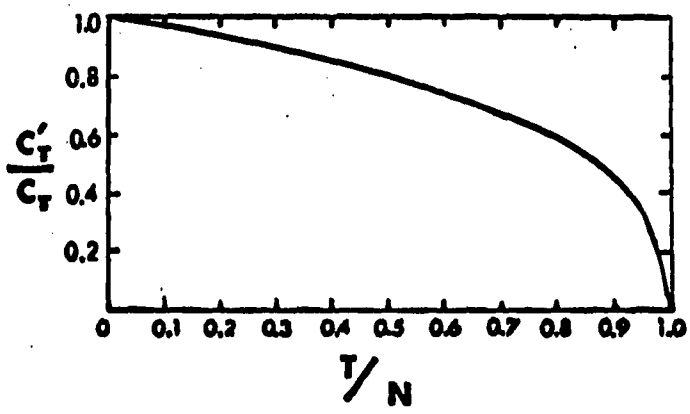

Fig. 3. Ratio of initial or "no slip" tangential compliance, C_T', to the "slip" compliance, C_T, for two like spheres in contact (Mindlin, 1949).

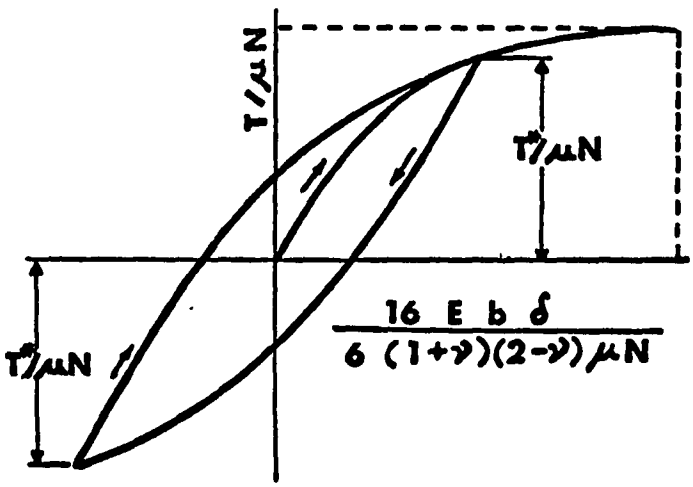

Fig. 4. Tangential force-displacement curve for two like spheres under a constant normal force N and acted on by an oscillating tangential force of maximum amplitude T* (Mindlin, et. al., 1951).

Reproduced with permission of the copyright owner. Further reproduction prohibited without permission.

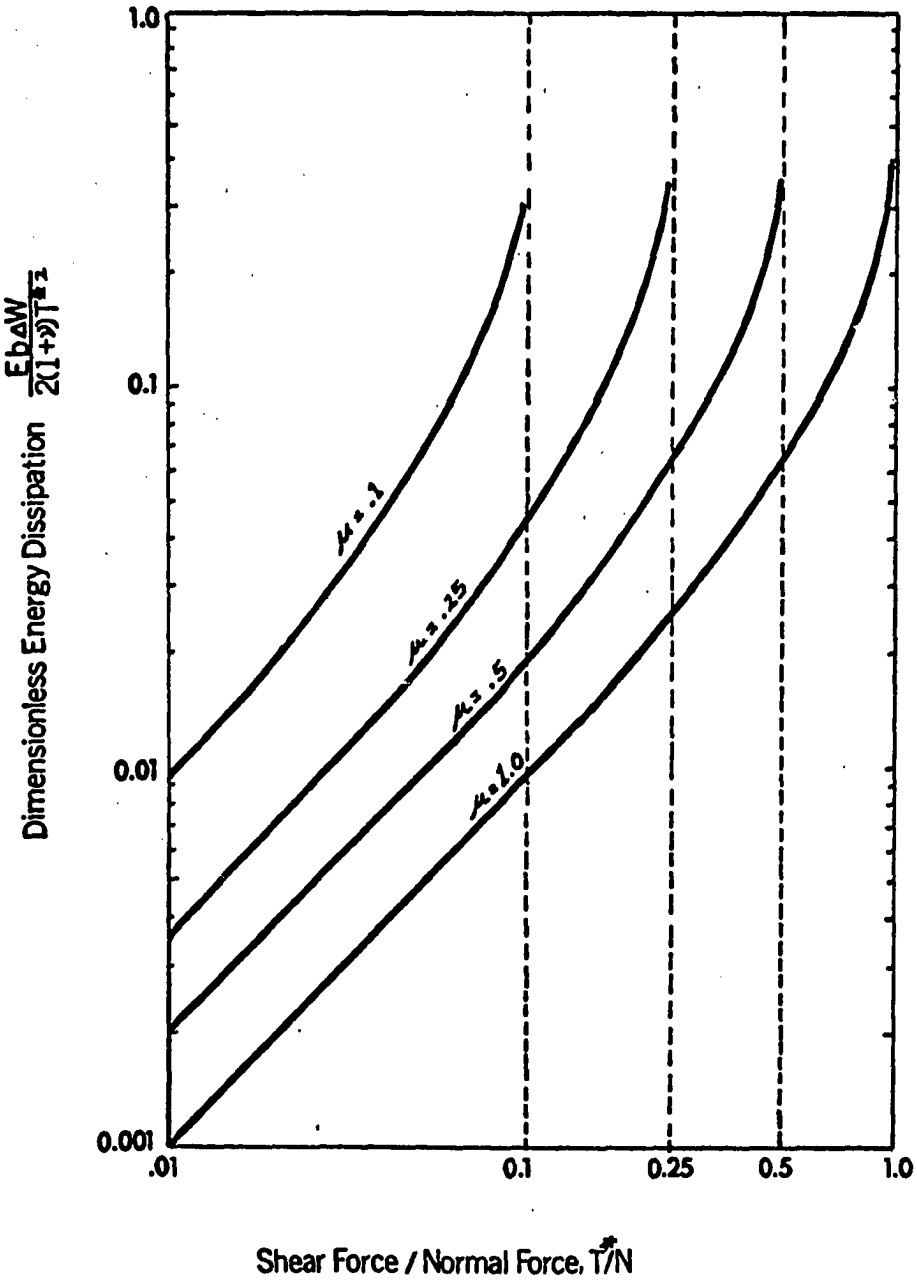

Fig. 5. Relation of energy dissipated per cycle to maximum amplitude T* of the oscillating tangential force acting on two like spheres for several values of the limiting coefficient of friction μ.

Reproduced with permission of the copyright owner. Further reproduction prohibited without permission.

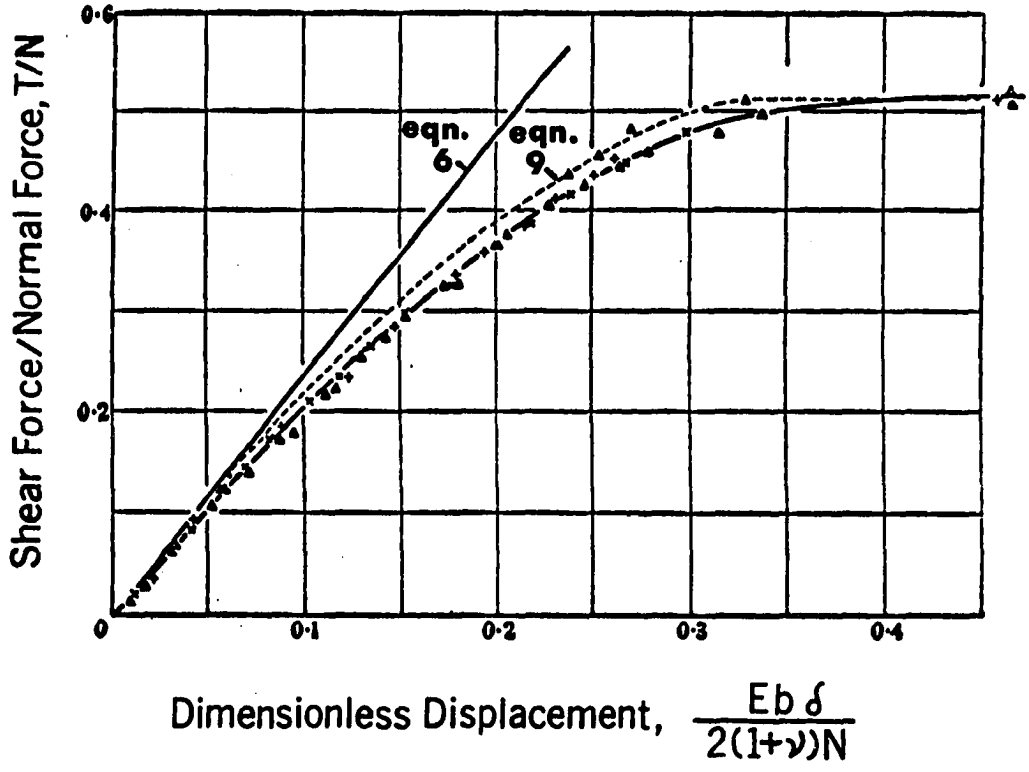

Fig. 6. Comparison of static force-displacement tests on single steel contacts with the theoretical relationships given by equations (6) and (9) taking μ=0.51 (Johnson, 1955).

Reproduced with permission of the copyright owner. Further reproduction prohibited without permission.

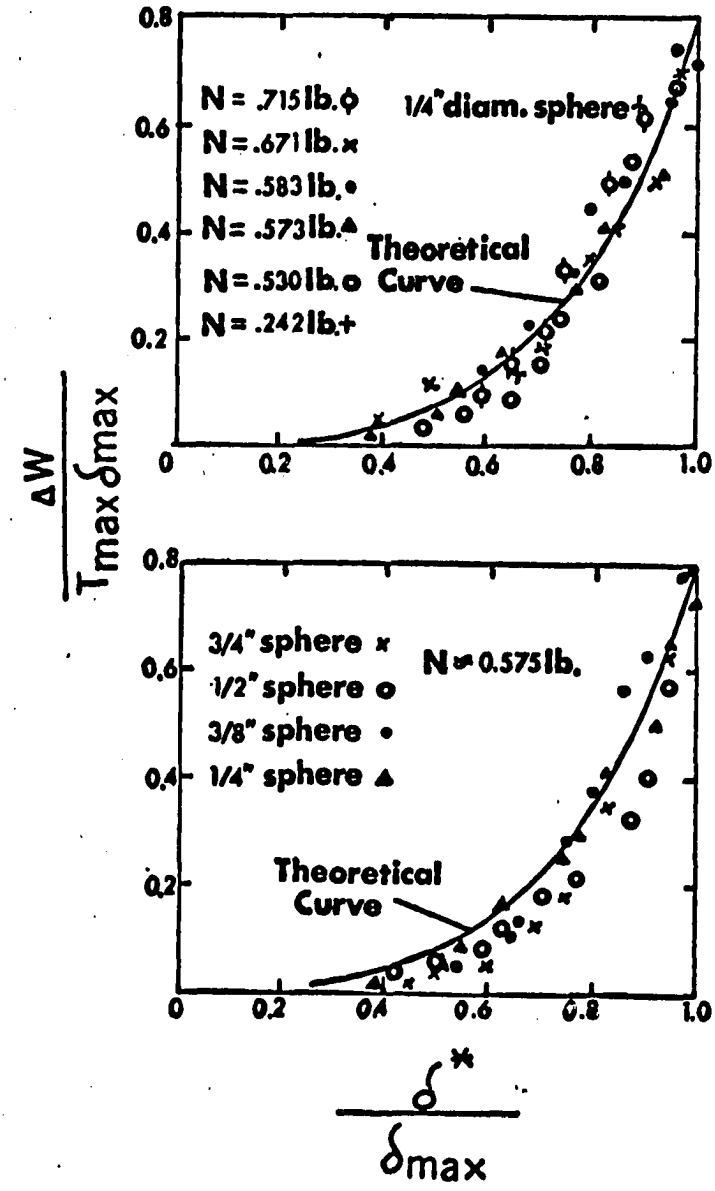

Fig. 7. Comparison of the energy dissipated per cycle at single circular steel contacts with the theoretical relation given by equation (13) (Goodman and Brown, 1962).

Reproduced with permission of the copyright owner. Further reproduction prohibited without permission.

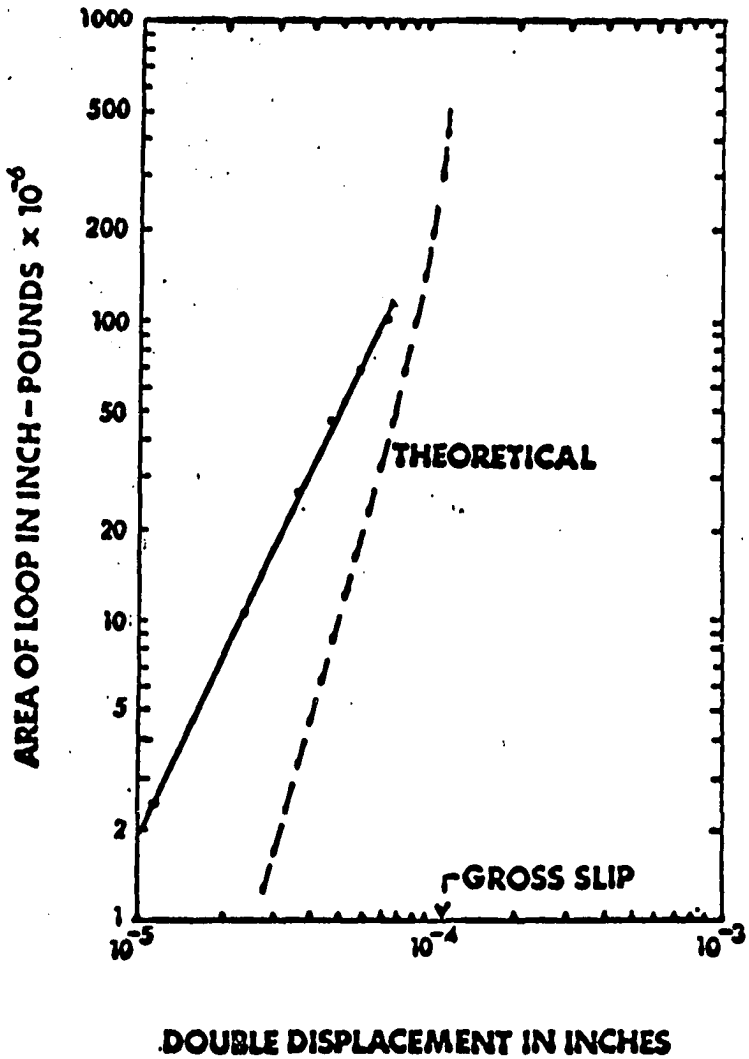

Fig. 8. Comparison of experimentally observed energy dissipation per cycle with the theoretical dissipation given by equation (13) for crown glass lenses (Mindlin, et. al., 1951).

Reproduced with permission of the copyright owner. Further reproduction prohibited without permission.

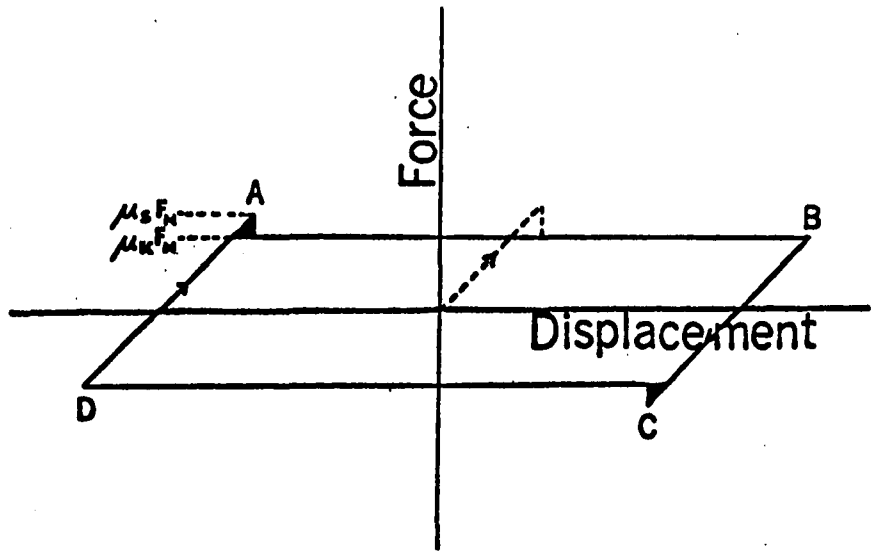

Fig. 9. Force-displacement curve for a spring-driven block sliding on a flat surface (White, 1966).

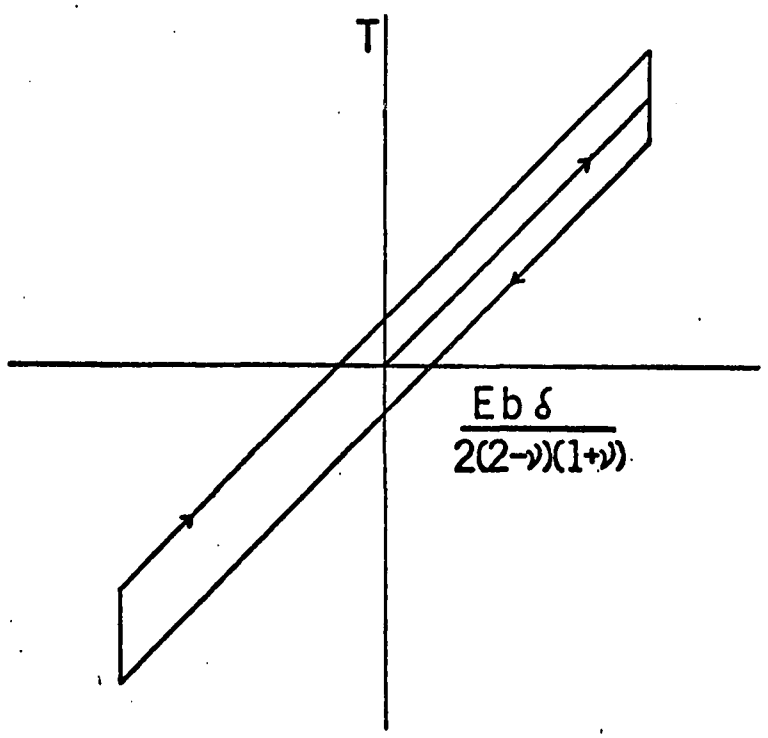

Fig. 10. White's modified force-displacement curve for two like spheres acted on by an oscillating tangential force of peak amplitude $T^* << \mu N$ (White, 1966).

Reproduced with permission of the copyright owner. Further reproduction prohibited without permission.

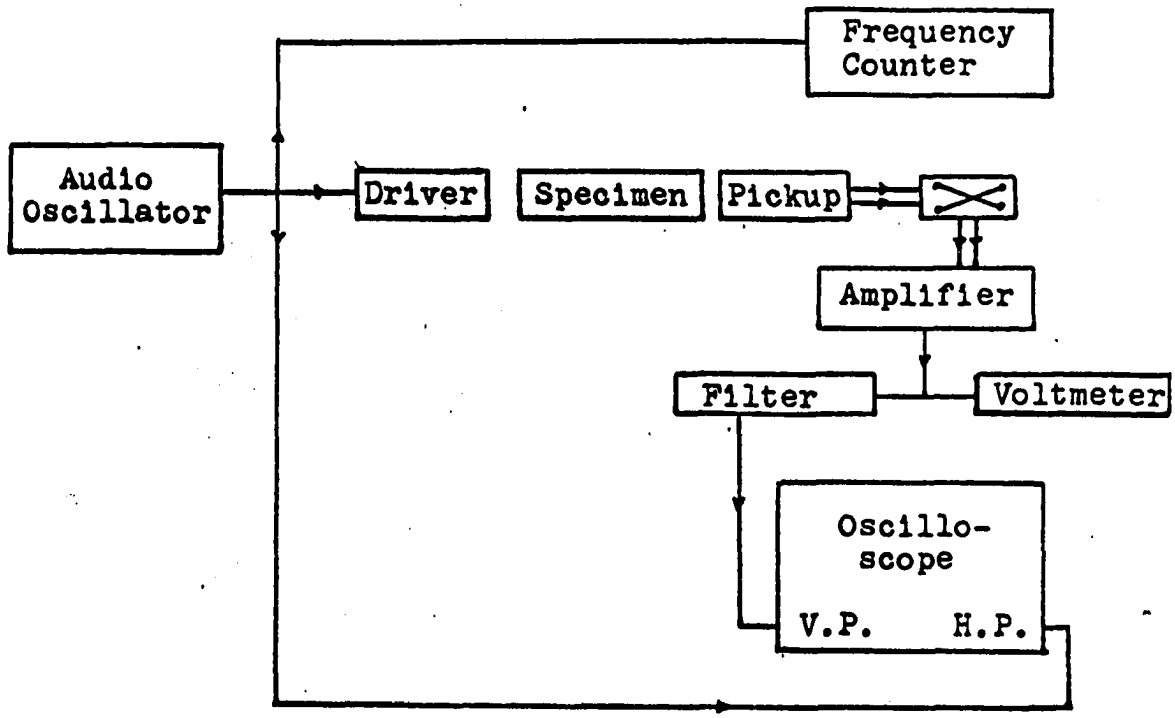

Fig. 11. Diagrammatic sketch of the basic setup for all acoustic experiments on granular bars.

Reproduced with permission of the copyright owner. Further reproduction prohibited without permission.

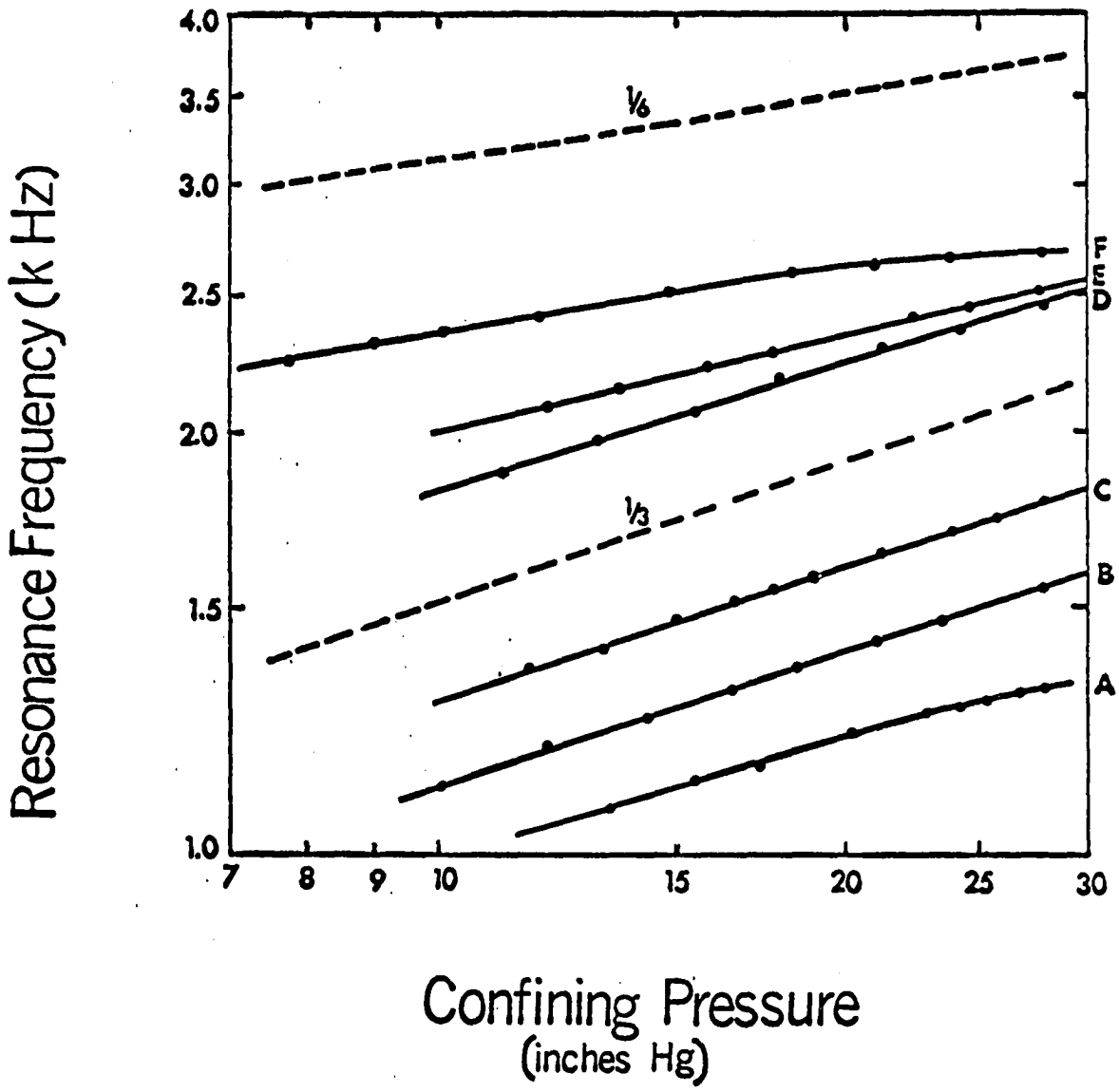

Fig. 12. Examples of frequency-pressure curves measured for clean granular aggregates. The differences in slope reflect the differences in grain shape and in type of deformation at contacts. A. crushed glass plate, B. spherical alumina, C. glass beads (-70+140 mesh), D. glass beads (-25+45 mesh), E. angular alundum, F. sodium chloride. (1 in. Hg = 3.38 X 10^{-2} bar)

Reproduced with permission of the copyright owner. Further reproduction prohibited without permission.

Reproduced with permission of the copyright owner. Further reproduction prohibited without permission.

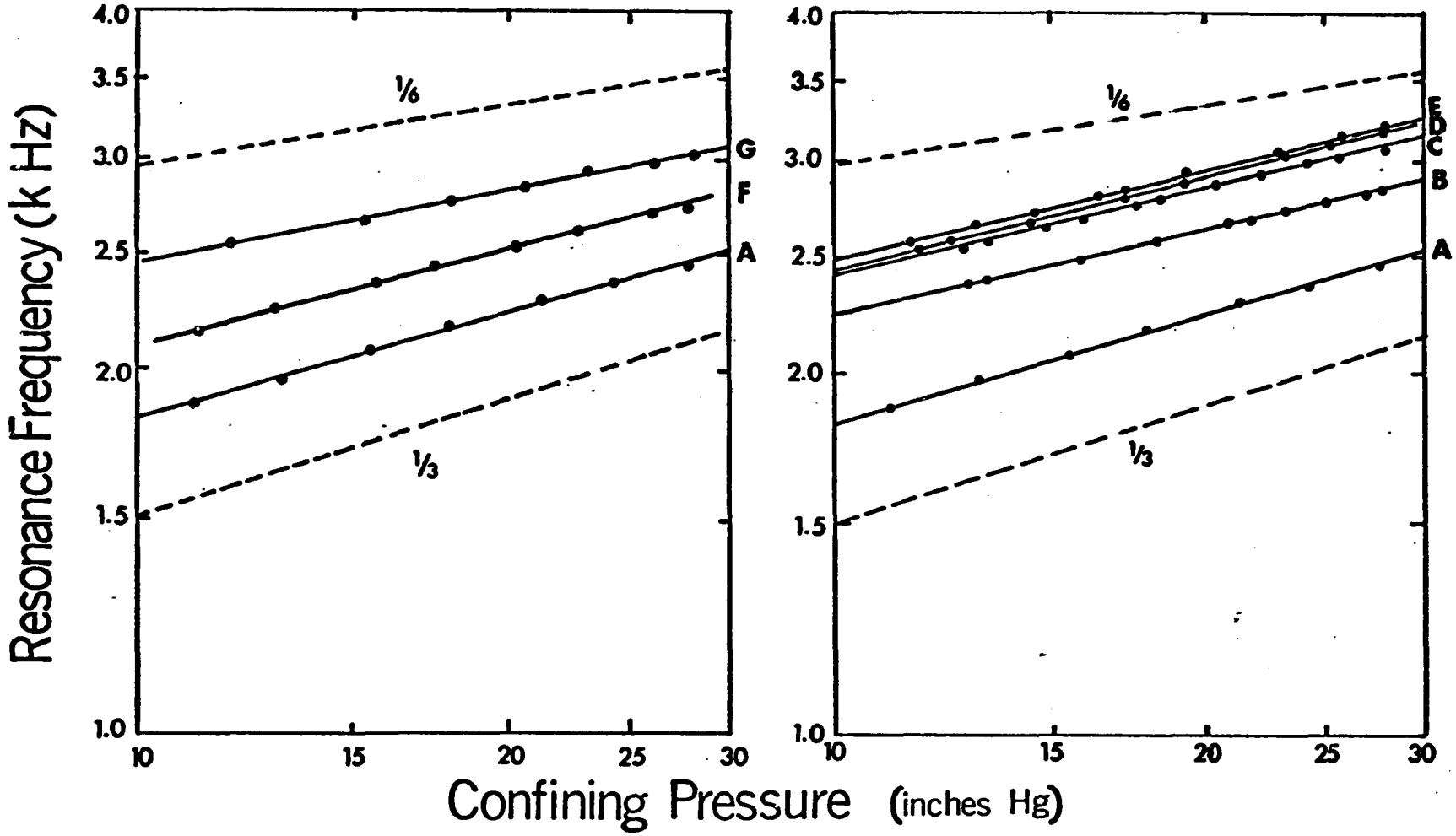

Fig. 13. Comparison of lubricated glass bead specimens with clean bead specimen. Lubrication generally brought the frequency-pressure slopes closer to the theoretically expected slope of 1/6. A. clean, B. 0.0045% oil, C. 0.0090% oil, D. 0.0050% sodium stearate, E. 0.0450% sodium stearate, F. Siliclad, G. molybdenum disulfide. (1 in. Hg = 3.38 X 10^2 bar)

Fig. 14. Q^{-1} versus resonance frequency for a representative sample of the specimens studied.

● Glass beads lubricated with 0.0090% oil

+ Glass beads lubricated with 0.0045% oil

⊙ Glass beads lubricated with 0.0504% glycerol

⊕ Glass beads lubricated with 0.0063% glycerol

▼ Glass beads lubricated with molybdenum disulfide

△ Glass beads lubricated with 0.0050% sodium stearate

■ Glass beads lubricated with 0.0450% sodium stearate

▣ Glass beads lubricated with Silicoled

✕ Glass beads, clean

⊡ Glass beads lubricated with 0.000063% glycerol

◐ Sodium chloride, unlubricated

▲ Spherical alumina (soft), unlubricated

● Angular alumdum, unlubricated

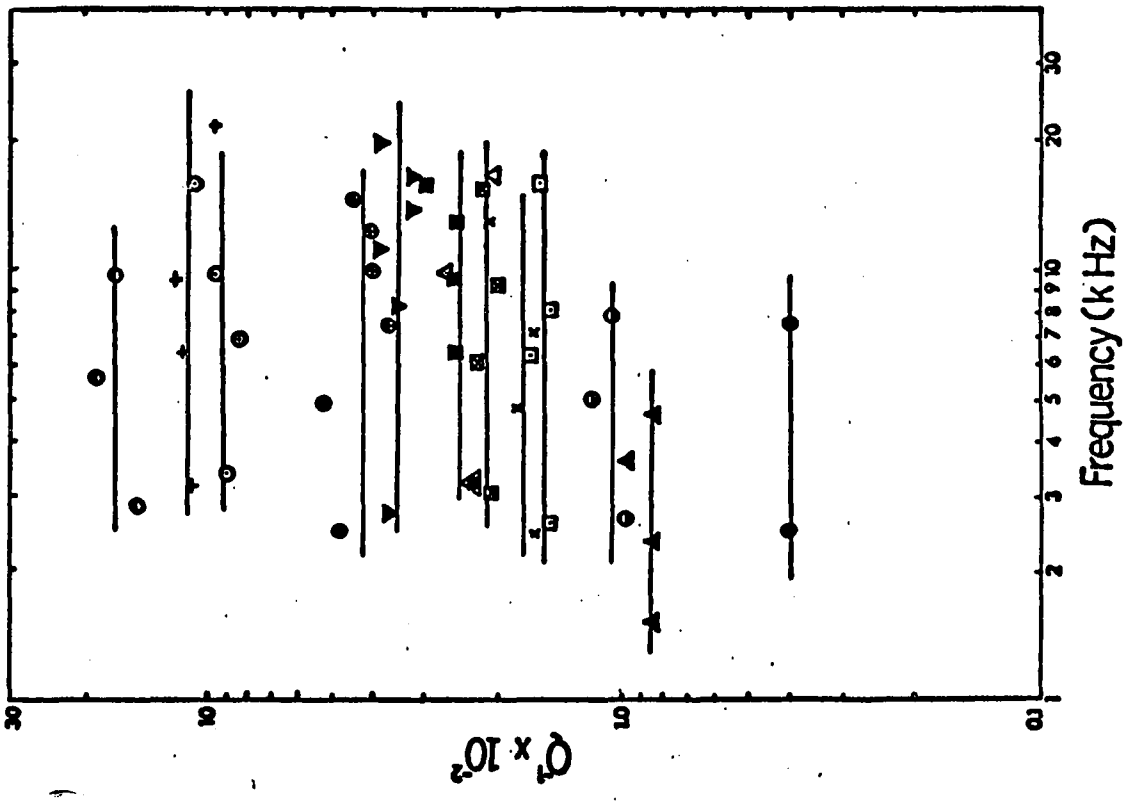

Reproduced with permission of the copyright owner. Further reproduction prohibited without permission.

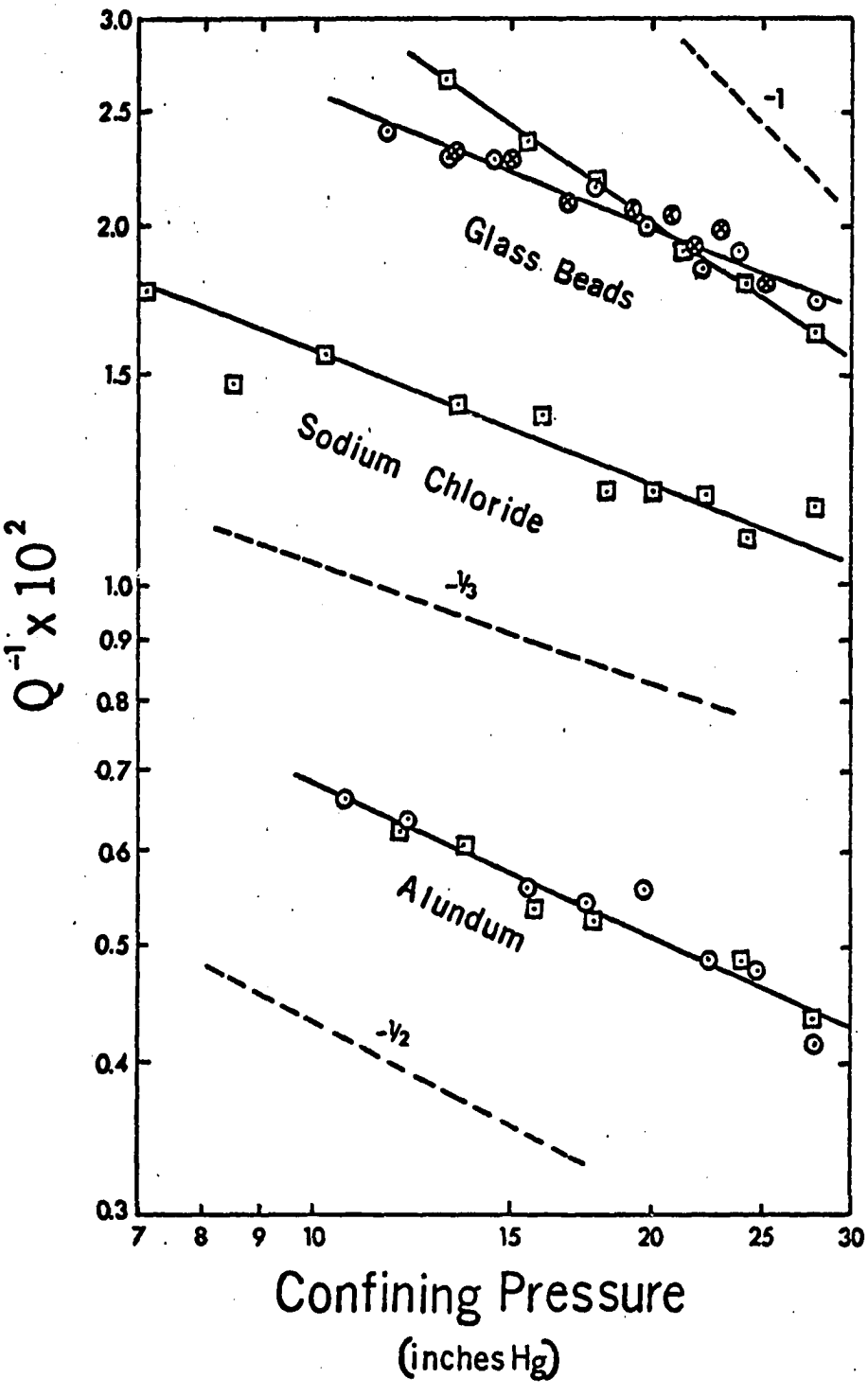

Fig. 15. Curves of Q^{-1} versus confining pressure for clean granular aggregates. ⊡ --First harmonic; ⊙ --third harmonic, increasing pressure; ⊛ --third harmonic, decreasing pressure. (1 in. Hg = 3.38 X 10^2 bar)

Reproduced with permission of the copyright owner. Further reproduction prohibited without permission.

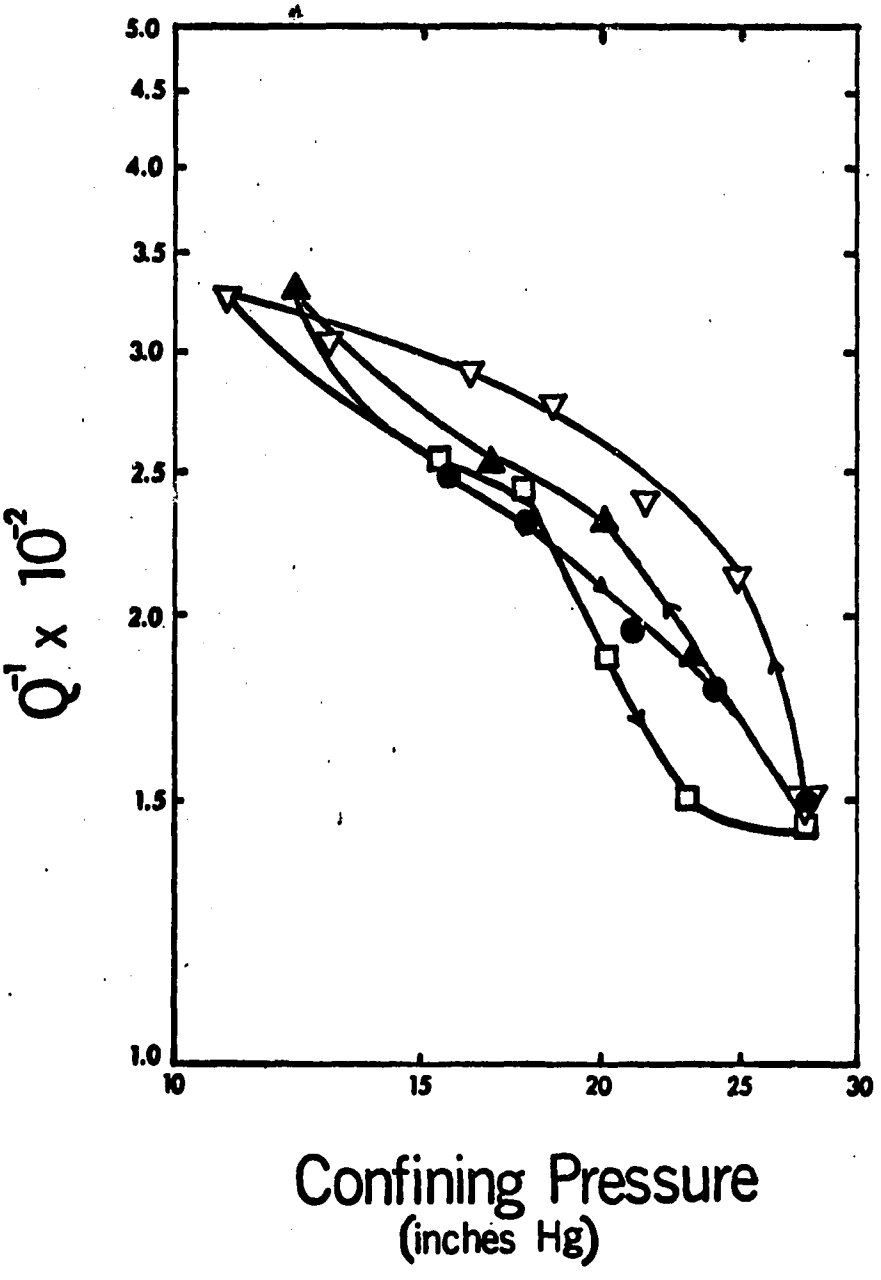

Fig. 16. Q^{-1} versus confining pressure for glass beads lubricated with 0.00063% glycerol showing hysteresis on pressure cycling. The first cycle is indicated by open symbols; the second cycle, by shaded symbols. (1 in. Hg = 3.38 X 10^2 bar)

Reproduced with permission of the copyright owner. Further reproduction prohibited without permission.

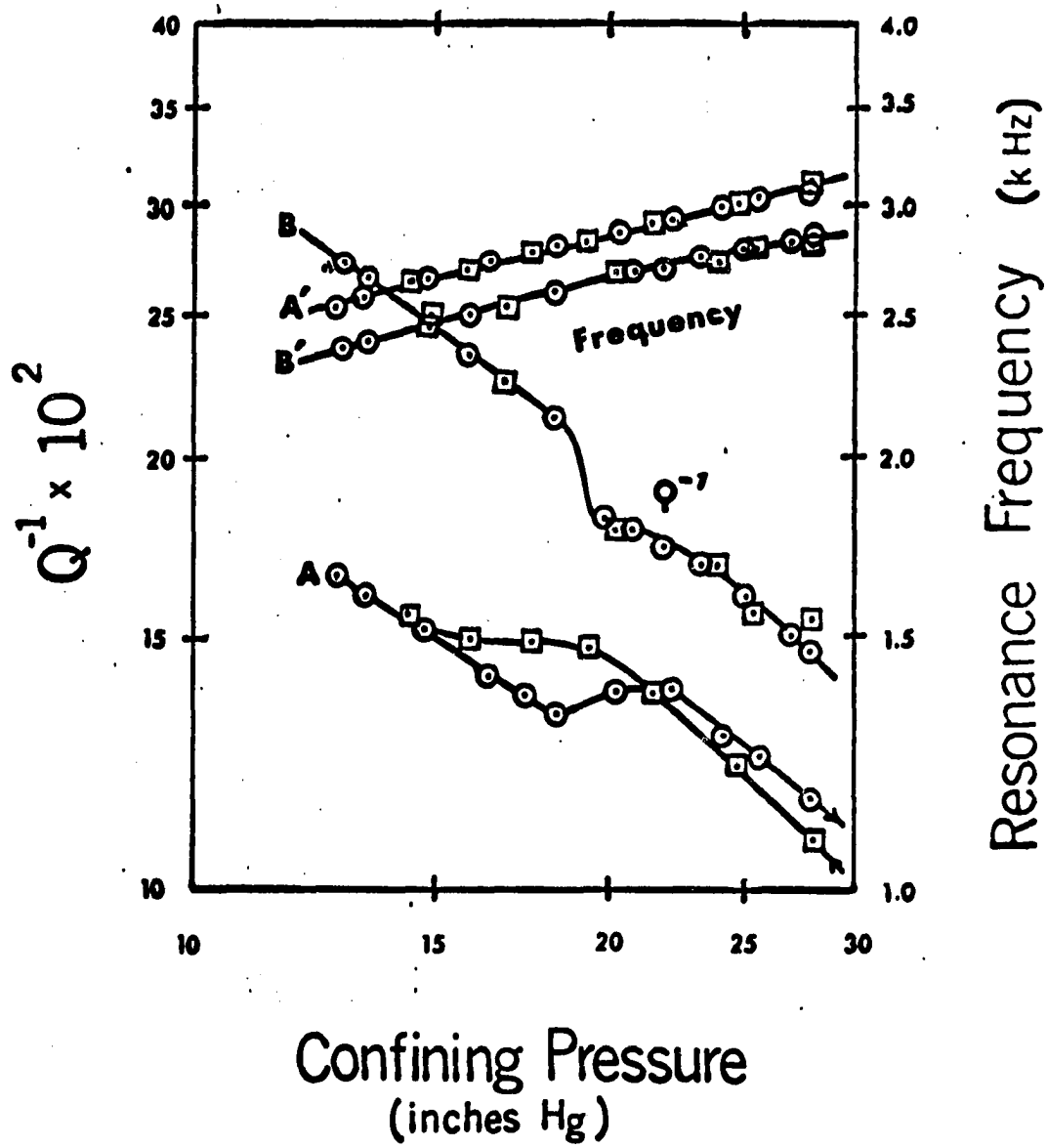

Fig. 17. Comparison of resonance frequency and Q^{-1} measurements as a function of confining pressure for glass beads lubricated with oil. A, A'--beads lubricated with 0.0045% oil; B,B'--beads lubricated with 0.0090% oil. Increasing pressure denoted by circles; decreasing pressure, by squares. (1 in. Hg = 3.38 X 10^2 bar)

Reproduced with permission of the copyright owner. Further reproduction prohibited without permission.

Reproduced with permission of the copyright owner. Further reproduction prohibited without permission.

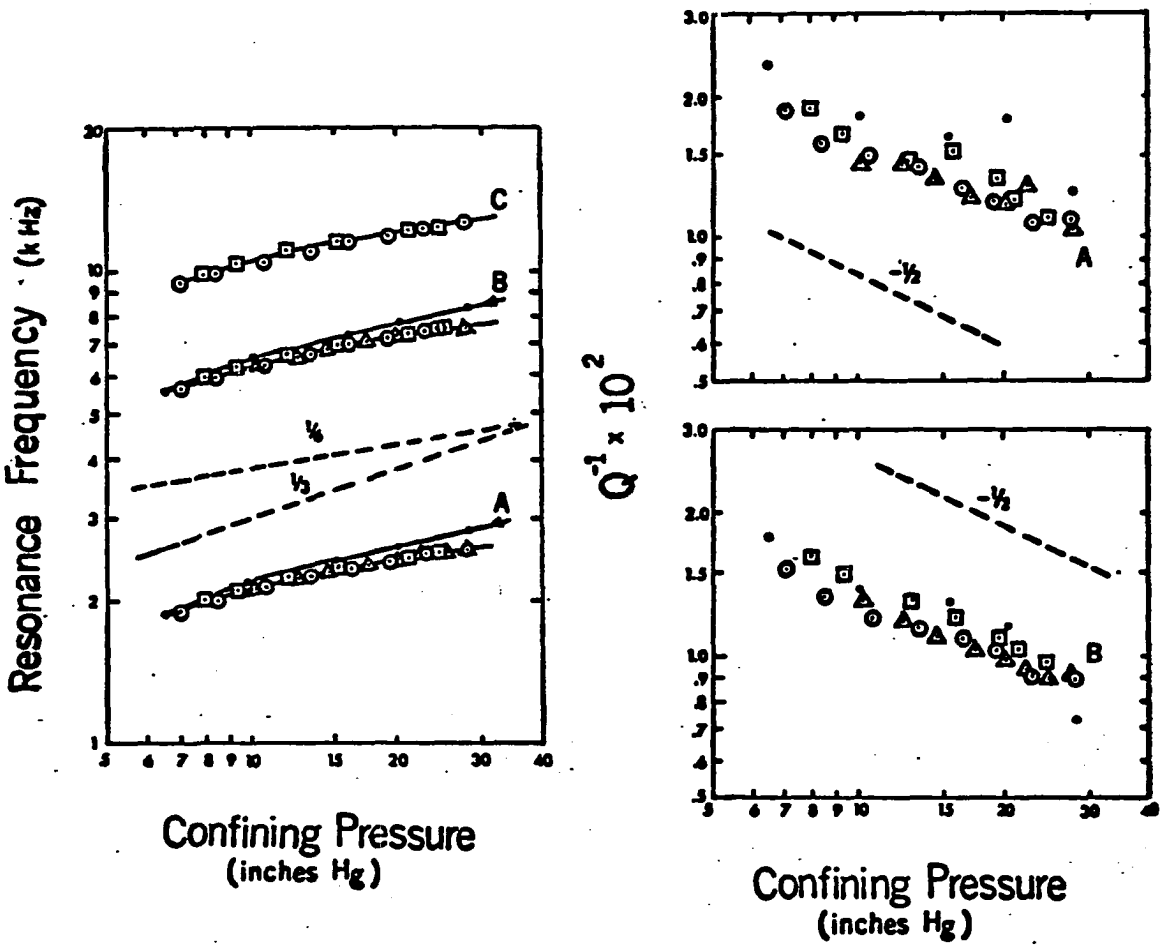

Fig. 18. Comparison of resonance frequency and Q^{-1} measurements as a function of confining pressure for alundum lubricated with 0.010% sodium stearate. A--first harmonic, B--third harmonic, C--fifth harmonic. First decrease and increase in pressure denoted by dots and circles, respectively; second decrease and increase, by squares and triangles, respectively. (1 in. Hg = 3.38 X 10^2 bar)

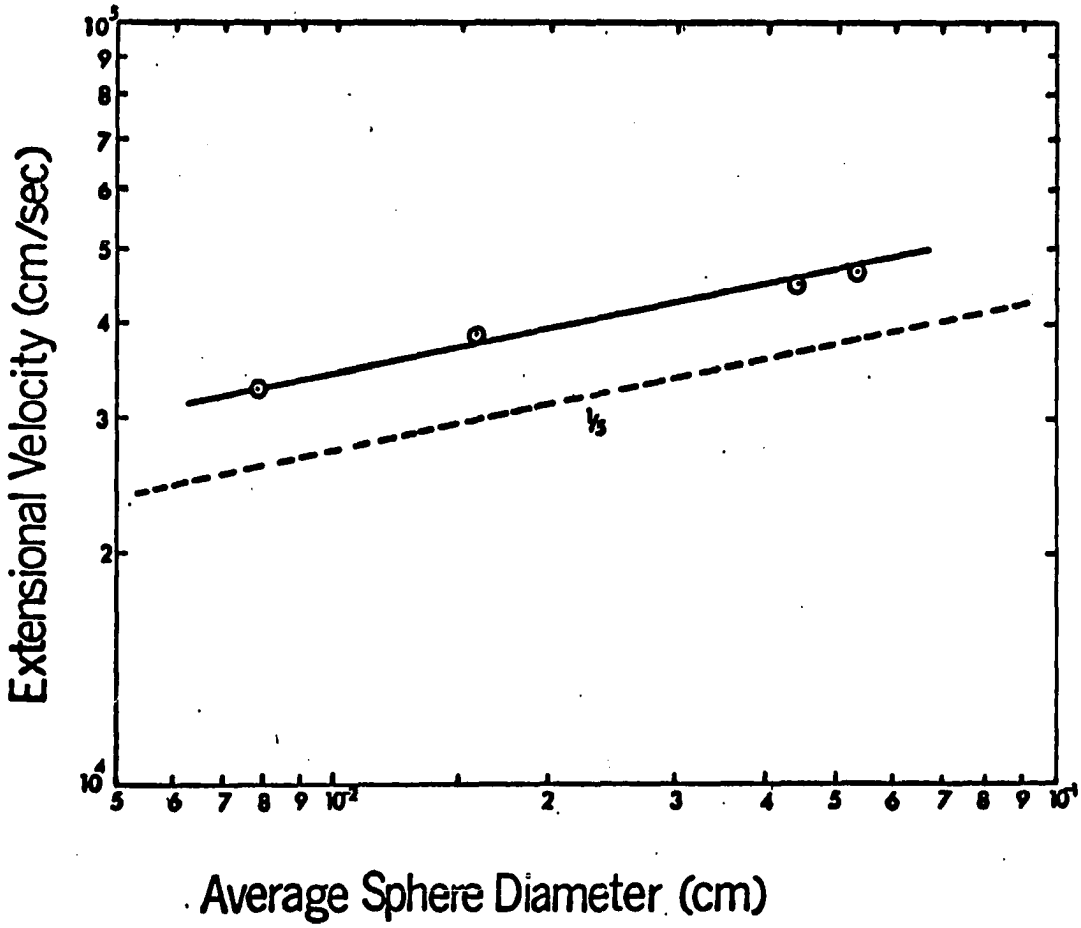

Fig. 19. Velocity versus average grain size for clean glass bead aggregates.

Reproduced with permission of the copyright owner. Further reproduction prohibited without permission.

Reproduced with permission of the copyright owner. Further reproduction prohibited without permission.

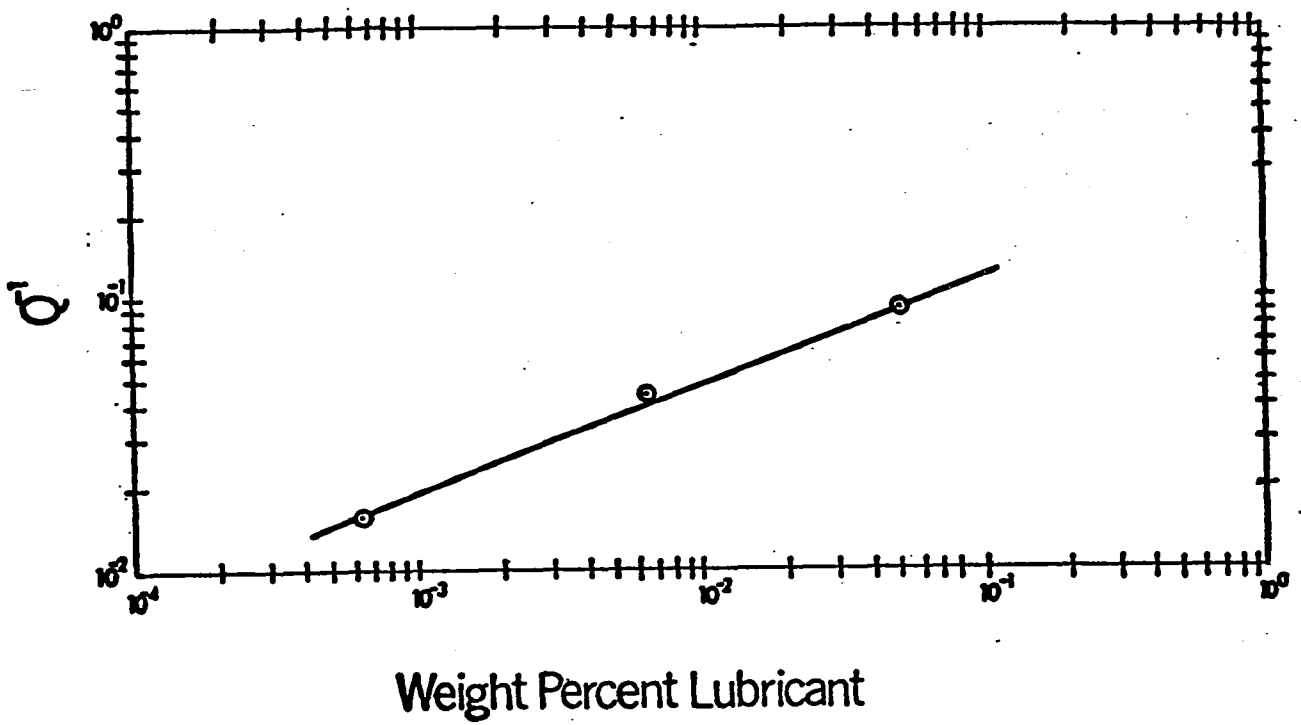

Fig. 20. Measurements of Q^{-1} of glass bead aggregates as a function of the amount of lubricant (glycerol) added to the specimens.

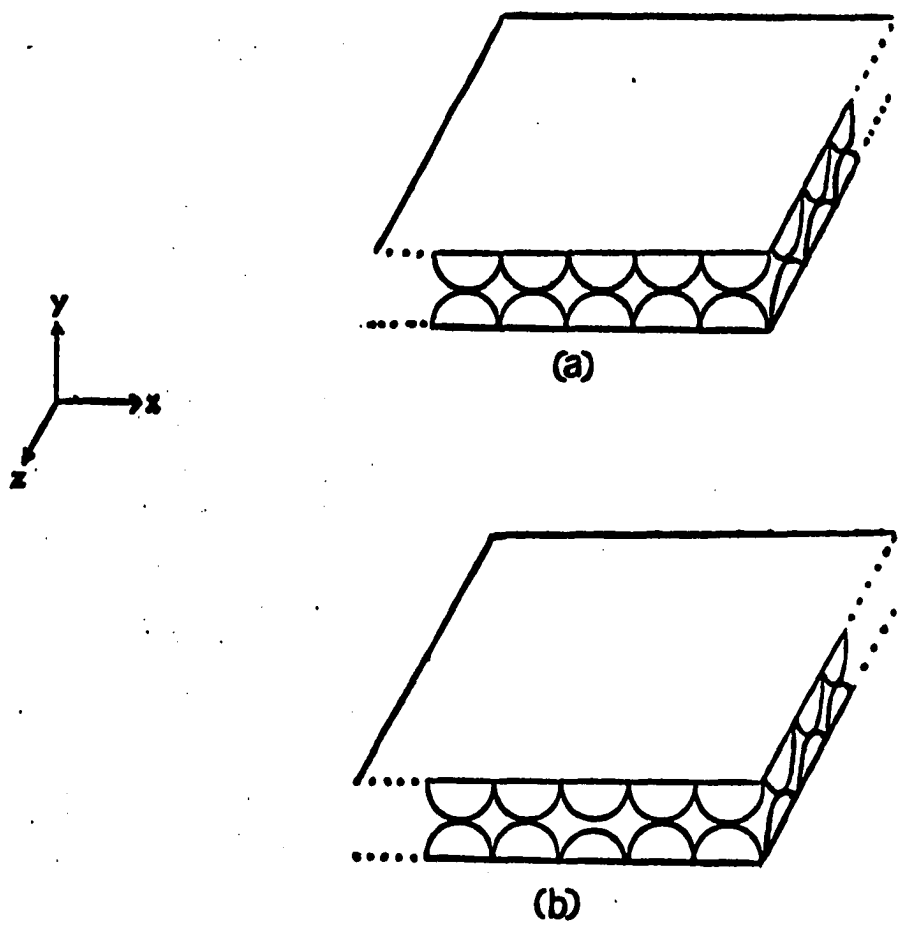

Fig. 21. Model for studying the effects of missing contacts.

Reproduced with permission of the copyright owner. Further reproduction prohibited without permission.

Reproduced with permission of the copyright owner. Further reproduction prohibited without permission.

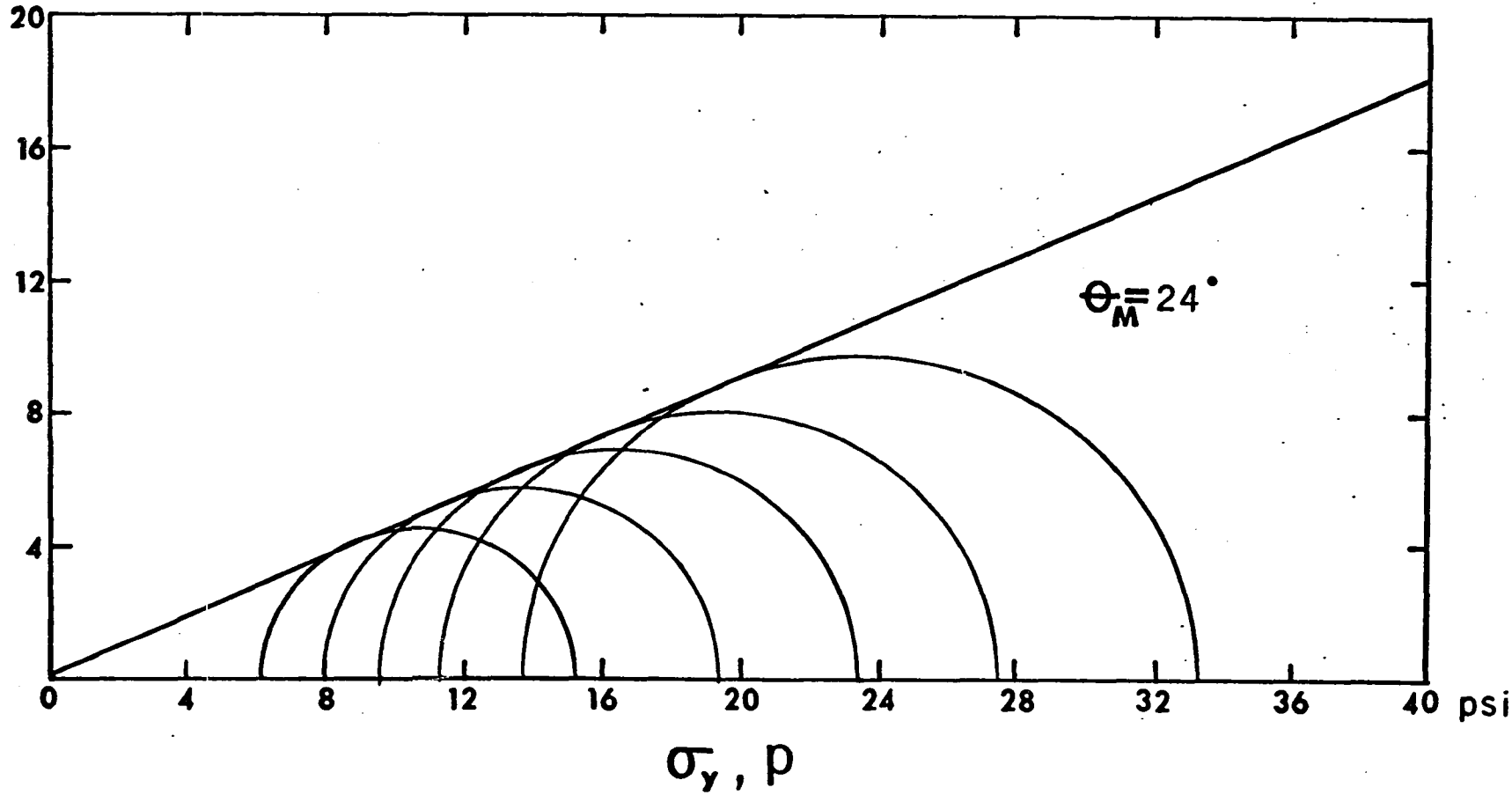

Fig. 22. Mohr circle diagram obtained in compression testing of glass beads lubricated with 0.0045% oil. (1 psi = 6.90 X 10^{-2} bar)

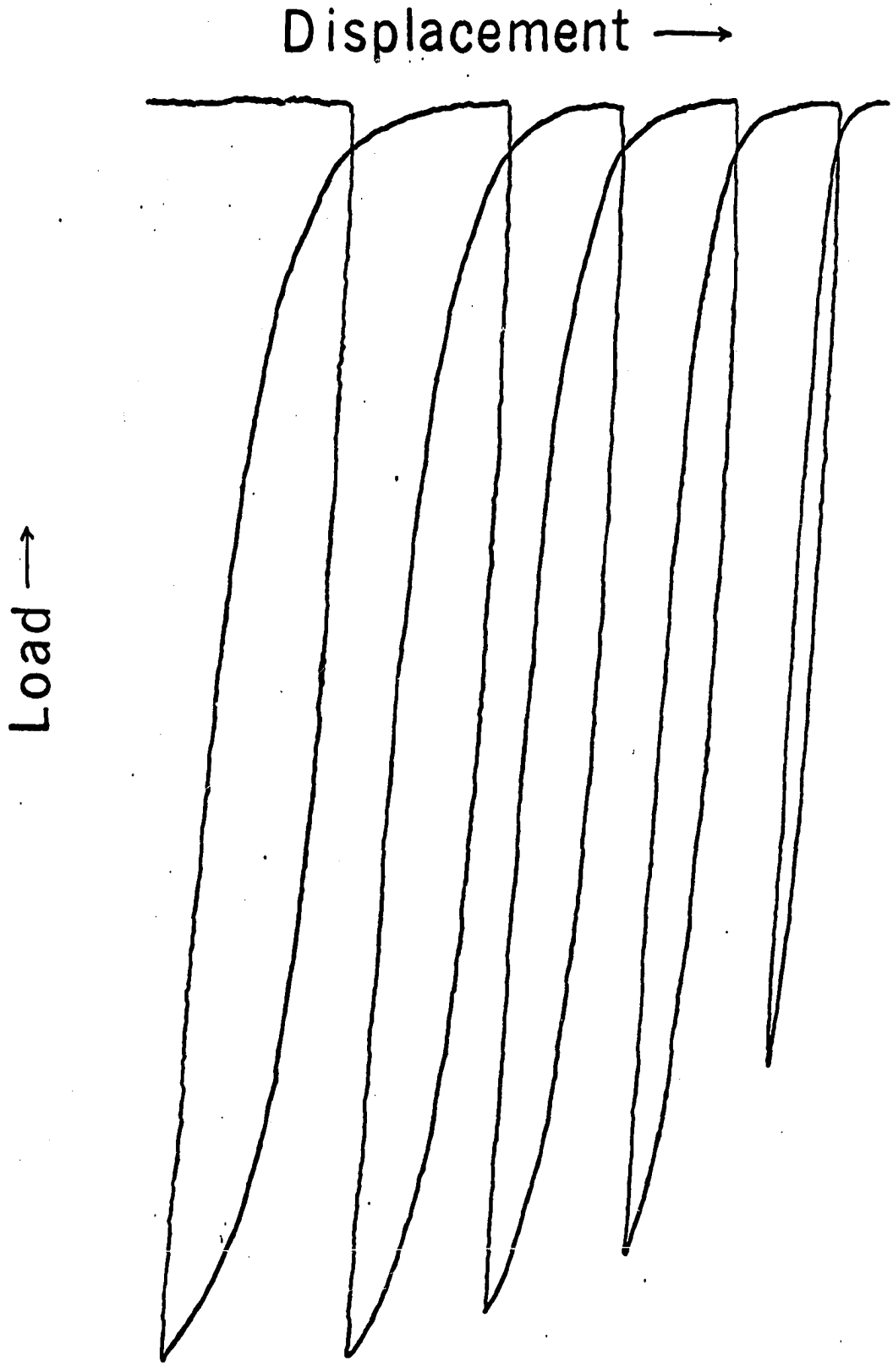

Fig. 23. Load-displacement hysteresis curves obtained during compression tests on alundum aggregates lubricated with 0.010% sodium stearate.

Reproduced with permission of the copyright owner. Further reproduction prohibited without permission.

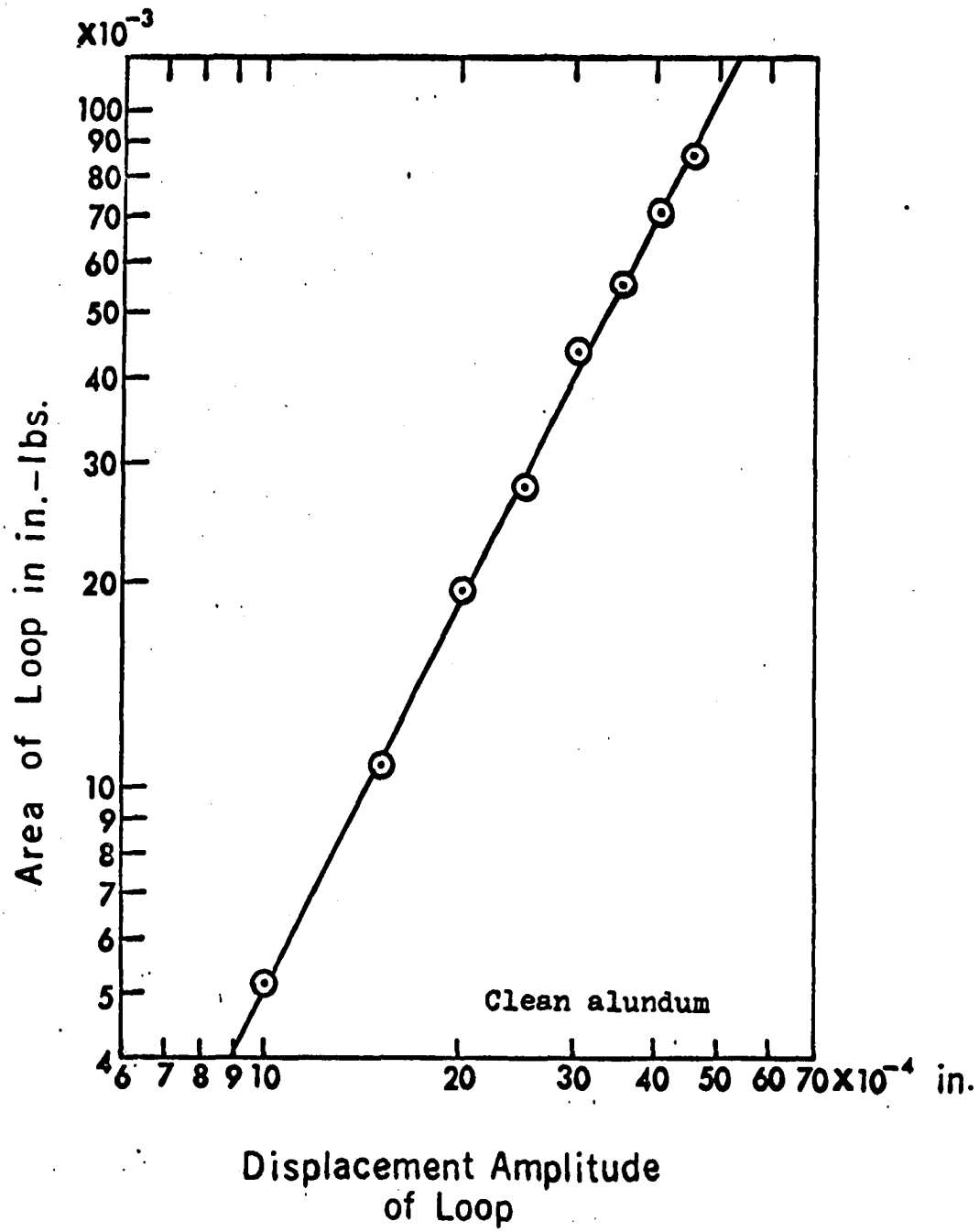

Fig. 24. Example of the relation of hysteresis loop area (or energy dissipation) to loop displacement amplitude.

Reproduced with permission of the copyright owner. Further reproduction prohibited without permission.